University of Alberta

An investigation into the Development of Ceramic Sorbents for High Temperature Air Separation for OxyFiring

by

Mehdi Mohammad Ali Pour

A thesis submitted to the Faculty of Graduate Studies and Research

in partial fulfillment of the requirements for the degree of

Doctor of Philosophy

in

Materials Engineering

Department of Chemical and Materials Engineering

© Mehdi Mohammad Ali Pour

Spring 2014

Edmonton, Alberta

Permission is hereby granted to the University of Alberta Libraries to reproduce single copies of this thesis and to lend or sell such copies for private, scholarly or scientific research purposes only. Where the thesis is converted to, or otherwise made available in digital form, the University of Alberta will advise potential users of the thesis of these terms.

The author reserves all other publication and other rights in association with the copyright in the thesis and, except as herein before provided, neither the thesis nor any substantial portion thereof may be printed or otherwise reproduced in any material form whatsoever without the author's prior written permission.

Abstract

Oxyfuel combustion as one of the alternatives to post-combustion carbon capture technologies requires an economically viable oxygen supply system. Cryogenic air separation, the main currently available technology, consumes above 30% of the energy produced as it involves separation of nitrogen from the oxygen in the inlet air stream. High temperature air separation is a promising technology for the purpose of oxygen production in oxyfuel combustion

Non-stoichiometric perovskite sorbents developed for use in high temperature air separation suffer from shortcomings that can affect their use in large applications. Development of alternatives to perovskite oxides as sorbents for high temperature air separation has been studied in this dissertation. Perovskite/spinel oxide has been considered as the first option for comparison of the properties as oxygen sorbent to those of the traditional perovskites. Copper oxide has been chosen as the second and main alternative to nonstoichiometric oxides. Despite numerous advantages, copper oxide has its own shortcomings for use as high temperature oxygen sorbent. Effect of synthesis method has been studied as the first approach for improving shortcomings of current sorbents - the most important of which is to increase the oxygen desorption rate. The citrate gel method has been shown to be the most effective ceramic synthesis method in this case by the positive effects that it has on surface chemistry of copper oxide as an oxygen sorbent.

Doping with alumina has been chosen to improve the properties through the chemistry of reactions occurring between CuO, $CuAl_2O_4$, $CuAlO_2$ and Cu_2O during oxygen absorption and desorption. Addition of alumina up to 30% has been shown to improve desorption kinetics without significantly affecting the absorption kinetics. High temperature stability is the other property that has been improved by addition of alumina. Zirconia and its derivatives doped with yttria and ceria were explored as support materials for copper oxide. Yttria stabilized zirconia was shown to have positive effects on oxygen desorption kinetics, high temperature stability and attrition resistance of the sorbents.

Acknowledgements

Hereby, I would like to thank everybody who helped me during my PhD and the past six years of my stay in Canada:

- I am extremely grateful to Dr. Richard Fox, who by his incredible knowledge and skill saved my life from the horrible ailment I was suffering from. I would also like to show my gratitude for Dr. Jeffrey Jirsch in managing the epileptic seizures in the past two years. My dear friends, Nima Shaygan, Ali Foroughi, Siavash Rezazadeh, Katayoon Navabi, Arash Ilbagi, Babak Shalchi, Farzad Mohammadi, Ali Hooshiar and Reza Hashemi supported me during this critical period without which it may not have been possible to reach this stage.
- I would like to acknowledge the support of my supervisors, Dr. John Nychka, Dr. Rajender Gupta along with Dr. Steve Kuznicki for their supervision and guidance. I had the opportunity to have access to their insights and knowledge at any time during the last four years. Their great suggestions have helped me in performing laboratory experiments, analyzing scientific data and writing scientific paper.
- I would like to thank Dr. Thomas Etsell for letting me using his lab equipment, my colleagues, Drs Farshid Vejahati, Moshfiqur Rahman, Arunkumar Samantha and Deepak Pudasaine for their help and assistance in technical matters. I would also like to thank Shiraz Merali, and Diane

Caird for XRD, Tina Barker and Gayle Hatchard for SEM and Dr Dimitre Karpuzov for XPS experiments

- Finally, I am very grateful to Alberta Innovates and Canadian Centre for Clean Coal/Carbon and Mineral Processing Technologies for financial support of this research.

Contents

List of Figures

List of Tables

Chapter 1: The Oxyfuel Process and High Temperature Air Separation

1.1. Research Objectives and Significance

Oxyfuel combustion as a pre-combustion carbon capture technology requires an economically viable oxygen supply system for its practical large scale use. Although high temperature air separation technologies have advantages over adsorption and cryogenic process, they suffer from shortcomings like poor oxygen desorption kinetics, CO_2 uptake and long-term structural stability of the sorbents. Development of a candidate material to improve these shortcomings is the main objective of this work. Addressing the parameters that have effect on absorption and desorption performance on the candidate material is the other objective of this research. The studies performed in this work can have important implications in other areas of research like ceramic synthesis, chemical looping combustion and catalysis.

1.2. Structure of Dissertation

This dissertation mainly consists of two parts. Chapters 1 and 2 deal with nonstoichiometric oxides with perovskite and perovskite/spinel structure as starting point for development of high temperature air separation sorbents. Chapter 1 provides a brief review of the oxyfuel power generation and air separation as the main challenge for practical development of this process.

Drawbacks of the currently available oxygen generation processes and the necessity for development of a new technology for supplying the oxygen requirements for oxyfuel power generation are discussed. An introduction to high temperature air separation and the materials that have been developed for use in this process, their advantages and disadvantages and the possible strategies for improvement of their propertied are also presented. In Chapter 2, a comparison is made between perovskite and dual phase sorbents for use in high temperature air separation. Oxygen sorption capacity, oxygen sorption/desorption kinetics and CO_2 uptake as important parameters of high temperature air sorbent are experimentally investigated. Chapters 3 to 5 focus on copper oxide as an alternative for nonstoichiometric oxides for use as an oxygen sorbent. In Chapter 3, the potential of copper oxide as a high temperature oxygen sorbent is discussed and the effect of ceramic synthesis methods on oxygen sorptive/desorptive propertied are experimentally tested. Chapter 4 deals with use of alumina as a dopant for improving the properties of copper oxide for high temperature air separation. In Chapter 5, a group of zirconia-based ceramics are introduced as a support material for copper oxide and their effect on high temperature oxygen absorption and desorption are experimentally investigated. Finally, an overall summary of the research is given in Chapter 6 and suggestions for future work are provided.

1.3. Oxyfuel Power Generation

Oxy-fuel or oxy-combustion processes are considered one of the important methods for reducing greenhouse gas emissions especially carbon dioxide. Carbon dioxide capture and sequestration techniques require separation of carbon dioxide from nitrogen which makes up the larger fraction of flue gases as air is currently used to burn fuels like coal and natural gas. The post-combustion capture technology currently available for separation of carbon dioxide from nitrogen in flue gases is monoethanolamine (MEA) solvents (Jadhav, P. D *et al.* 2007). In oxy-fuel processes, an oxygen-enriched stream of carbon dioxide is produced to burn the fuel in oxygen/CO_2 mixture rather than in air; as a result, a pure carbon dioxide exhaust is produced that requires little separation, facilitating carbon dioxide capture. Furthermore oxy-combustion reduces NO_x emissions while improving combustion characteristics like decreasing the unburned carbon content (Toftegaarda, M. B. *et al.* 2010). An economically viable oxygen production method is essential to making oxy-combustion power plant a future option when carbon dioxide capture becomes strongly regulated. Oxygen removal using ceramic sorbents takes advantage of high oxygen sorption capacity of these materials and their high sensitivity to oxygen composition. Perovskite sorbents can comparatively absorb large amounts of oxygen but no other gases (Lin,Y.S. *et al.* 2000). This oxygen sensitivity gives such materials the potential to be used as an integral part of the combustion process to provide high selectivity of oxygen in the feed gas. Another technology based on perovskite ceramics is the membrane technique which has shown high selectivity and efficiency for oxygen separation

but a fabrication technique to produce membranes with a low level of defects at the industrial scale is a major challenge (Sunarsoa, J. *et al.* 2008). The sorbent version of ceramics does not require a very high level of structural integrity and the porosity usually produced in ceramic fabrication processes can even help with the efficiency of the process through the increase in surface area. However the technology is quite new and requires much more in depth investigation of various parameters such as structural stability, effect of catalyst poisons on the long term efficiency and the kinetics of sorption and desorption. Slow desorption rate of oxygen during the generation stage is a major challenge but use of CO_2 as a purge gas has been shown to improve this effect (Qing Yang and Y. S. Lin. 2007).

1.3.1. Oxyfuel Combustion and Related Phenomena

Oxyfuel or O_2/CO_2 recycle combustion is among the most important technologies for zero emission power generation. This process provides opportunities for reducing boiler size and cost, CO_2 capture, and use of advanced steam technologies. Another important advantage of this process, especially in case of oxy-firing of pulverized coal is its ability for being retrofitted in existing thermal power plants. Oxyfuel combustion is carried out in an atmosphere of oxygen and CO_2 instead of a mixture of oxygen and nitrogen (air), which leads to a high CO_2 concentration in the flue gas which can be easily and economically separated from the water vapour which is the other major component of the flue gas. In this process (Figure 1.1) oxygen is fed into the boiler via an air separation unit. In

addition to oxygen the major part of CO_2-rich exhaust is also recycled back to the boiler to control combustion temperature and reduce NO_x emission. CO_2 recycle is a necessary step especially in coal combustion in oxygen because high flame temperature enhances the formation of NO_x in the boiler (Hadjipaschalis, I. *et al.* 2009).

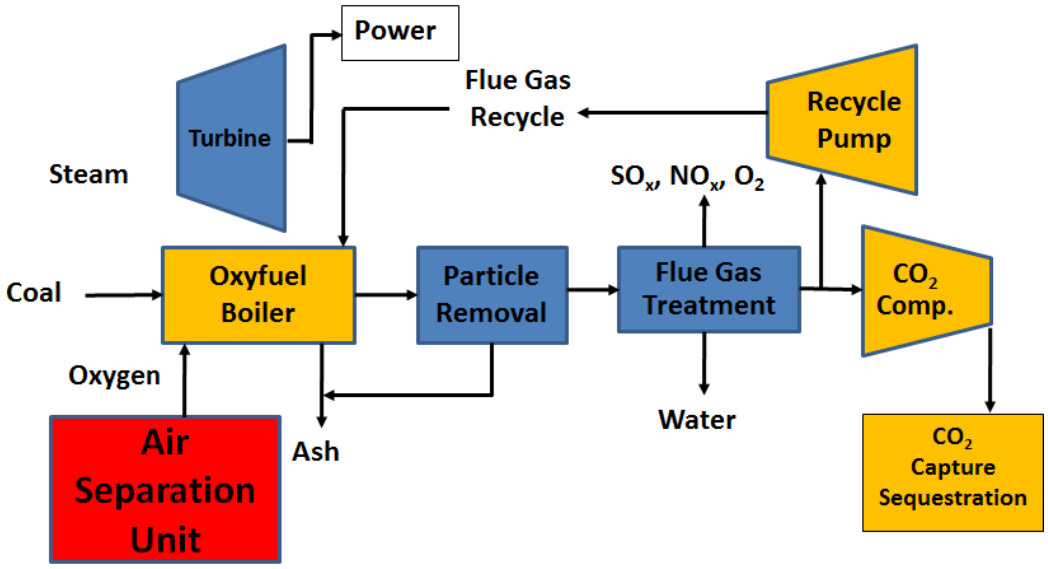

Figure 1.1. Basic principles of Oxyfuel technology

(reproduced using the idea from Hadjipaschalis, I. *et al.* 2009)

The major advantage in oxyfuel combustion is that a CO_2-rich flue gas is produced which is almost nitrogen free which means a simpler CO_2 capture and sequestration process compared to other technologies as the other component is water vapour which is easily condensable. The other advantage is the reduction

(elimination) of SO_x and NO_x emission due to absence of nitrogen and high oxygen fugacity in the feed gas which means lower cost of desulphurization and nitrogen oxide removal as a result of lower volume of the relevant equipment (Jordal, K. *et al.* 2004). The composition of flue gas in oxyfuel combustion is 55-65% CO_2, 25-35% H_2O and the rest being nitrogen, oxygen and argon depending on the type of fuel used (e.g. pulverized coal, dry or raw lignite) (Kakaras, E. *et al.* 2007). After condensation and cleaning, the flue gas is around 96% CO_2 which can be compressed and transported for storage or enhanced oil recovery (Hellfritsch, S. and Gampe, U. 2007). The amount of recycled CO_2 is a critical factor as it can affect the flame temperature and plant efficiency. It is generally desired that the amount of CO_2 recycled be reduced to increase the plant efficiency and prevent the need for excessive O_2 concentration to keep the flame temperature high as the high heat capacity of CO_2 can adversely affect this parameter (Toporov, D. *et al.* 2007). Another method for increasing oxyfuel plant efficiency is the substitution of the air separation unit (ASU) by other technologies for pure oxygen or oxygen mixed with CO_2 that is less demanding in terms of auxiliary plant requirements (Marion, J., 2004). A typical cryogenic air separation unit can consume up to 20% of plant gross output which is detrimental to plant efficiency. Replacement of the conventional air separation units by technologies like ceramic auto-thermal recovery and chemical looping combustion can improve the plant efficiency by a few percent (Ishida, M. and Jin, H. 1994), however the cryogenic air separation process remains the only available large-scale technology at present time (Wall, T. *et al.* 2009).

1.4. Air Separation Techniques

In addition to its crucial importance in oxy-fuel combustion, air separation is an essential chemical process as it produces oxygen and nitrogen as two basic commodities used in many processes. Oxygen is used in a variety of applications from medical care, smelting furnaces and steel making. Nitrogen is extensively used in welding, petroleum and petrochemical engineering, low temperature storage and food packing. Currently, the separation of oxygen and nitrogen is performed by using the three processes (Ruthven, D. M. *et al.* 1994):

1. ***Cryogenic distillation***: This technique exploits the relative volatilities of the two components. This is the most developed process and has a number of advantages for large scale production of high purity gases but in low to medium scale production due to transportation cost of the cryogenic products and power consumption it is inefficient (Li, G.Q and Govind, R. 1994).
2. ***Adsorption Processes:*** This technique is most suitable for on-site production (i.e. medium to large scale throughputs). For large scale production of oxygen and nitrogen at high purity these processes are usually preferred over membrane separation (Rege, S.U. and Yang, R.T, 1997).
3. ***Membrane separation***: This technique is based on the difference in solubility and diffusivity of nitrogen and oxygen in the membrane

material. It is most suitable for small scale production of nitrogen. For air separation, this technique is limited to a single stage process which puts an upper limit of 50% mole fraction on oxygen purity (Burdyny, T. and Struchtrup.1997).

1.4.1. Adsorption Processes (Ruthven, D. M. 1984)

Pressure swing adsorption (PSA) is the dominant processes for air separation. These systems composed of two separate beds which perform the separation process continuously. Compressed air enters the bottom of one bed and one component is desorbed while the other enriched components pass through the bed to achieve separation. After reaching saturation, the process is switched to desorption while the other bed starts the adsorption simultaneously. This process exploits the preferential adsorption of one component on an adsorbent to separate the two components. PSA can be done either by utilizing the equilibrium or kinetics aspects of the adsorption phenomena. Equilibrium controlled separation is achieved by exploiting the difference in adsorption isotherms or the adsorption capacities of the two major components which in air separation are oxygen and nitrogen. In this case both species have rapid diffusion rate in the adsorbents and separation depends on the preferential adsorption of nitrogen. In kinetic-controlled processes, the difference in molecular size of the two species leads to faster desorption rate for oxygen. Equilibrium processes are generally used for production of oxygen whereas kinetic processes are more favourable when

Nitrogen production is considered. In kinetic-controlled processes, the choice of the cycle time is very critical for the performance of the adsorption process. For acceptable adsorption performance high selectivity, large adsorption performance, fast sorption and desorption kinetics and ease of regeneration are the general required properties.

For equilibrium-controlled production of oxygen, usually the first generation zeolite adsorbents like 5A or 13X are used. These adsorbents require pressures above atmospheric pressure and can have a separation factor ($\alpha_{N2/O2}$) of 3.0-3.5 when totally dehydrated (Rege, S.U. and Yang, R.T. 1997). For second generation zeolites like CaX, higher separation factors can be achieved but the desorption process is difficult at atmospheric pressures (Chou C. *et al.* 1998). For both types of sorbents the maximum oxygen purity is 95-96% due to presence of argon which has nearly the same sorption affinity as oxygen (Anson, A. *et al.* 2009). Industrial production of nitrogen is through a kinetic-controlled process. Zeolite 4A and carbon molecular sieve are usually used as the adsorbent. The fine pore size (4Å) of these materials is crucial to the high separation of the species because it is the difference in molecular size of the two molecules that leads to the higher sorption rate of O_2 despite their similar sorption affinity on the adsorbents. By choosing proper cycle time nitrogen purity as high as 98-99% can be achieved that is adequate enough for most applications. In these cases adsorption is generally carried out at temperatures below 50°C because the best results are obtained at low temperatures due to their physical adsorption mechanism (Yang, R.T. 2003). 5A and X zeolites have been extensively used in the production of

oxygen. Zeolites with low silicon/aluminum ration can achieve high selectivity for nitrogen adsorption. The interaction between nitrogen and cation in zeolite is much stronger than that of oxygen and in addition the nitrogen sorption capacity is much more sensitive to the choice of cation present in the adsorbent therefore by exchanging the cations with some ions like Li high nitrogen selectivity and adsorption can be achieved but synthesis of such compounds are rather expensive and difficult. Figure 1.2 shows the adsorption capacities of nitrogen and oxygen on Li-X zeolite. Nitrogen is selectively adsorbed on this zeolite. This is one of the best available adsorbents for air separation based on Zeolite structure. Carbon molecular sieve is the other type of adsorbent used for air separation especially in nitrogen production. Many studies have been performed for using preparing oxygen selective adsorbents and their use in the PSA process. An example of this type of adsorbent is the use of char from coconut shell pyrolysis which has been found to have high oxygen volumetric capacity when crushed and sized to form granules (Rege, S. U. and Yang, R. T. 1997).

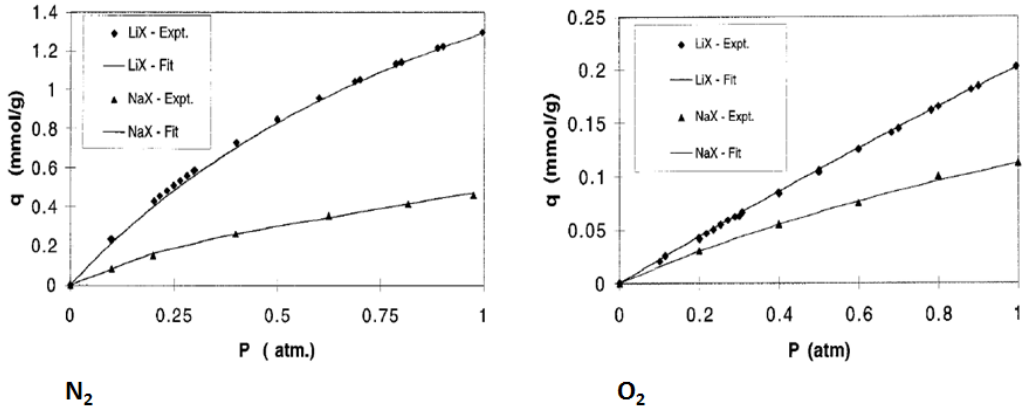

Figure 1. 2.Comparison of oxygen and nitrogen adsorption on two types of x zeolites
(Rege, S. U. and Yang, R. T. 1997)
(Reprinted with written permission from American Chemical Society)

Use of cerium and silver sites on SiO_2 support has also been reported by Jarayaman and Yang (Jayaraman, A. and Yang, R. T. 2005). These salts have shown high selectivity for oxygen with selectivity increasing with pressure. The reason for oxygen selectivity is the large magnetic susceptibility of this molecule. Dispersion of silver on high surface area substrate of SiO_2 has been shown to increase the sorption capacity. The sorbent is also stable on exposure to water and can be regenerated (Jayaraman A. and Yang R. T. 2005).

1.4.1.1. Drawbacks of the Current Adsorption Processes

Years of research on the PSA process and adsorbent developments has improved the performance of adsorption processes but these processes still suffer from

major drawbacks when it comes to their use in air separation. Therefore the need for research and development of new adsorbents is still felt. These problems can be summarized in the following categories (Sircar, S. *et al.* 1998):

1. Under normal conditions, there is no thermodynamic selectivity for adsorption between oxygen and nitrogen on most zeolite adsorbents due to their weak or non-polar nature and comparable polarizabilities.
2. Using equilibrium processes alone, the maximum purity obtainable is limited to 95-96% due to low selectivity.
3. Large oxygen adsorption capacity required for industrial applications is not possible by the current adsorbents.
4. Presence of other species like H_2O, CO_2 in the gas stream can affect the adsorption properties. Pre-treatment is usually necessary to maintain the performance of the system which makes the process design more complicated. This is crucially important in the oxy-fuel application considered in this work. CO_2 is an essential component of oxy-fuel technology and its use with the available adsorbents can lead to low efficiency of the bed and a complicated design.
5. Most of the available adsorbents have the highest sensitivity at rather low temperatures. Use of these sorbents in the oxyfuel process will require heating and cooling of the gas streams causing waste of energy which is in contrast with the goal of reaching higher efficiency in the oxyfuel process.

6. Due to relatively high cost of oxygen production by these methods (Figure 2.3), their application to oxyfuel power generation is not economically viable

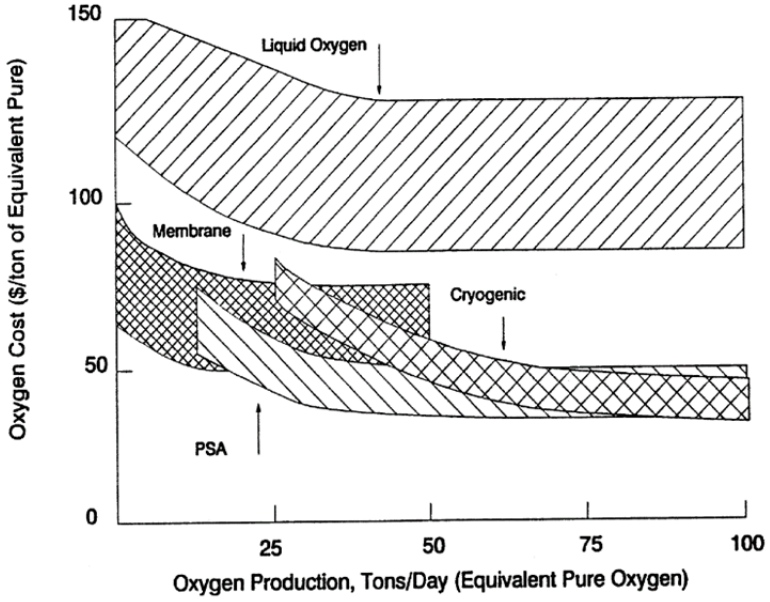

Figure 1.3. Cost of oxygen production for different conventional methods (Kobayashi, H., and Prasad, R., 1999)

1.5. Ceramic Membranes for Air Separation

Membrane oxygen separation exploits the properties of the pure oxygen conducting and mixed ionic-electronic conducting ceramics. For oxygen permeation through the membrane a driving force is required which can be either an electrical or chemical potential gradient (Figure 1.4). In the case of mixed ionic-electronic conducting membranes the amount of oxygen produced can be

controlled by application of an electric current. The ceramic membranes are usually oxides based on perovskite or fluorite structures. Oxides with these structures are usually known for exhibiting favourable oxygen permeation properties suitable for use as oxygen conducting membranes. Fluorite structure (Figure 1.5A) has a face centered cubic packing in which the empty interstice in a space at the center is located within the cubic anion lattice. A solid solution like $(ZrO_2)_x(CaO)_{1-x}$ exhibit high electrical conductivity due to its high oxygen mobility. In fluorite structures the cation sites are occupied while many of the oxygen anion sites are empty leading to high oxygen deficiency. Perovskite type oxides (Figure 1.5B) are the second group of compound in membrane manufacture (Sunarsoa J. *et al.* 2008).

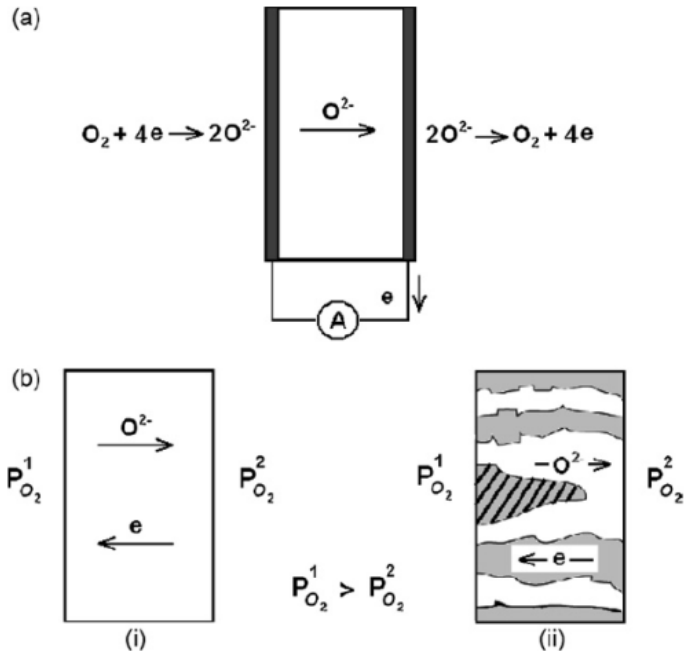

Figure 1. 4. Types of Ceramic Membrane**:**

(a) solid electrolyte . (b) i. Single and ii. Dual phase mixed ionic-electronic

(Sunarsoa, J. *et al.* 2008, *reprinted with written permission from Elsevier*)

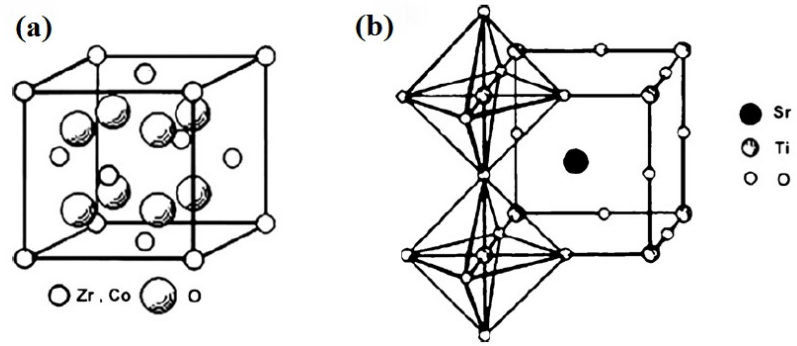

Figure 1.5: A. Fluroite and B. Perovskite Structure

(Sunarsoa, J. *et al.* 2008, *reprinted with written permission from Elsevier*)

These oxides have the general formula of ABO_3 and have been studied for their important physical properties like pyro-electricity, magnetism and electro-optic properties since the 1950s. In the past three decades compounds like $LaMnO_3$, $LaCoO_3$ and $LaCrO_3$ have been used as cathode materials in solid oxide fuel cells. They have also been extensively investigated as catalysts for partial oxidation of hydrocarbons, oxidative coupling of methane in production of syn-gas (Navrotsky, A. 1989). If doped with aliovalent impurities such as strontium, perovskite materials can exhibit oxygen non-stoichiometry. Doping is the partial substitution of A-site or B-site ions by ions of different oxidation states which leads to formation of vacancies and free electrons or electron holes to maintain electrical neutrality which gives the material both electronic and ionic conduction. Depending on the chemistry, type of impurities and extent of doping either of ionic or electronic conduction properties can change significantly which leads to different materials for different applications (Kingery, W.D. and Bowen, H.K. 1976).The driving force for oxygen permeation across the membrane is the difference in partial pressure on the two sides; a concentration gradient in the material is created across which oxygen can diffuse. For this purpose the molecular oxygen in the gas phase should first be adsorbed on the surface, dissociate and then enter the structure to diffuse to the other side provided the ionic mobility is high enough by the existence of desirable conditions most significant of which is high temperature (>600°C) (Tejuca, L. G. 1989). These steps can be described by the following reaction as represented by the Kröger-Vink notation (Kroger, F.A. and Vink, H.J. 1958):

$$\frac{1}{2}O_2 + V_O^{\bullet\bullet} \Leftrightarrow O_O^x + 2h^{\bullet} \qquad \text{(Eqn. 1-1)}$$

Where the forward reaction is dominant on the high pressure side and the reverse is on the low pressure side. In this reaction $V_O^{\bullet\bullet}$ is oxygen vacancy, $h^{\bullet}$ an electron hole and O_O^x the lattice oxygen.

Systematic works on the oxygen conduction properties of these oxides have been in progress since 1980s to understand and optimize dense membrane properties as related to oxygen separation and other applications. Currently the thickness of ceramic membranes for air separation is around 0.5 to 2 mm with a measured oxygen flux of 0.1 to 1 μmol/cm^{2}s which is in the same range as microporous membranes. The oxygen flux can be increased by decreasing the thickness for example by depositing a thin film on a porous support. In spite of all advances in this area, this technique in practice has to deal with a number of obstacles which make its use more limited (Sunarsoa, J. 2008):

1. Lack of a technique for large scale fabrication of membranes with desired properties
2. Unavailability of high temperature sealing materials and techniques
3. Long term structural and chemical stability of the membranes
4. Lack of fundamental understanding of oxygen transport properties used for the design of the membrane processes.

1.6. Sorbents for High Temperature Air Separation

Economic development of emission free power generation requires, as one of its essential components, an air separation process that lacks the draw-backs mentioned in the previous sections for the currently available processes. Development of new sorbents is a key step to development of processes suited to requirements of emission-free power generation processes like oxy-fuel combustion. (Lin, Y. S. *et al.* 2002) has recently introduced, in a US patent, a new group sorbents based on the perovskite structure which have the potential to eliminate the drawbacks of current adsorption processes. These new sorbents are non-stoichiometric oxides in the strontium-lanthanum-cobalt system which can selectively adsorb a considerable amount of oxygen (0.6-0.9 mmol/g) at elevated temperatures (> 300°C). The nonstoichiometry of these oxides has an important consequence which is highly beneficial to oxygen separation. The oxygen-deficiency property makes these oxides highly selective to oxygen over nitrogen and other non-oxygen containing species as a result the effect of other gas species are expected to be minimal (Lin, Y. S. *et al.* 2002).

1.6.1. Concept of High Temperature Sorption Process

Two major types of oxides (LSCF1: $La_{0.1}Sr_{0.9}Co_{0.5}Fe_{0.5}O_{3-\delta}$, LSCF2: $La_{0.1}Sr_{0.9}Co_{0.9}Fe_{0.1}O_{3-\delta}$) based on the Lanthanum cobaltite system ($LaCoO_3$) have been studied by (Lin, Y. S. *et al.* 2002) for high temperature air separation. Different impurity elements have been used for partial substitution of A-site (La)

and B-site (Co) atoms and their effects on air separation have been studied using thermogravimetric and packed bed methods. Doping by aliovalent impurities induces oxygen deficiency due to oxygen non-stoichiometric effect which is essential to maintain charge neutrality. For a fixed composition, this property is a function of temperature and pressure (P_{O2}) which can be used to absorb and desorb oxygen by changing temperature and pressure (e.g., TSA and PSA). Figure 1.6 shows a description of TSA process on these two types of sorbents. As seen in this figure, the oxide reaches equilibrium at 600°C and then with a decrease in temperature the value of nonstoichiometry (δ) decreases to lower values. Decrease of oxygen nonstoichiometry corresponds to increase of oxygen content in the perovskite solid which can be considered as the sorption part of the TSA process. In the desorption part with an increase in temperature δ can return to its original value (Yang Z. *et al.* 2002).The same effects can be observed by changing the flowing gas above the ceramic sample which forms the basis for PSA process. Figure 1.7 shows the PSA process for LSCF sorbent at 600°C. At a total pressure of 1 atm switching the gas from oxygen to helium results in desorption which has been shown as an increase in oxygen non-stoichiometry. By switching the gas back to oxygen, the sample abruptly loses its oxygen deficiency (δ) and absorbs oxygen (Figure 1.7A). The same effect is observed when air is used instead of pure oxygen (Figure 1.7B). In both cases oxygen uptake is very fast and occurs instantaneously but desorption is rather slow.

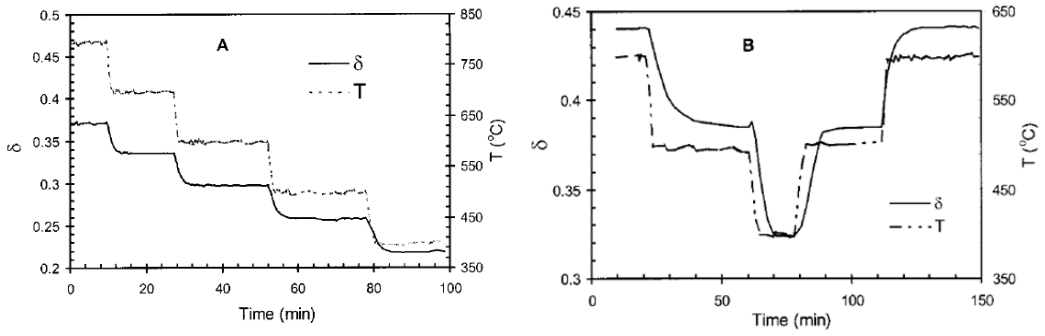

Figure 1.6. Schematic description of TSA process for oxygen sorption on perovskite LSCF: A.LSCF1: P_{O2} = 1 atm, B.LSCF2: P_{O2} = 0.01 atm. (After:Yang, Z., *et al.*, 2002.

(*reprinted with written permission from American Chemical Society*.)

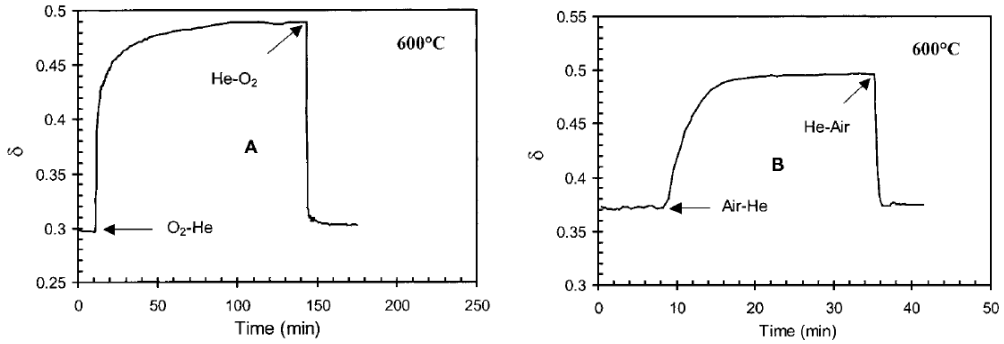

Figure 1. 7. Schematic description of PSA process for oxygen sorption on perovskite LSCF: A.LSCF1, B.LSCF2 (After Yang Z. *et al*. 2002.)

(*reprinted with written permission from ACS Publications*.)

The obvious advantage of these processes over the conventional air separation techniques is their high selectivity for oxygen; production of nitrogen and oxygen at high purities is possible which cannot usually be reached with established processes. Figure 1.8A compares the nitrogen and oxygen sorption equilibrium properties of perovskite-type ceramic sorbents with those of a representative

conventional adsorbent, zeolite LiX. The zeolite compound shows a preferable sorption of nitrogen and gives an equilibrium selectivity of around 10 in the pressure of interest. LSCF shows a relatively large sorption capacity for oxygen for but zero for nitrogen. This mono-sorption gives an infinitely large selectivity for oxygen over nitrogen, argon and any other gas in air. In this comparison the different operating conditions over which the sorption takes place should be taken into consideration. Using the density of the two materials the ratio of oxygen concentration in the gas phase to that in the solid can be calculated which is shown for the two sorbents as function of oxygen pressure in Figure 1.8B. Over this pressure range, LSCF has a higher (1 order of magnitude or higher) oxygen partition amount in the solid phase than LiX zeolite which is a sign of its better sorption equilibrium properties (Yang, Z. H. and Lin Y. S. 2003).

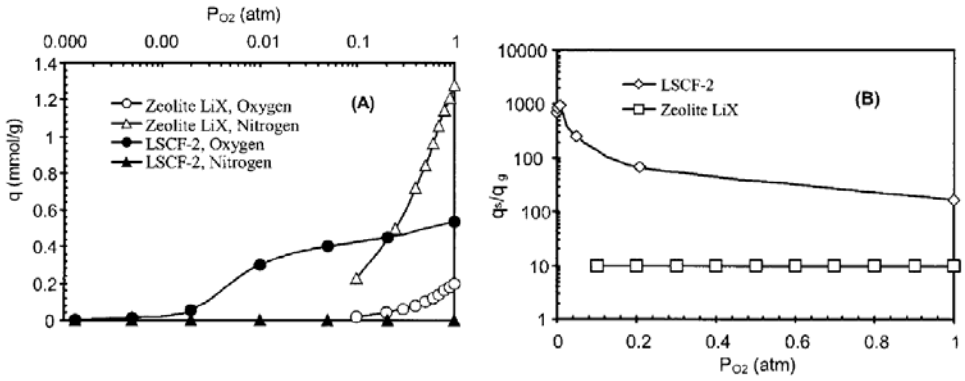

Figure 1. 8. Comparison of sorption capacities of LSCF Perovskite and LiX Zeolite (Yang, Z. H. and Lin Y. S. 2003).

(*reprinted with written permission from ACS Publications.*)

1.6.2. Nonstoichiometry and Oxygen Deficiency in Perovskite Oxides

Development and use of ceramic sorbents for air separation requires a fundamental understanding of oxygen non-stoichiometry in perovskite oxides. Oxygen non-stoichiometry is a phenomenon that occurs due to existence of defects in the crystal structure of the oxide. It is well known that perfect crystal structures are rare and that the presence of defects is thermodynamically and geometrically necessary for stability of the material. Creation of defects causes a considerable increase in the entropy of the material which minimizes the Gibbs free energy of the system. Defects can generally be classified as electrical and structural defects. Electronic defects are related to intrinsic ionization or excitation of electrons from valence to conduction bands or their formation to maintain charge neutrality. The structural defects are divided into point, line and area categories. These defects are important in this discussion as they provide pathways for diffusion in the material. Point defects can be created internally or by introduction of impurities through formation of oxide solid solutions. This way, the material maintains charge neutrality by reduction of ions in the lattice sites which is either by anion vacancy or cation interstitial formation and vice versa. In some systems, anion vacancy is the dominant while the other mechanism operates in some other systems.

Stoichiometric oxides are compounds that contain an equivalent number of positively and negatively-charged defects. In these oxides concentration of defects is a function of the internal equilibrium of the material. In nonstoichiometric oxides, where there is an excess of anion or cation defects, defect concentration is a function of temperature and pressure of the surrounding component (oxygen in

the case of oxides). Non-stoichiometry in oxides can be caused by deficiency of oxygen (or excess of metals) as well as deficiency of metals (excess of oxygen) which forms the basis for oxygen nonstoichiometry in oxide ceramics. Non-stoichiometry in oxides can exist as both an excess and deficiency of oxygen. Oxidative non-stoichiometry or oxygen-excess means that there are more oxygen ions available than the number of sites in the oxygen sublattice of the oxide crystal structure whereas in the case of oxygen-deficiency the reverse conditions exist. A group of perovskite oxides have the ability to exhibit the two types of behaviour as a function of temperature and pressure. As mentioned in the previous sections, perovskite oxides have the general formula of ABO_3. Among these oxides LSCF oxides ($La_{1-x}Sr_xCo_{1-y}Fe_yO_{3-\delta}$) have been the subject of numerous studies. It's been shown that A-site substitution of La by Sr enhances the amount of oxygen adsorbed while B-site substitution of Co by Fe affects the bonding strength of adsorbed oxygen leading to changes in the properties of adsorbed oxygen. Fe is also believed to stabilize the perovskite crystal structure by inhibiting the perovskite to brownmillerite phase transformation. LSCF oxides can absorb relatively large amounts of oxygen (0.2-0.4 mmol/g) while preserving their structure. With increase of Sr and Co content oxygen deficiency, and as a result oxygen sorption capacity becomes more sensitive to changes in temperature or oxygen partial pressure. The high sensitivity and the stability of the structure can facilitate a reversible sorption and desorption over a large period of time. Table 1 summarizes the dependences of oxygen nonstoichiometry (δ) on temperature and oxygen partial pressure for a number of LSCF oxides. As shown,

with an increase in Sr content at the A site the change in oxygen nonstoichiometry ($\Delta\delta$) to a given change in temperature or oxygen partial pressure increases (Mizusaki, J. *et al.* 1985).

Table 1.1. Dependence of oxygen nonstoichiometry on T and P_{O2} for various LSCF materials (Mizusaki, J. *et al*. 1985, Mizusaki, J. *et al.* 1989, Yang, Z. H. and Lin Y. S. 2003).

LSCF Oxide	X	Experimental conditions	$\Delta\delta$
$La_xSr_{1-x}Co_{0.2}Fe_{0.8}O_{3-\delta}$	0.6	P_{02} = 0.21 atm, T: 300 to 1200°C	0.14
	0.4		0.25
	0.2		0.32
$La_xSr_{1-x}CoO_{3-\delta}$	0.8	P_{O2}: 0.2 to 0.001 atm, T = 800°C,	0.032
	0.6		0.075
	0.3		0.083
$La_xSr_{1-x}CoO_{3-\delta}$	0.8	P_{02} = 0.01 atm, T: 725 to 950°C	0.045
	0.6		0.092
	0.3		0.092
$La_xSr_{1-x}FeO_{3-\delta}$	0.9	P_{O2}: 1 to 10^{-5} atm , T = 1000°C,	0.039
	0.75		0.092
	0.5		0.131

Chapter 2: Dual Phase Sorbents vs. Perovskite Sorbents

2.1. Introduction.

Slow desorption rate of oxygen during regeneration stage is a major challenge for use of perovskite sorbents in high temperature air separation. Use of CO_2 and generation of oxygen through carbonization of the Perovskite oxide has been shown to improve this effect (Lin, Y.S., *et al*. 2009). Another approach for improving the oxygen generation kinetics is addition of a second phase to the Perovskite sorbents. The second phase which has a spinel structure improves the oxygen recombination reaction in the desorption stage without affecting the recombination reaction in the absorption stage (Lu, F.H. and Dieckman, R. 1995). In this section, the oxygen sorptive/desorptive properties of two dual phase sorbents are compared with those of the Perovskite sorbents discussed in the previous sections.

2.2. Powder Synthesis

The citrate gel method of Marcilly (Marcilly, C. *et al.* 1970) was used to synthesize strontium and barium based oxides with $Sr_1Co_1Fe_1O_{3\pm\delta}$ (SCF) and $Ba_1Co_1Fe_1O_{3\pm\delta}$ (BCF) respectively. Nitrates of the cobalt, iron and strontium (for SCF) and barium (for BCF) were mixed in distilled water according to the intended stoichiometry. Citric acid (100% excess of the nitrate ions) was then

added to the mixture. The mixture was then vigorously stirred at 100-105°C for 4 hrs. The resultant viscous gel was then dried at 110°C before combustion was performed at 600°C for 5 hrs. The resultant powders were then sintered under stagnant air at 1000 and 1100°C for 12 hrs. 3 grams of the final oxides were produced each synthesis procedure.

2.3. Sorbent Characterization

Figures 2.1 to 2.4 show the scanning electron micrographs of the sintered powders. Figure 2.2 shows an acicular morphology which is the result of an intergrowth structure (Yin, Q. *et al* 2008). Compared to the perovskite structures (Figures 2.3 and 2.4) morphology is more porous which is considered an important additional advantage. The higher porosity is due to the fact that a more crystalline structure can be obtained at a lower sintering temperature whereas for perovskites LSCF1 ($La_{0.1}Sr_{0.9}Co_{0.1}Fe_{0.9}$) and LSCF2 ($La_{0.1}Sr_{0.9}Co_{0.5}Fe_{0.5}$) a higher sintering temperature is required due to presence of La_2O_3 in green powder. A Rigaku Geigerflex powder diffractometer with a cobalt Kα radiation with a scan rate of 0.6 °/min and a step size of 0.02° was used for crystal structure analysis of the samples.A dual phase structure is shown in figures 2.5 and 2.6 by matching the observed peaks with perovskite and spinel phases from the JCPDS standards PDF#46-0335 ($SrCo_{0.5}Fe_{0.5}O_3$) and PDF#22-1086 ($Co_2Fe_4O_x$)respectively.

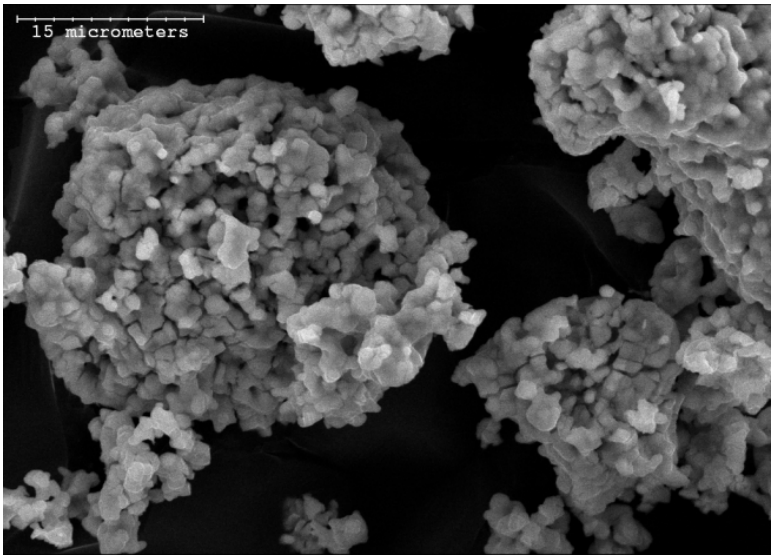

Figure 2.1. Secondary Electron SEM micrograph of the sorbent BCF

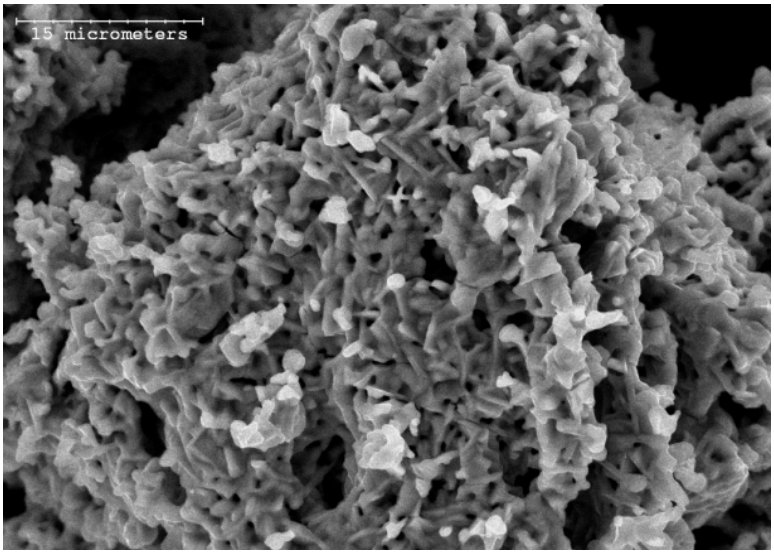

Figure 2.2. Secondary Electron SEM micrograph of the sorbent SCF

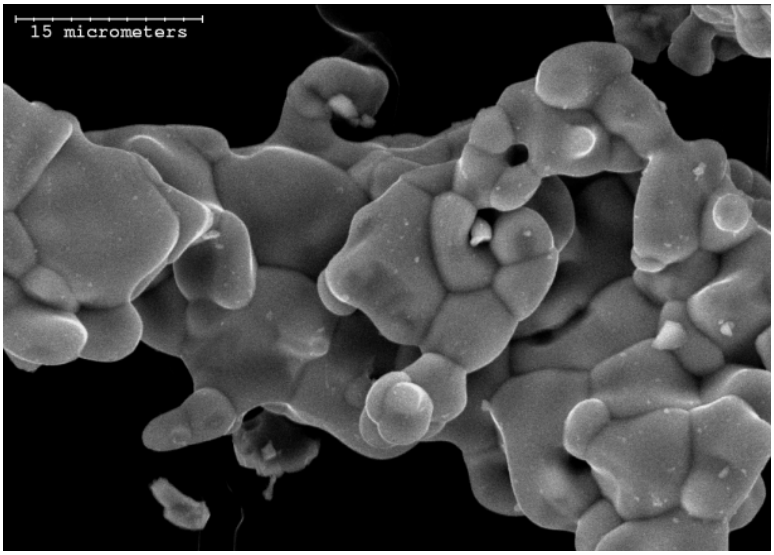

Figure 2.3. Secondary Electron SEM micrograph of the sorbent LSCF1

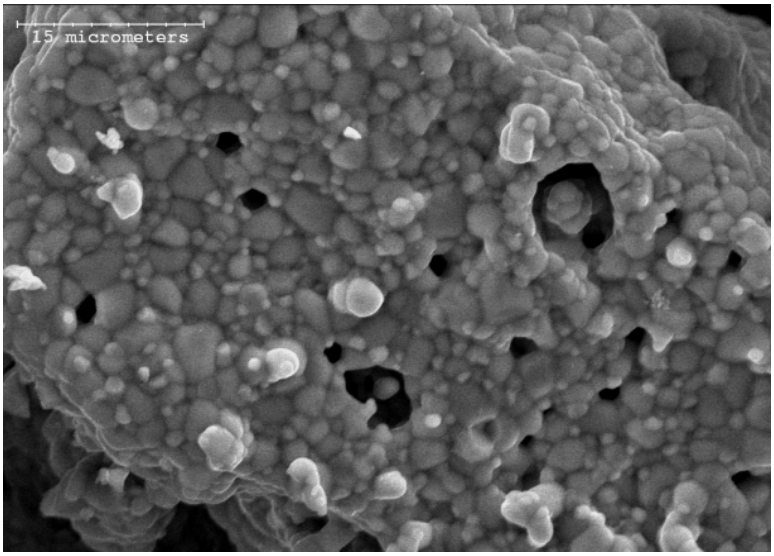

Figure 2.4. Secondary Electron SEM micrograph of the sorbent LSCF2

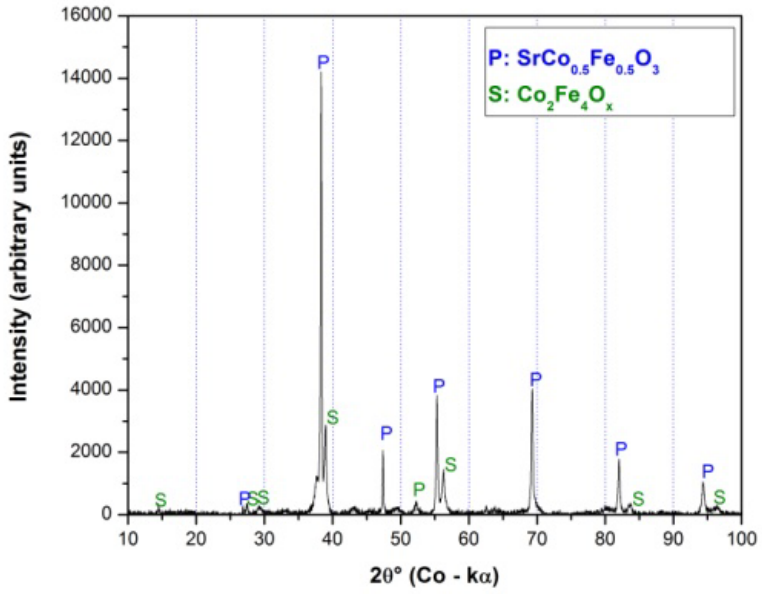

Figure 2.5. X-ray diffraction pattern of SCF111

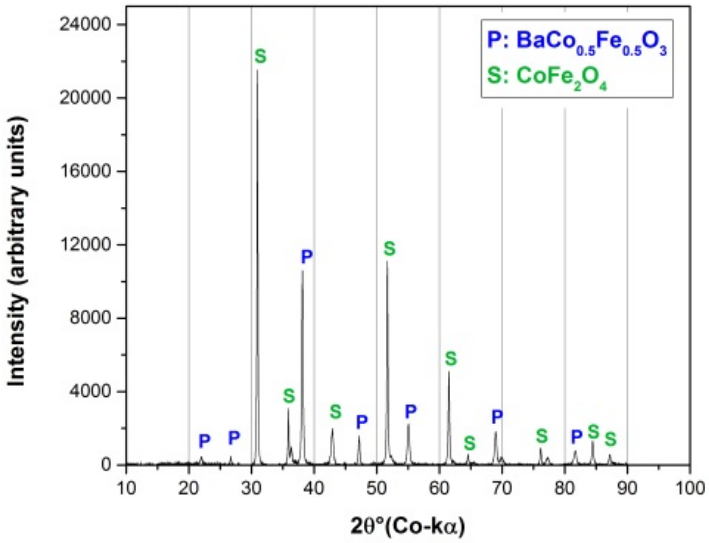

Figure 2.6. X-ray diffraction pattern of BCF111

2.4.Thermogravimetric studies

The synthesized sorbents were tested in a TA-SDT-Q600 TG-DSC for measuring their oxygen sorptive/desorptive properties. A 15-20 mg sample of the sorbents was heated to 1000°C at a rate of 10°C/min under 100 ml/min of Nitrogen (P_{O2} = 10^{-6} atm). It was then cooled the desired temperature at the same rate, held at that temperature for 10 minutes for weight to become stabilized before the gas is switched to air. Sample was then held under air for 30 minutes and then switched back to N_2 for desorption stage which usually took 60 minutes. To investigate the CO_2 uptake properties of the sorbents, the same amount of all samples were heated with the same heating rate under a 100 ml/min flow of CO_2.

2.5. Results and Discussion

The difference between weight of the sample under N_2 and air was used to calculate the sorption capacity according equation 2.1. Figure 2.7 compares the oxygen sorption capacity (OSC) of the dual phase samples (SCF and BCF) with that of the perovskite sorbents (LSCF1 and LSCF2). The comparison between desorption rate of the samples is shown in figure 2.8. The dual phase samples show both higher sorption capacity and desorption rate at nearly all temperatures. This can be explained using the difference between the defect structure of the samples. In perovskite samples, oxygen conduction (storage) occurs by movement of oxygen vacancies through the anion sublattice therefore oxygen storage requires higher activation energy. In dual phase samples, existence of the second

Spinel phase and consequently interstitial oxygen ions increases the flux of oxygen ions and therefore oxygen storage properties are greatly improved. This is more prominent in case of oxygen desorption rate because it is much more dependent on oxygen diffusion. In addition the Spinel oxides are thought to be good catalysts for oxygen recombination reaction which produces and additional advantage for use of these materials as oxygen sorbents (Lu, F.H. and Dieckman, R. 1995).

$$OSC = \frac{wt\ of\ sample\ at\ T^{\circ C}\ and\ air - \ wt\ of\ sample\ at\ 1000^{\circ C}\ and\ N_2}{wt\ of\ sample\ at\ 1000^{\circ C}\ and\ N_2} \qquad \text{Eqn. 2.1}$$

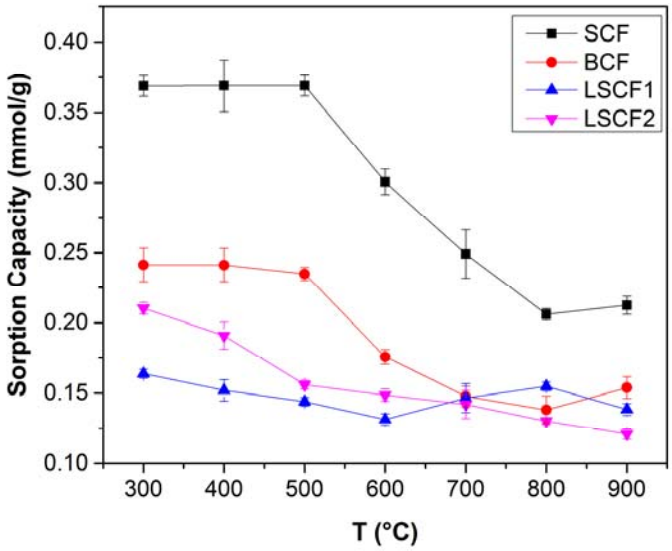

Figure 2.7. Comparison of sorption capacity of samples

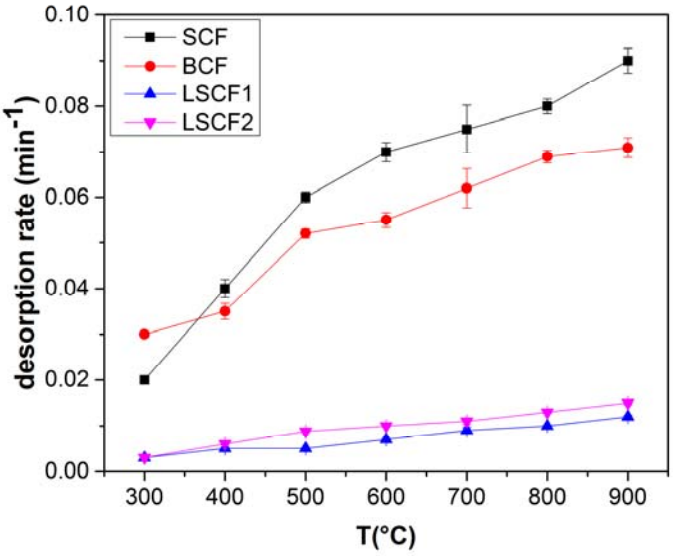

Figure 2.8. Comparison of oxygen desorption rate of samples

Figure 2.9 shows the CO_2 uptake curves of the sorbents. The perovskite sorbents absorb large amounts of CO_2 at nearly all temperatures. The amount of CO_2 absorbed is much lower for the Spinel sorbents. In the intermediate temperature range there is virtually no absorption which is crucially important for the use of sorbents in oxy-fuel power generation. CO_2 absorption occurs through carbonization reaction of the sorbents which can degrade them over long period of operation.

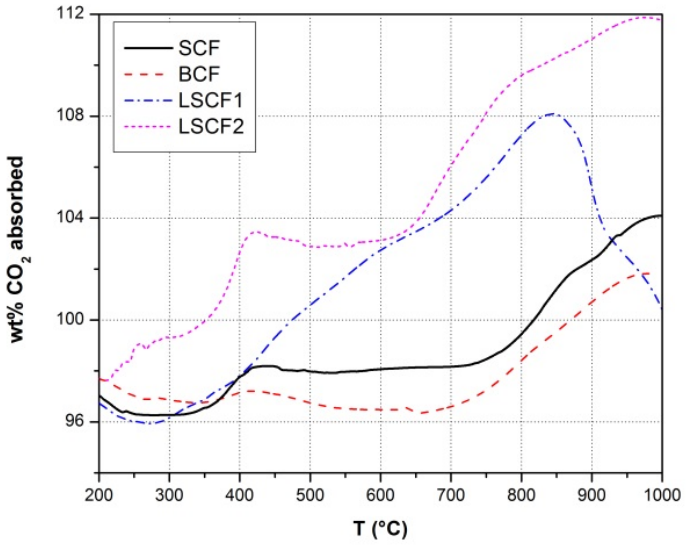

Figure 2. 9. CO_2 uptake curves of the sorbents

2.6. Conclusion

Dual phase sorbents show an improved a higher oxygen sorption capacity and desorption rate compared to their perovskite counterparts. The improved properties can be associated with the existence of the Spinel phase which contributes to the kinetics and thermodynamics of the reaction through the existence of oxygen interstitial spices. Negligible CO_2 uptake is an additional advantage of the dual phase sorbents, which is extremely important in use of these materials as oxygen sorbents in oxy-fuel power generation.

Chapter 3: CuO as an Alternative to Perovskite Sorbents: Effect of Synthesis Method on Oxygen Sorptive/Desorptive Properties

3.1. Introduction

As discussed in chapters 1 and 2, in high temperature air separation using perovskite and dual phase sorbents, the oxygen generation step involves reaction of CO_2 with the perovskite oxide and formation of carbonates of alkaline earth metals like strontium, barium or calcium usually present in these materials. In the oxygen storage step, carbonates decompose and CO_2 diluted with N_2 will be released into the atmosphere (Figure 3.1). During oxygen desorption some CO_2 is used in the formation of carbonates whereas during oxygen sorption, carbonates decompose to get some CO_2 released as shown in Fig below. This leads to failure in complete capture of CO_2 from the flue gas (Li, Z., *et al.*, 2008).

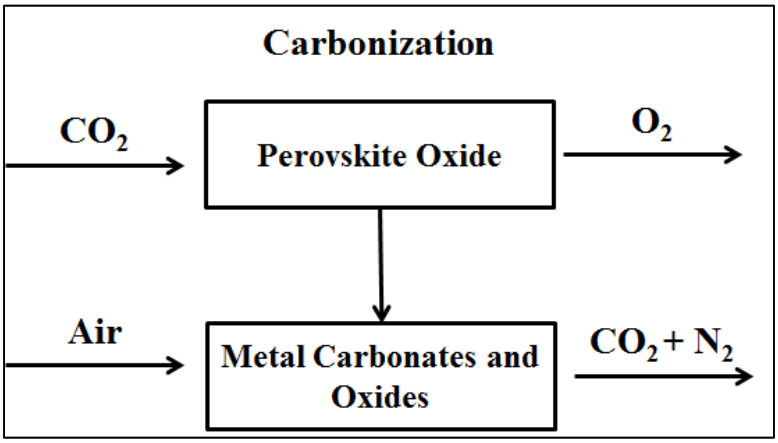

Figure 3. 1. Effect of oxygen sorbent carbonization on CO_2 capture (reproduced using the idea from (Li, Z., *et al.*, 2008).

Presence of SO_x and NO_x in the recycled flue gas used as the purge gas has also been observed to adversely affect the reactivity of perovskite oxides causing a decrease in oxygen release kinetics and storage capacity (Watterud, G., 2005). An oxygen carrier with inertness to CO_2 and acid gases, high oxygen sorption capacity and high sorption/desorption kinetics is critical for the CAR and oxyfuel process. Transition metal oxides are considered as an appropriate material for use as oxygen sorbents for this application (Andez, J., *et al.*, 2004). Figure 3.2 compares the theoretical oxygen sorption capacity of these oxides with perovskite and dual phase sorbents. Zhang *et al*. have used CO_3O_4/CoO equilibrium for oxygen storage and in the CAR process (Zhang, T., *et al.*, 2009).

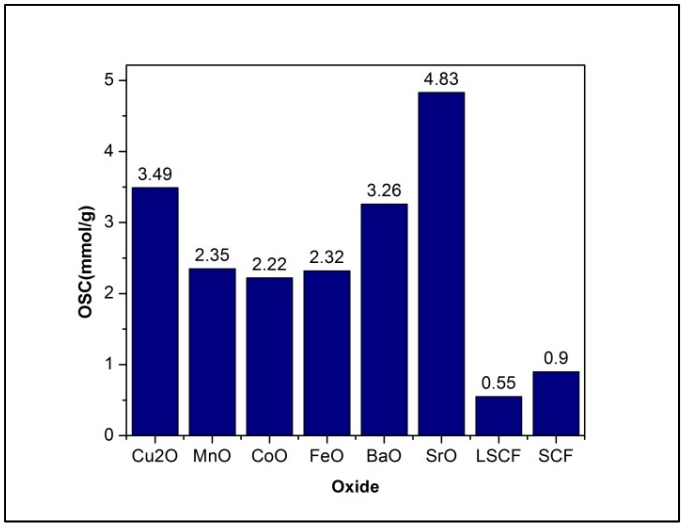

Figure 3.2. Theoretical oxygen sorption capacity of candidate oxides for high temperature air separation

Copper oxide has also been extensively studied as oxygen carrier for chemical looping processes (Garcı´a-Labiano, F., *et al.*, 2004). Due to its high oxygen sorption capacity, inertness to carbon dioxide and relatively high oxygen sorption/desorption kinetics; this compound can be a suitable candidate for the CAR process (Mattison, T., *et al.*, 2009). In addition, use of copper-based oxygen carriers has fewer environmental implications and lower cost compared to oxides of cobalt and nickel (Andez, J., *et al.*, 2004). The CuO/Cu_2O equilibrium involves electronic and ionic conduction in CuO and Cu_2O layers that form during oxidation and reduction respectively (Li, J. and Wang, Q., 1989). Oxygen molecule dissociation and oxygen ion recombination are also rate controlling steps during the reduction and oxidation reactions (Grzeski, Z. and Migdalska, M., 2009). The surface chemistry and crystallinity can also contribute greatly to the dynamics of oxygen absorption and desorption (Li, J. and Wang, Q. 1989). One efficient way to control these properties is through use of different ceramic synthesis methods. Solid state methods use metallic copper as the precursor and copper oxide is synthesized by high temperature oxidation of metal powders or plates. The oxides produced this way tend to be more compact with high heterogeneity in composition and crystal structure (Raynaud, G. M., *et al.* 1984). In case of copper, a combination of CuO, Cu_2O, Cu_3O_4 and metallic copper exist in the oxidation product that can affect the properties of the product as an oxygen carrier (Cuang, S.Y. *et al.,* 2008). Calcination and sintering at higher temperatures (<1053°C under air) reduce the concentration of compounds other than CuO to much lower amounts but a single phase homogeneous oxide product is hard to

obtain (Tannyan, N.J., *et al.*, 2002). Precipitation and sol-gel methods use water soluble salts of copper (usually nitrate) as precursor and copper oxide is produced through calcination of copper hydroxide or hydroxy carbonates (Bluthardt, C., 2008). These methods have the advantage of producing more homogeneous composition with finer crystallite size (Filipic, G., 2012). The presence of residual carbonates in calcined samples has been shown to produce copper suboxide species which increase the chemical activity of the oxide (Baltes, C. *et al.* 2008). The purpose of this chapter was to study the effect of synthesis route on the oxygen sorptive/desorptive properties of copper oxide as a high temperature oxygen carrier. Four common sol-gel methods are compared with solid state oxidation product from two precursors of different purity. The morphology, crystal structure and surface chemistry were the properties compared as well as the oxygen absorption kinetics from air and oxygen desorption into CO_2 as is the purge medium in Oxyfuel (Scheffknecht, G., *et al.*, 2011) and chemical looping with oxygen uncoupling (Xu, L., *et al.*, 2013).

3.2. Experimental Procedure

3.2.1. Sorbent Synthesis

Six sorbents were prepared using the following synthesis methods. All the chemicals and reagents used were of high purity.

3.2.1.1. Citrate gel

(Marcilly, C., et al., 1970)

A 1:2 molar ratio aqueous solution of copper nitrate hexahydrate (Sigma Aldrich 99.9999%) and citric acid (Sigma Aldrich 99.95%) was prepared. The solution was stirred and heated on a hot plate in the temperature range of 95-100°C to prepare a blue-colored transparent gel. The gel was then dried at 105°C for 24 hours in an oven. The dried gel (Figure 3.3) was ground by mortar and pestle and calcined at 650°C for 8 hours on alumina panels under an air flow of 100 ml/min. The calcined powder was then ground by mortar and pestle and sintered at 1000°C for 5 hours in zirconia crucibles under an air flow of 20 ml/min.

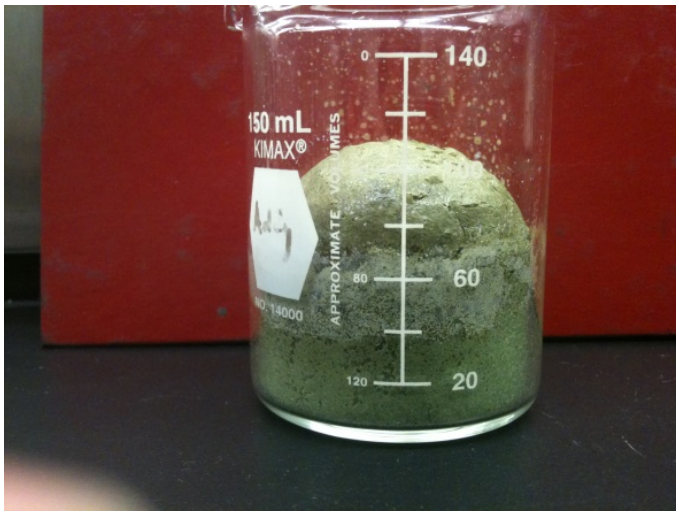

Figure 3.3. Dried gel of the copper nitrate/citric acid mixture

3.2.1.2. Pechini

(Pechini, M.P., 1967)

A 1:1 molar ratio aqueous solution of copper nitrate hexahydrate (Sigma Aldrich 99.9999%) and citric acid (Sigma Aldrich 99.95%) was prepared. The mixture was magnetically stirred until a clear solution was obtained. Ethylene glycol was added to the solution at a molar ratio of 1 to the amount of citric acid present. The solution was then heated at 95°C to evaporate the excess water present and prepare a blue glassy resin. The resin was then heated in an oven at 105°C for a period of 24 hours. The dried resin (Figure 3.4) was then ground by mortar and pestle and calcined at 650°C for 8 hours on alumina panels under an air flow of 100 ml/min. The calcined powder was attrition milled once more and sintered at 1000°C for 5 hours in zirconia crucibles under an air flow of 20 ml/min.

Figure 3.4. Top view of dried gel copper oxide precursor form Pechini method

3.2.1.4. Alanine-assisted combustion

(Raja, M.W., et al., 2007)

Copper nitrate hexahydrate (Sigma Aldrich 99.9999%) and α-alanine (Sigma Aldrich 99.95%) were used to prepare the combustion mixture. Three solutions with oxidant (copper nitrate) to fuel (alanine) molar ratios of 0.5, 1 and 2.5 were prepared. The mixtures were heated and magnetically stirred to evaporate the water followed by auto-ignition and combustion producing a fine ash. In mixtures with oxidant to fuel ratios of 0.5 and 1, the ignition and combustion was too intense and very small amount of combusted powder remained in the beakers. These powders were collected for characterization. The combustion product of mixture with oxidant to fuel ratio of 3.5 (Figure 3.5) was ground by mortar and pestle and calcined at 650°C for 8 hours on alumina panels under an air flow of 100 ml/min. The calcined product was attrition milled once more once more using mortar and pestle for 5 minutes and sintered at 1000°C for 5 hours in zirconia crucibles under an air flow of 20 ml/min.

Figure 3.5. Plan view of the combustion product of oxidant to fuel ratio of 2.5 in Alanine assisted combustion method

3.2.1.4. Precipitation

(Du, G.H. and Van Tendeloo, G., 2004)

1 g of copper nitrate hexahydrate was first dissolved in 100 ml distilled water. Then 30 ml of $NH_3.H_2O$ (0.15M) solution was added to the nitrate solution under constant stirring. A blue precipitate of $Cu(OH)_2$ was produced when NaOH (1 M) solution was added dropwise to the above solution to adjust the pH value to 9–10. The blue precipitate was then filtered and washed several times to obtain a solid product. The precipitate was then dried in an oven at 105°C for a period of 24 hours. The dried precipitate was then ground by mortar and pestle and calcined at 650°C for 8 hours on alumina panels under an air flow of 100 ml/min. The calcined powder was attrition milled once more and sintered at 1000°C for 5 hours in zirconia crucibles under an air flow of 20 ml/min.

3.2.1.5. High Temperature Oxidation

(Wood, G. C. and Stott, F. H., 1980)

High purity (99.9999%) copper plate and Canadian pennies (98%Cu, 1.75%Sn, 0.25% Zn) were used as precursor for synthesis using high temperature oxidation. The samples were first washed in a 0.15M solution of HCL, after rinsing and drying, they were annealed at 650°C for 24 hours under an air flow of 100 ml/min. The samples were quenched to 25°C to peel off the scales. The oxide

scales were ground by mortar and pestle and sintered at 1000°C for 5 hours in zirconia crucibles under an air flow of 20 ml/min.

3.2.2. Morphology, Crystal Structure and Surface Chemistry

The morphology of samples was investigated using scanning electron microscopy (Hitachi S-2700) and the crystal structure was determined by X-ray diffraction (Rigaku rotating anode TTRAX III, Auburn Hills, MI) with Cu-Kα as the radiation. A Kratos AXIS 165 spectrometer with Al Kα radiation and sample charge neutralization capability was used for X-ray photoelectron spectrometry (XPS) analysis of the samples. An area of approximately 1 mm in diameter was selected for the analysis using a selected area aperture.

3.2.3. Oxygen Sorption/desorption Investigation by Thermogravimetry

A TA instrument SDT Q600 TGA instrument was used for thermogravimetric analysis. The instrument consisted of a stainless steel tube placed in a horizontal furnace that can be operated to temperatures up to 1200°C with a computer continuously recording the data. The instrument had two separate reactant gas inlets that can be operated automatically. Air and CO_2 were used as reactive gases for sorption and desorption stages. Small amounts of the sample (5-10 mg) were

placed in alumina pans and heated with a heating rate of 50°C/min to 750-900°C under 100 ml/min of air and then gas is switched to CO_2 to study desorption. After complete desorption, the gas was switched to air to study absorption. As recommended by (Ollero, P., *et al.* 2002) to reduce the diffusion effects between the sample and bulk gas phase , sample pans were ground from the original 4 mm to about 0.5 mm deep.

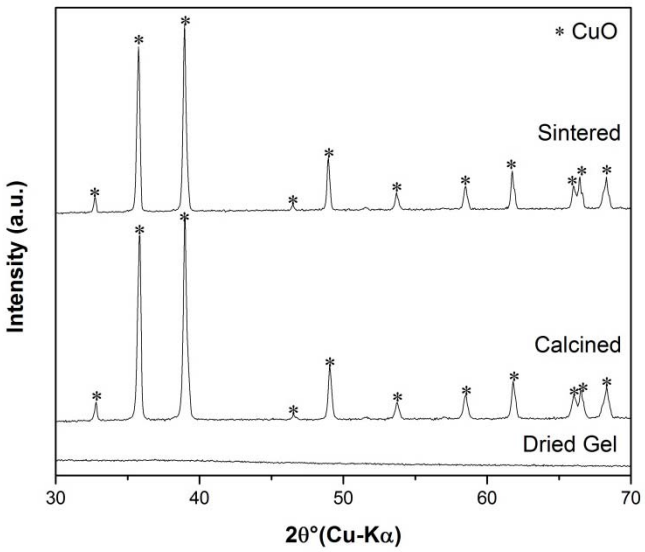

Figure 3.6. Crystal Structure Evolution in Citrate Gel Synthesis Route

3.3. Results and Discussion

3.3.1. Crystal structure Analysis of the Sorbents

Figure 3.6 shows the XRD pattern during different synthesis stages of the sample produced through citrate gel method. The dried gel is, as expected, a completely

amorphous structure. The single phase CuO structure is observed in the calcined sample. The sintered sample's peaks have a relative higher intensity and finer width compared to the calcined sample which is due to growth of the crystallites and increase in density.

Figure 3.7 shows the same pattern for the sample synthesized by the Pechini method. In this case broad peaks of low intensity are observed in the dried gel (resin) which can be due to crystallization of citric resin (PDF4: 01-077-0047) as already reported by (Marquez, A. G., *et al.*, 2011). The calcined and sintered sample's patterns behave similarly to those of the sample synthesized by the citrate gel method.

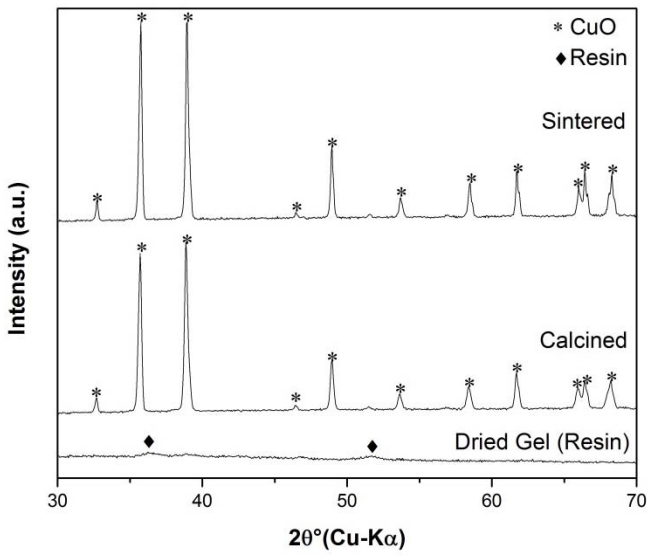

Figure 3.7. Crystal Structure Evolution in the Pechini Route

Figure 3.8 shows the effect of oxidant to fuel ratio (O/F) on the structure of the combusted gel in the Alanine assisted combustion method. The sample with O/F = 0.5 is single phase cuprite and the sample with O/F = 1 is two phase cuprite and metallic copper. The presence of metallic copper can be explained by reduction of the cupric oxide by the carbonaceous materials available and increase in the temperature. The sample with of O/F = 2.5 is single phase cupric. The single phase cupric oxide sample has a relatively broadened peak but the half width is below the limit (0.05-0.1° in the 2θ range 30-50°) allowed for measurement of crystallite size.

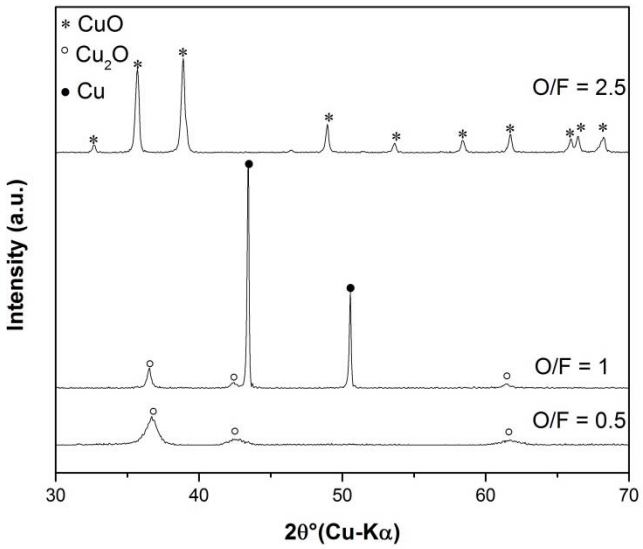

Figure 3.8. Effect of oxidant to fuel ratio on the structure of combusted gel in Alanine assisted combustion method

Figure 3.9 compares the crystal structure for the as-prepared, calcined and sintered samples prepared by the alanine assisted combustion method with an

O/F=2.5. The structure remains the same (CuO) through the sintering process with minor changes in peak widths and intensities due to sintering and crystal growth.

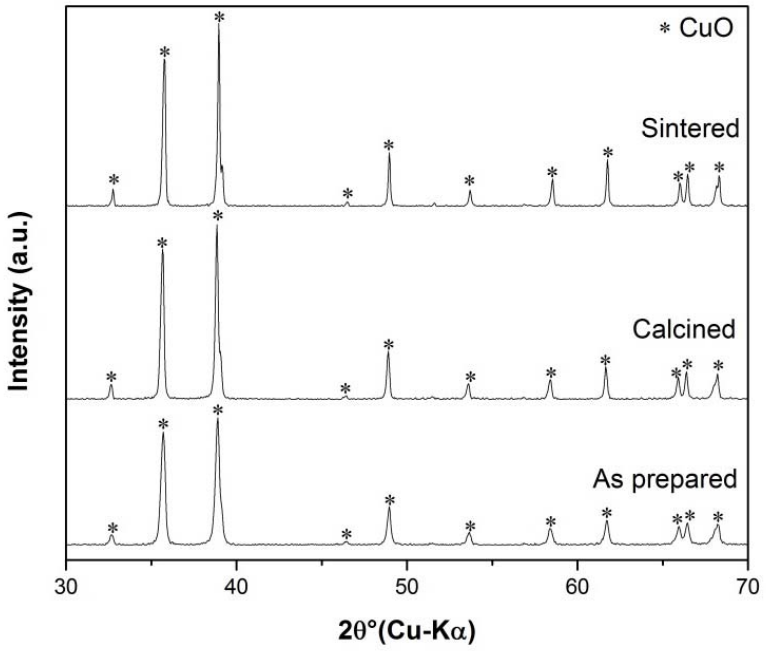

Figure 3.9. Crystal Structure Evolution in Alanine Assisted Combustion method using Oxidant to Fuel ratio of 2.5

Figure 3.10 shows the evolution of crystal structure during synthesis by the precipitation method. The as-prepared sample is one phase copper hydroxide with broad peaks showing its fine crystallite size. However, due to high number of overlapping lines, the full refinement of the pattern to calculate crystallite size was not possible. Individual refinement of certain peaks with pseudo-Voight function and crystallite size calculation with Scherrer equation (Klug, H.P., 1954)

shows a value in the 50-100 nm range. Calcination converts the structure to cupric oxide and the sintering increases the crystallite size as evidenced by decrease in the peaks' width and increase in their intensity.

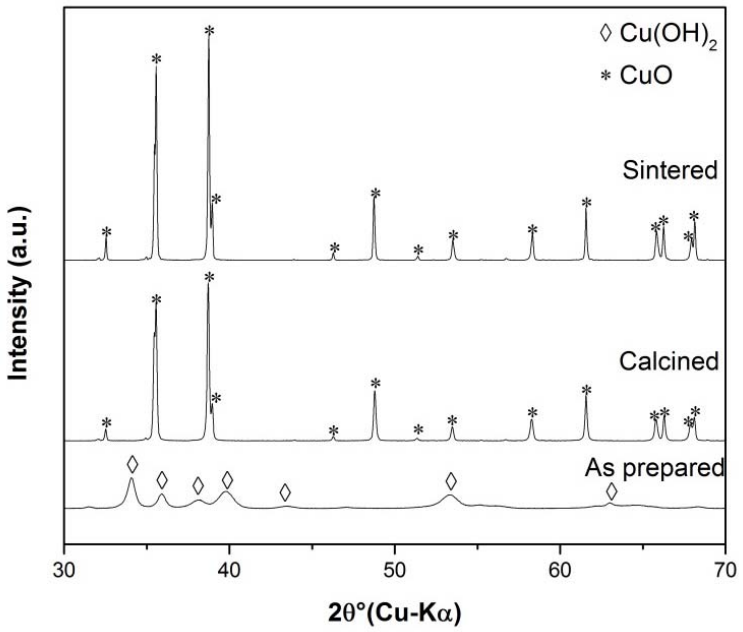

Figure 3.10. Evolution of crystal structure in the precipitation method.

Figures 3.11 and 3.12 show the crystal structure evolution in the high temperature oxidation synthesis of samples using copper plate and penny coin respectively. Both samples have the crystal structure of pure copper in the as-received form. The calcined samples are a mixture of cupric and cuprous oxides. The relative intensity of cuprous oxide peaks are higher in the penny sample which can be due to promoting effect of impurities, which are higher in concentration in this sample, in the formation of this type of oxide. The same trend is observed in the

sintered samples. In both samples a small amount of cuprous oxide remains after sintering. This can have important effects on the oxygen sorption capacity and oxygen sorption and desorption kinetics.

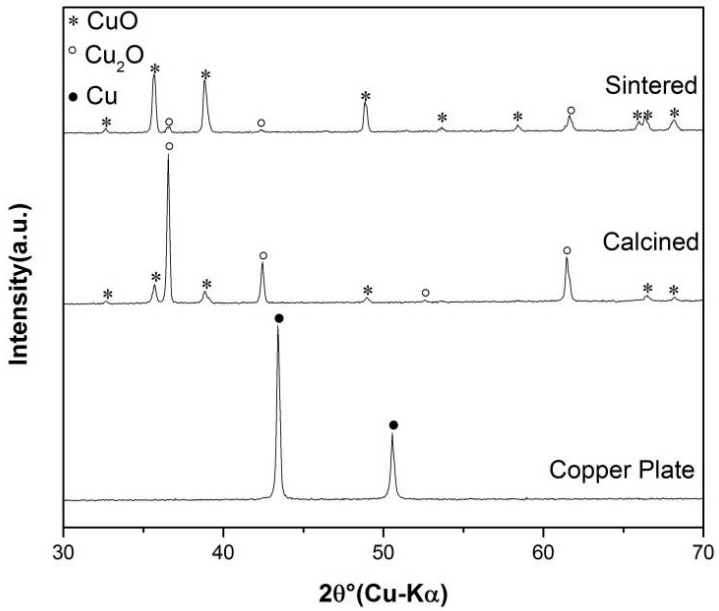

Figure 3.11. Evolution of crystal structure in the high temperature oxidation method using copper plate as precursor

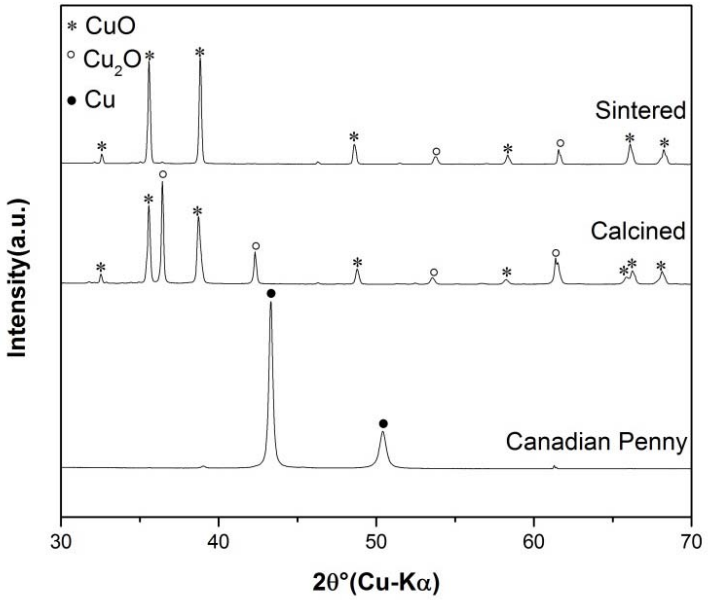

Figure 3. 12. Evolution of crystal structure in the high temperature oxidation method using Canadian penny as precursor

3.3.2. XPS Analysis of the Sorbents

Figure 3.13 shows the main and shake up satellite $Cu2P_{3/2}$ and $Cu2P_{1/2}$ of the synthesized samples. The satellite peaks are the sign of cupric oxide presence but both cuprous (Cu_2O) and cupric oxides (CuO) and metallic copper contribute to the $Cu2P_{3/2}$ peak (Poulston, S., *et al*., 1996). The binding energy for each of these compounds is listed in Table 3.1. Given the highly oxidizing conditions under which the samples were synthesized and as observed in the x-ray diffraction patterns discussed in the previous section the existence of metallic copper is highly improbable. Deconvolution of the $Cu2P_{3/2}$ peak and the relative area of

satellite peak to this peak can be used to quantify the concentration of the two types of oxide on the surface.

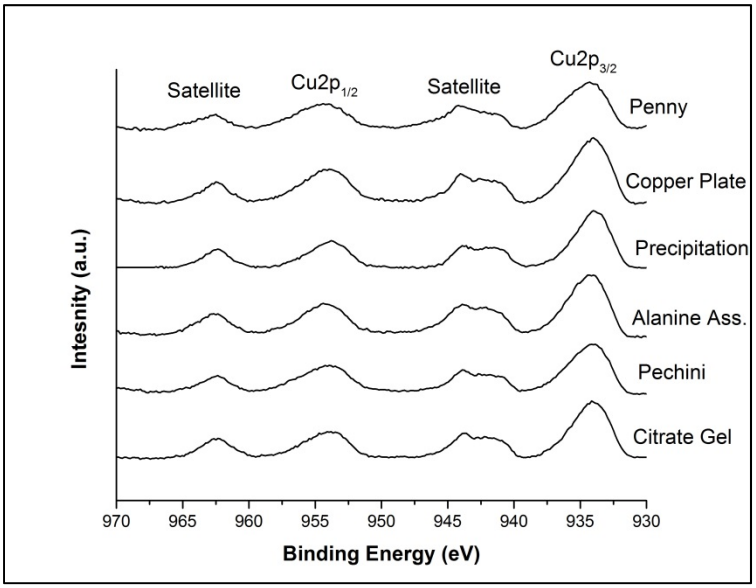

Figure 3.13. The XPS $Cu2P_{3/2}$ and $Cu2P_{1/2}$ spectra of the samples using different methods

Table 3.1. Binding energies of $Cu2P_{3/2}$ for metallic Cu, Cu_2O, and CuO

(Poulston, S. *et al.* 1996)

	$Cu2P_{3/2}$ Binding Energy (eV)
Metallic Cu	932.6
Cu_2O	932.4
CuO	933.6

Deconvolution of the $2P_{3/2}$ was used to calculate the relative content of Cu_2O and CuO in the surface. The CASAXPS® software was used for this purpose. A Gauss-Lorentzian distribution function was used for representing each of the peaks. Figure 3.14 shows the deconvoluted peaks for each of the samples. The results of deconvolution are listed in Table 3.2.

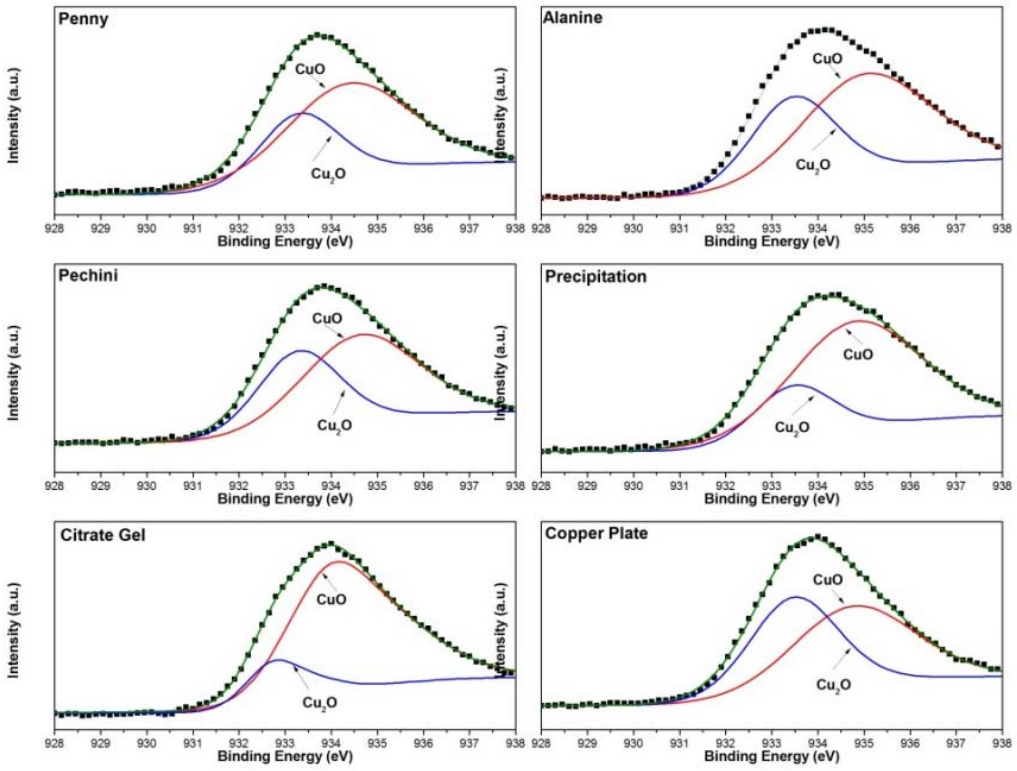

Figure 3.14. Deconvolution of $Cu2P_{3/2}$ of samples synthesized using different methods

The O1S regions of the XPS spectra are shown in Figure 3.15. The main peak was attributed to lattice oxygen and the shoulder appearing on the high energy side of the peak was due to presence of hydroxyls on the surface of the samples (Tobin, J.P., *et al*, 1983). Contribution to the area under the peak from the two types of

Cu-O bonds is considered when the area under the O1S peak is used for calculating the surface copper to oxygen ratio. These ratios are listed in Table 3.3. In all samples, the O/S ratio shows a deviation from the stoichiometric value of 1 which is in agreement with the values reported by (Poulston, S., *et al.*, 1996).

Table 3. 2. The results of deconvolution of XPS Cu $2P_{3/2}$ peak: The binding energy and FWHM of peaks.

	Binding Energy of $Cu2P_{3/2}$ (eV)		FWHM of $Cu2P_{3/2}$ (eV)		$\%Cu_2O$
Synthesis route	Cu_2O	CuO	Cu_2O	CuO	
Citrate Gel	932.7	934.7	1.6	2.9	31.92
Precipitation	933.5	934.7	1.9	3.1	41.69
Alanine Assisted	933.5	935.2	1.6	3.5	70.00
Pechini	933.2	934.6	2.0	3.5	77.24
Copper Plate	933.5	934.7	2.3	2.8	86.02
Penny	933.3	934.5	1.9	2.4	65.00

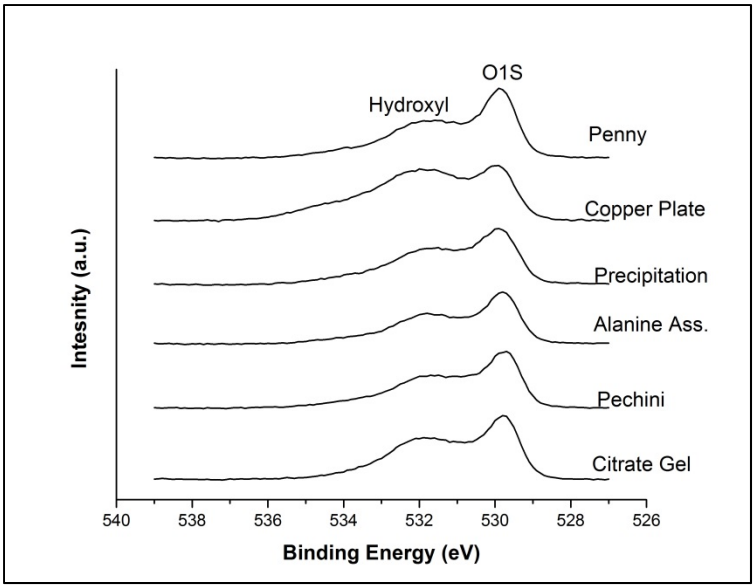

Figure 3.15. The XPS O1S spectra of the samples using different methods

Table 3. 3. The O/Cu Oxygen ratio calculated using the area of O1S and $Cu2P_{1/2}$ peaks

Synthesis Route	O/Cu
Citrate Gel	0.8404
Precipitation	0.79155
Alanine Assisted	0.6500
Pechini	0.6138
Copper Plate	0.5699
Penny	0.675

3.3.3. SEM Morphology of the Sorbents

Figure 3.16 shows the evolution of microstructure of the samples synthesized using the citrate gel method. The morphology was highly dense after the gel was dried. Calcination da relatively porous structure which tended to become dense after sintering. However, a very small of amount of porosity was maintained even after sintering.

Figure 3.17 shows the evolution of microstructure of the samples synthesized using Pechini method. The same trend is also observed in this type of sample. The calcined sample however was less porous which can be correlated to the type of gel and its crystallization as it was mentioned in the synthesis and x-ray diffraction sections. (3.3.1)

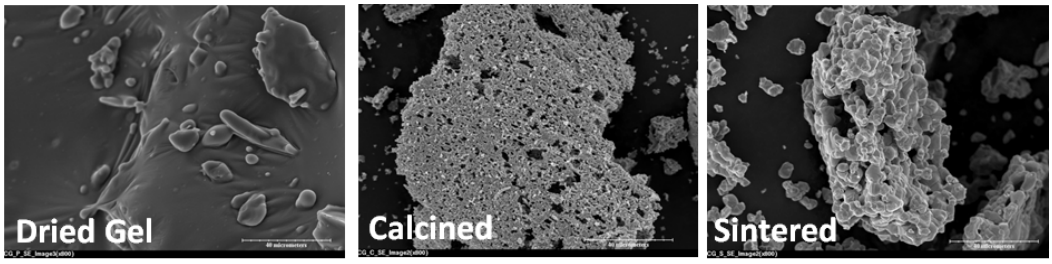

Figure 3.16. Evolution of morphology in the citrate gel method

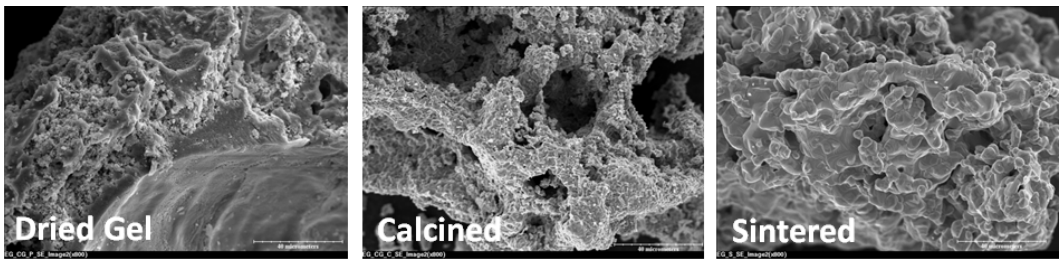

Figure 3.17. Evolution of morphology in the Pechini method

Figure 3.18 shows the evolution of microstructure of the samples synthesized using the alanine assisted combustion method with an oxidant to fuel ratio of 2.5. The combusted gel had a porous structure which was maintained during calcination. The sintered sample was more porous compared to the previous sintered samples.

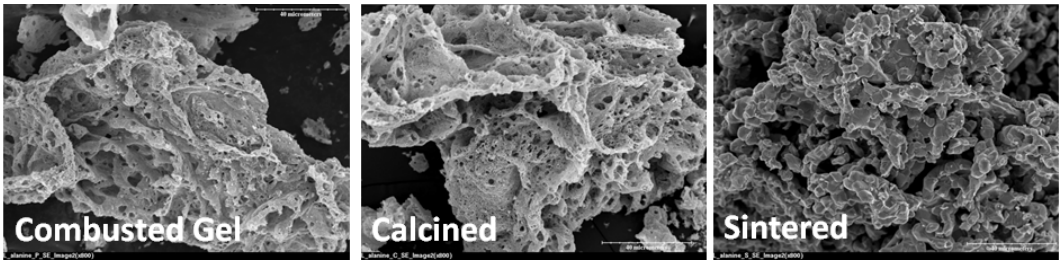

Figure 3. 18. Evolution of morphology in the Alanine assisted combustion method

Figure 3.19 shows the evolution of microstructure of the samples synthesized using the precipitation method. The morphology does not shown any sign of macroporosity as was observed in the previous samples. The inset figure in the dried precipitate micrograph shows fine crystallites which is in agreement with the broadening observed in the X-ray diffraction pattern shown in Figure 3.10. The morphology remained unchanged during the synthesis process which means that the annealing of the sample led to growth of the fine crystallites without significantly changing the porosity structure of the sample.

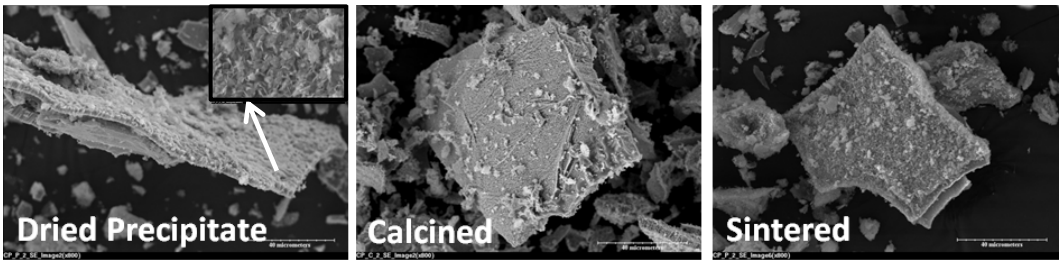

Figure 3. 19.Evolution of morphology in the precipitation method

Figure 3.20 shows the evolution of microstructure of the samples synthesized using the high temperature oxidation with high purity copper plate as the precursor. The metal surface washed by HCl had a rough structure. The roughness is important in accelerating oxidation during the calcination stage as seen in the mid figure which shows the acicular structure of the oxides formed on the surface. The sintered has a dense morphology with large grains formed as a result of the sintering process. The needle shaped grains have become more spherical in the final sample.

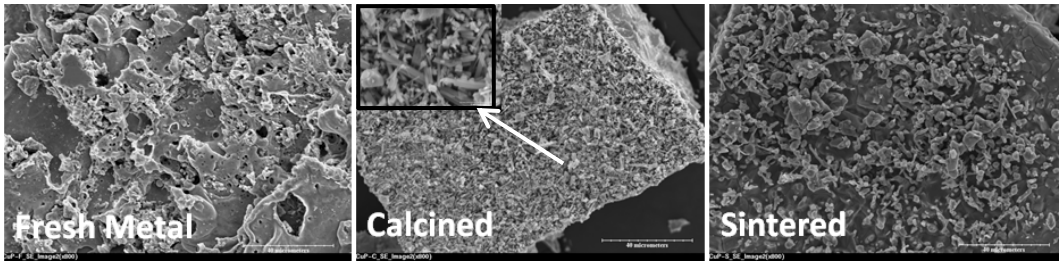

Figure 3.20. Evolution of morphology in the high temperature oxidation method using copper plate as precursor

Figure 3.21 shows the evolution of microstructure of the samples synthesized using the high temperature oxidation of pennies. The precursor in this case, the penny, was less porous although the scratches due to wear and the coining process were observed and the acid wash caused scale formation in these places. The calcined sample has a similar morphology to that of the copper plate with acicular shapes in the grains. The sintered sample was denser compared to the copper plate which can be due to presence of oxides of tin and zinc (Dubey, N. M. *et al.*).

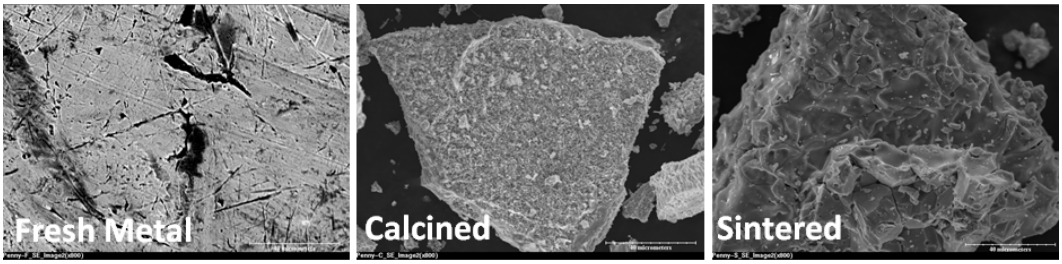

Figure 3.21. Evolution of morphology in the high temperature oxidation method using penny as precursor

3.3.3.1. Thermal Faceting in the Sorbents

Figure 3.22 compares the microstructure of sintered sorbents at the highest magnification possible by the scanning electron microscope available. One feature common in all of the samples is the polygonal shape of the grains with the size varying from one sample to the other. In all samples, except the one synthesized by the Pechini method, step like features are also observed. These features known as facets (Heffelfinger, J.R., *et al.*, 1995) have different directions and their extent is also different in various samples. This increase in the surface area occurring at

high temperature can have important effects on surface chemistry of the sorbents and therefore the oxygen sorption and desorption kinetics from these samples (Reinecke, N. and Taglauer, 2000).

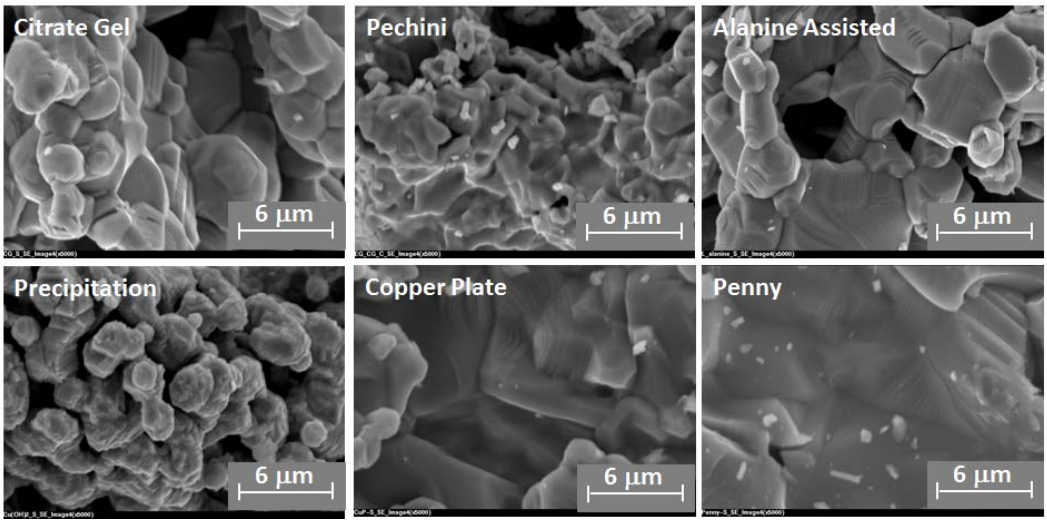

Figure 3. 22. Thermal faceting in sintered samples.

2.3.4. Kinetics of Oxygen Sorption/Desorption

The results of TGA experiments discussed in section 2.1 were used to calculate the kinetics of oxygen sorption and desorption. The change in sample mass was used to calculate conversion according to the following equations:

$$X_{des} = \frac{w_0 - w_t}{w_0 - w_f}$$ (Eqn. 3.1 (Brown, M. E. and Gallagher P. K., 2008))

$$X_{abs} = \frac{w_t - w_0}{w_f - w_0}$$ (Eqn. 3.2 (Brown, M. E. and Gallagher P. K., 2008))

where w_0, w_t and w_f are initial weight, weight at time t and final weight of the sample and X_{des} and X_{abs} the desorption and absorption conversion. The differential rate relation shown by the following equation was used to calculate the rate constant (k) from the slope of isoconversional plots of $\frac{\ln\left(\frac{dX}{dt}\right)}{f(X)} vs. \frac{1}{T}$.

$\frac{dX}{dt} = k_0 exp\left(-\frac{Q}{RT}\right) f(X)$ (Eqn. 3.3 (Brown, M. E. and Gallagher P. K. 2008)),

where *f(x)* represents the dependence of reaction rate on its progress. By integrating Eqn. 3.3, the following Eqn. is obtained:

$g(X) = \int_0^X \frac{dX}{f(X)} = kexp\left(-\frac{Q}{RT}\right) t$ (Eqn. 3.4 (Brown, M. E. and Gallagher, P. K. 2008)),

where *g(X)* is the integral form of the reaction model. Table 3.4 lists a number of common reaction models used in the kinetics of solid state reactions. To find the appropriate model, the reduced time plot method suggested by (Brown, M. E. and Gallagher, P. K., 2008) was used. Figures 3.23 to 3.26 show the reduced time plot curves for oxygen desorption and absorption using different samples. The symbols used to label the curves in these figures are according to those listed in Table 3.4. The experimental reduced time plots obtained at various operating temperatures should be identical provided the kinetic triplet is independent of temperature. It can be seen from Figures 3.23 and 3.24 that the reduced time plots for absorption and desorption do not correspond to any of the models and a great disparity exists among them. These changes can be due to variation of at least one

of kinetic components with temperature. The dependence on temperature requires use of empirical kinetic models for comparison of the sorption/desorption kinetics of the samples.

Table 3.4. Expression for *f(X)* and *g(X)* functions for some of the common mechanisms

(Brown, M. E. and Gallagher, P. K. 2008)

No.	Symbol	Reaction Model	*f(X)*	*g(X)*
1	P1	Power Law	$4X^{3/4}$	$X^{1/4}$
2	P2	Power Law	$3X^{2/3}$	$X^{1/3}$
3	P3	Power Law	$2X^{1/2}$	$X^{1/2}$
4	P4	Power Law	$2X^{1/2}$	$X^{3/2}$
5	R1	Zero Order	1	X
6	R2	Contracting area	$2(1-X)^{1/2}$	$1-(1-X)^{1/2}$
7	R3	Contracting volume	$3(1-X)^{2/3}$	$1-(1-X)^{1/3}$
8	F1	First order	$(1-X)$	$-\ln(1-X)$
9	A2	Johnson-Mehl-Avrami (*m=2*)	$2(1-X)[-\ln(1-X)]^{1/2}$	$[-\ln(1-X)]^{1/2}$
10	A3	Johnson-Mehl-Avrami (*m=3*)	$3(1-X)[-\ln(1-X)]^{2/3}$	$[-\ln(1-X)]^{1/3}$
11	A4	Johnson-Mehl-Avrami (*m=4*)	$4(1-X)[-\ln(1-X)]^{3/4}$	$[-\ln(1-X)]^{1/4}$
12	D1	One-dimensional diffusion	1/2X	X^2
13	D2	Two-dimensional diffusion	$1/[-\ln(1-X)]$	$(1-X)\ln(1-X)+X$
14	D3	Three dimensional diffusion	$3/2[(1-X)^{-1/3}-1$	$(1-2X/3)-(1-X)^{2/3}$

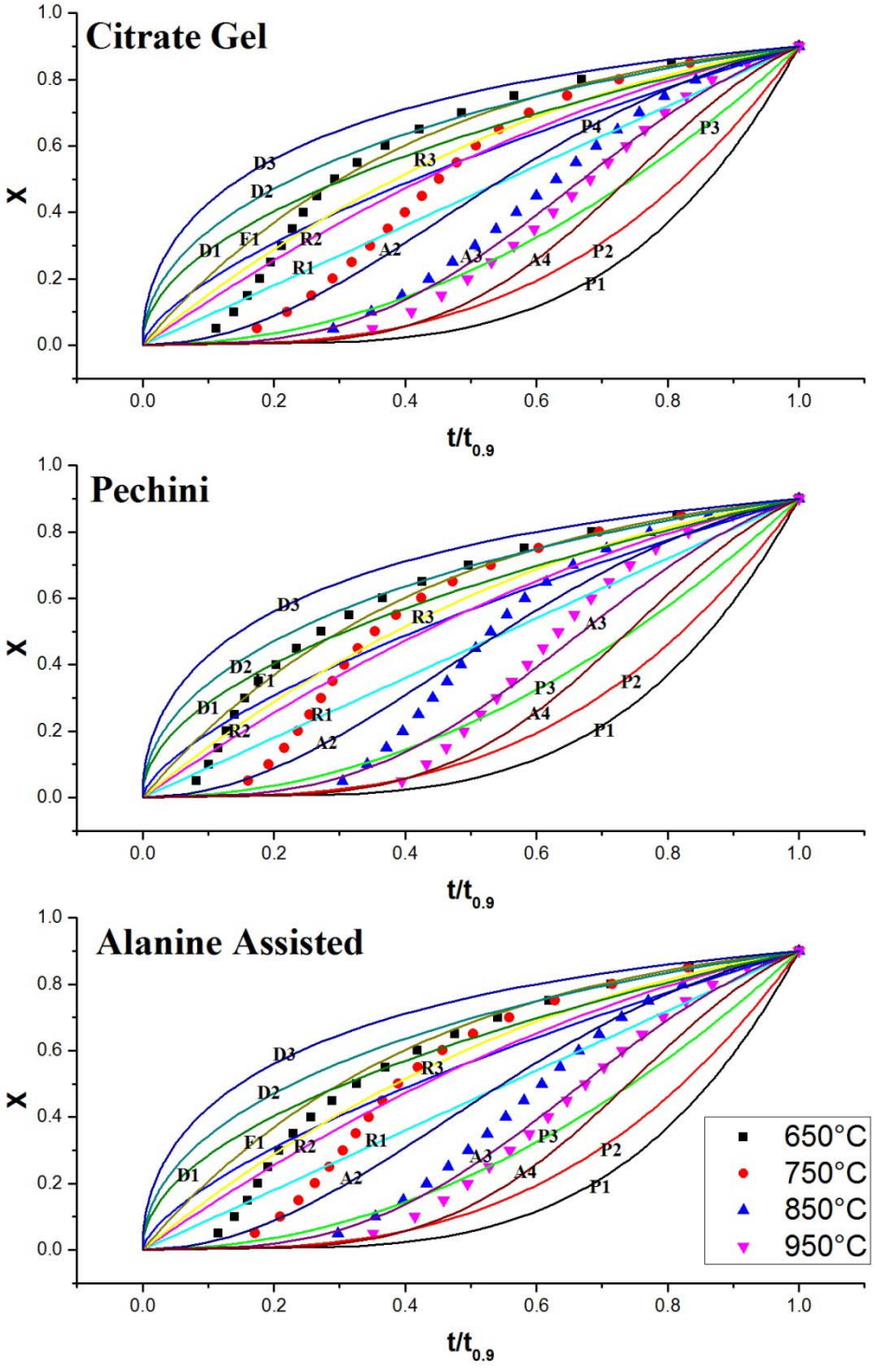

Figure 3.23. Reduced time plot for absorption experiments of first three samples

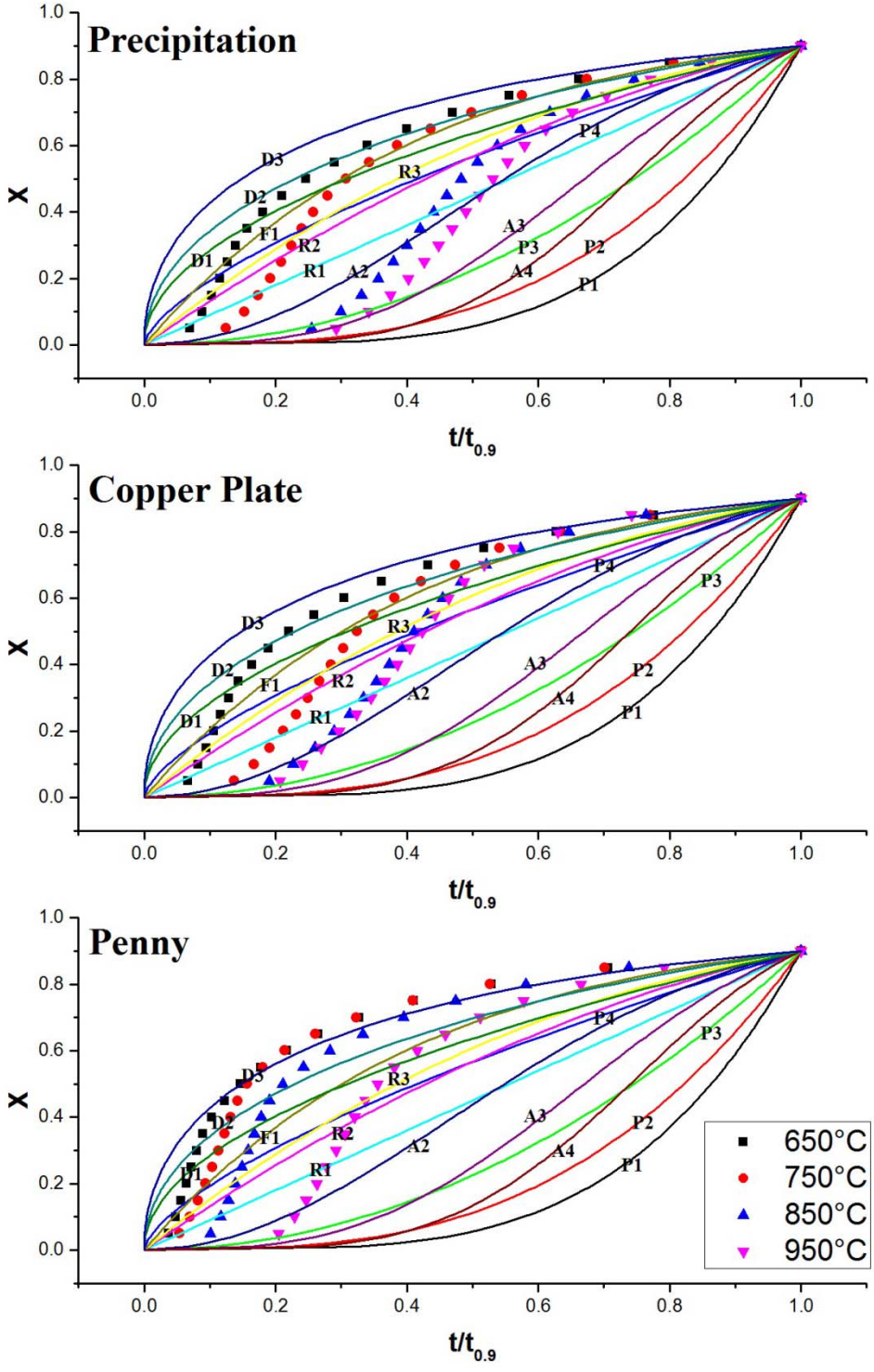

Figure 3.24. Reduced time plot for absorption experiments of second three samples

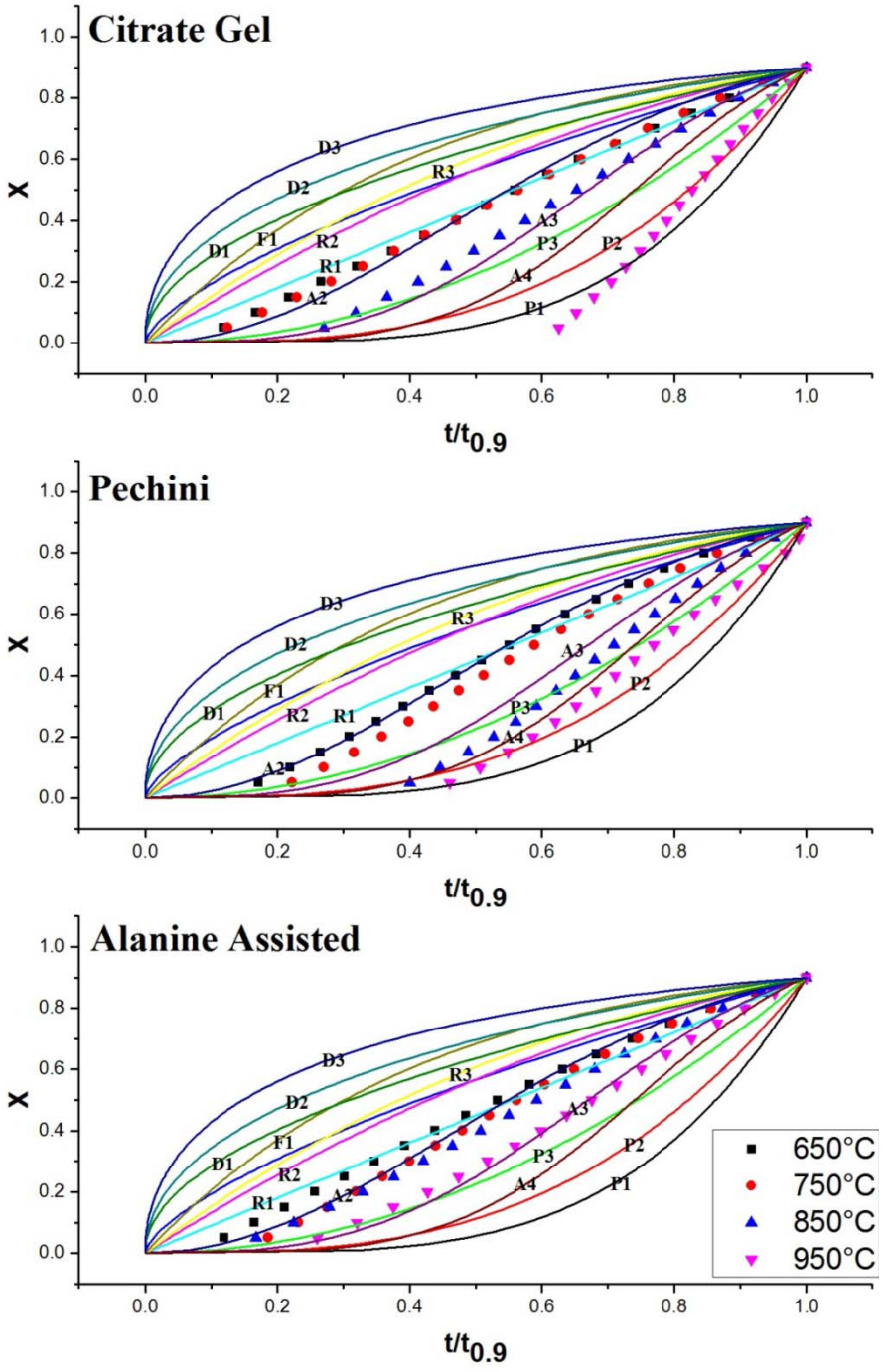

Figure 3.25. Reduced time plot for desorption experiments of first three samples

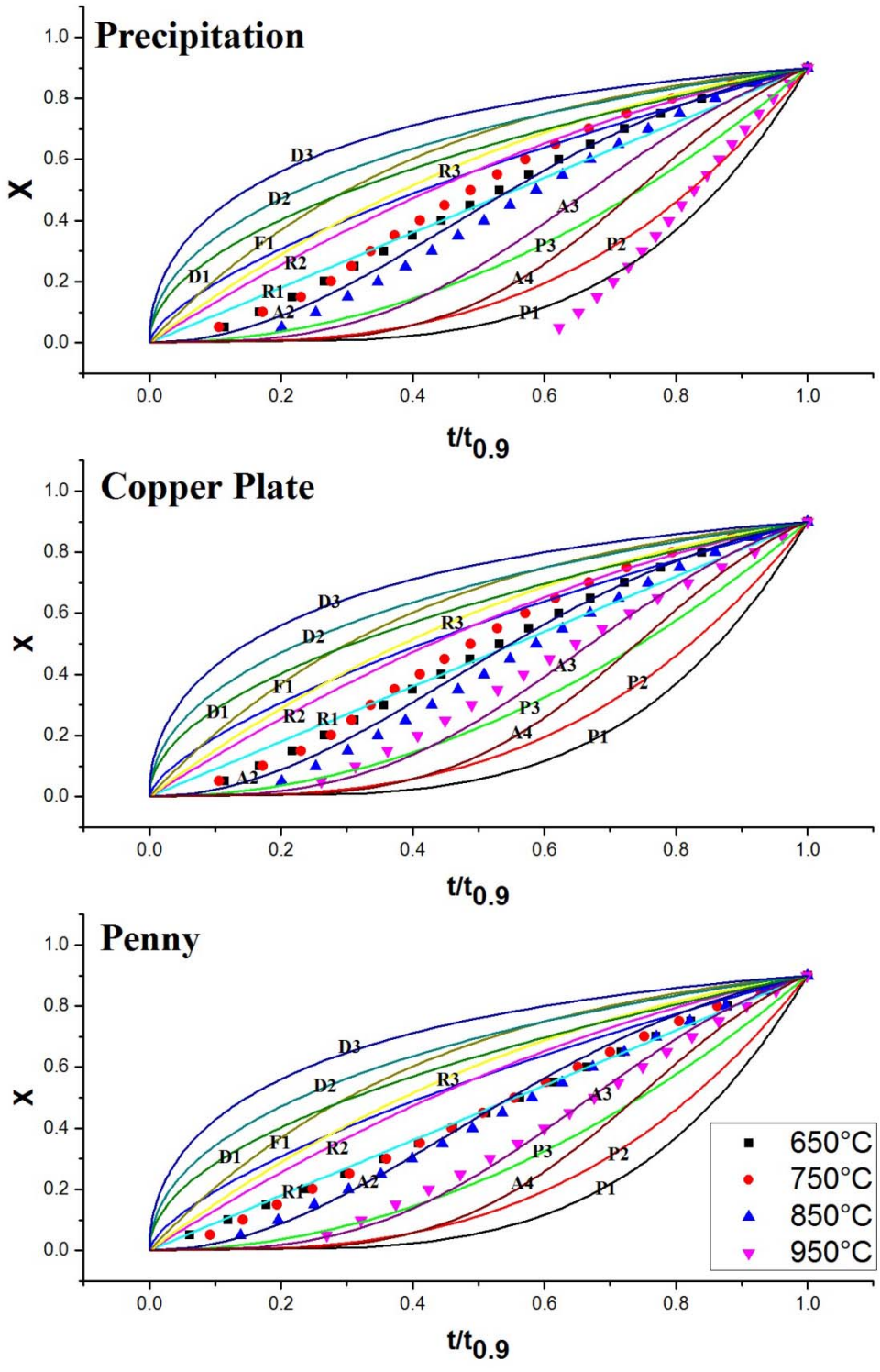

Figure 3.26. Reduced time plot for desorption experiments of second three samples

(Malek, J., 1992) has proposed an algorithm for kinetic analysis using empirical models which can be used in cases like this where kinetic triplet parameters are dependent on temperature. The algorithm uses the maximum following functions to choose the models listed in Table 3.25.

$$Y(X) = \frac{dX}{dt} \approx f(X) \text{ (Eqn. 3.5 (Malek, J., 1992))}$$

$$Z(X) = \left(\frac{dX}{dt}\right) t = f(X)g(X) \text{ (Eqn. 3.6 (Malek, J. 1992))}$$

Figure 3.27 shows a graphical description of the Malek algorithm.

Table 3.5. The empirical kinetic models and their corresponding selection criteria

(Malek, J. 1992)				
Model	Symbol	F(X)	X_p^{∞} (maximum of Z(X)	X_M (maximum of Y(X)
Reaction order	F_n	$(1-X)^n$	$1-n^{1/(1-n)}$	0
Johnson Mehl Avrami	JMA(m>1)	$m(1-X)[-ln(1-X)]^{1-1/m}$	0.632	1-exp(1/m-1)
Sestak-Berggren	SB(M,N)	$X^M(1-X)^N$	$(0,X_p)$	M/(M+N)

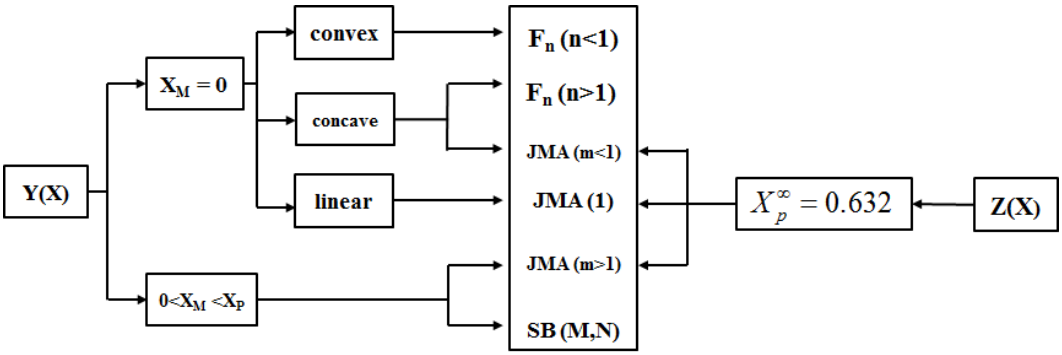

Figure 3.27. Schematic diagram of the kinetic model determination

(Malek, J. 1992)

The *Y(X)* and *Z(X)* functions of different samples for sorption and desorption are shown in Figures 3.28 to 3.31. Tables 3.6 and 3.7 list the X_M and X_p^∞ derived from these curves. It's seen that for all samples at all temperatures, the relation $0 < X_M < X_p^\infty$ is satisfied and considering that the maximum values of *Y(X)* (X_p^∞) are not equal to *0.632*, based on the algorithm described in Figure 3.27, the Sestak-Berggren model can be used to describe the kinetic of the reactions studied. The agreement of the sorption and desorption reactions with shows the possibility for the presence of an autocatalytic mechanism in the oxygen absorption and desorption from the sorbents studied here (i.e. increase in the rate of the reaction by its advance) (Burnham, A. K. and Braun, R.L., 1999).

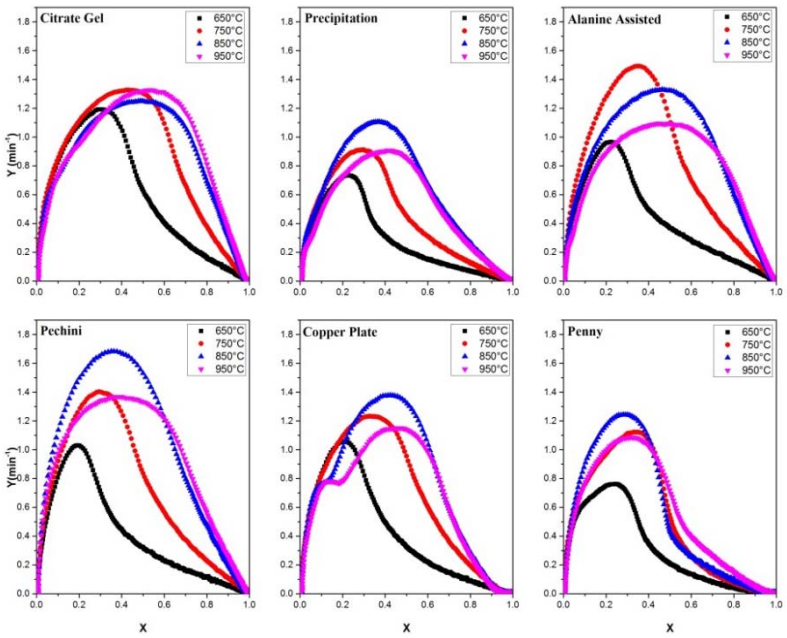

Figure 3.28. The *Y(X)* functions of absorption runs

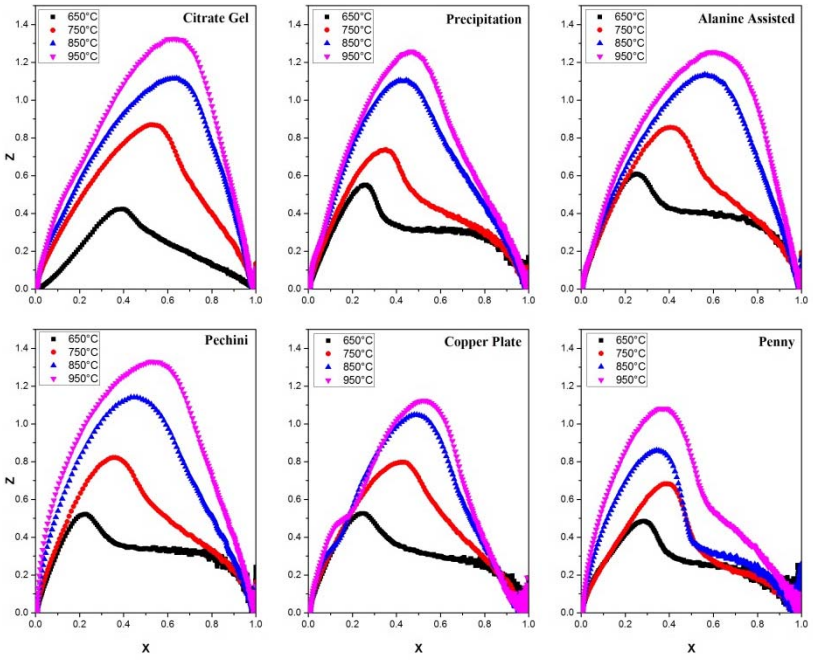

Figure 3.29.The *Z(X)* functions of absorption runs

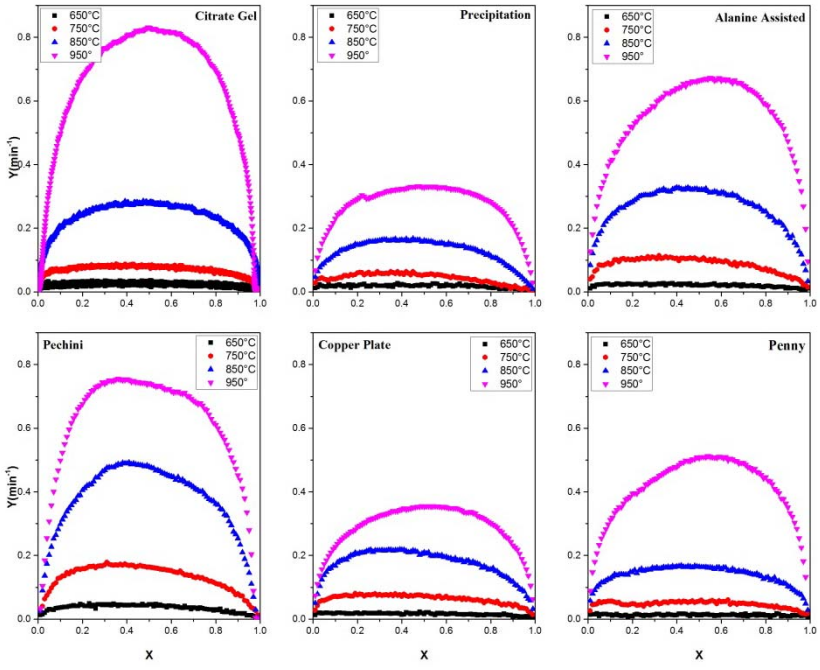

Figure 3. 30. The *Y(X)* functions of desorption runs

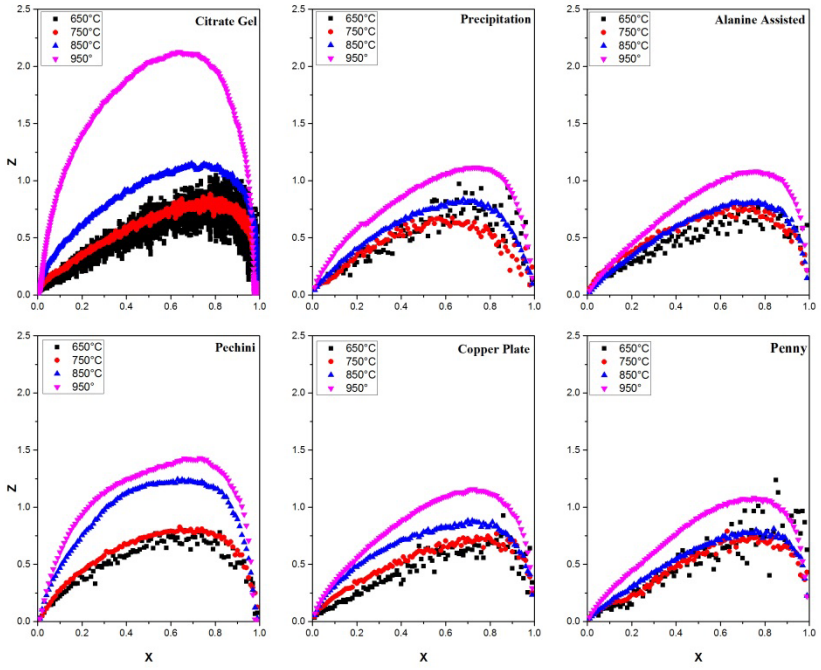

Figure 3. 31. The *Z(X)* functions of desorption runs

Table 3.6. The Y*(X)* and *Z(X)* maxima values for absorption

T(°C)	Citrate Gel		Precipitation		Alanine		Pechini		Cu Plate		Penny	
	X_M	X_p^∞	X_M	X_p^∞	X_M	X_p^∞	X_M	X_p^∞	X_M	X_p^∞	X_M	X_p^∞
650	0.30	0.39	0.23	0.26	0.23	0.25	0.19	0.23	0.21	0.25	0.25	0.29
750	0.43	0.53	0.29	0.35	0.36	0.41	0.29	0.35	0.33	0.43	0.34	0.38
850	0.49	0.64	0.37	0.44	0.46	0.56	0.36	0.45	0.42	0.49	0.29	0.34
950	0.53	0.63	0.42	0.47	0.49	0.60	0.39	0.52	0.45	0.52	0.31	0.36

Table 3.7. The *Y(X)* and *Z(X)* maxima values for desorption

T(°C)	Citrate Gel		Precipitation		Alanine		Pechini		Cu Plate		Penny	
	X_M	X_p^∞	X_M	X_p^∞	X_M	X_p^∞	X_M	X_p^∞	X_M	X_p^∞	X_M	X_p^∞
650	0.39	0.8	0.38	0.66	0.26	0.66	0.23	0.66	0.48	0.86	0.35	0.6
750	0.35	0.78	0.29	0.63	0.32	0.72	0.31	0.64	0.19	0.83	0.63	0.63
850	0.39	0.75	0.45	0.68	0.4	0.77	0.41	0.63	0.39	0.88	0.42	0.84
950	0.4	0.73	0.48	0.74	0.55	0.76	0.36	0.76	0.42	0.85	0.54	0.75

Using the relation $X_M = \frac{M}{M+N}$ and the equation 3.3, the parameters *N*, *M* and

K(=$k_0$exp(-/RT) and from the slope of *ln(K)* vs. 1/T, the Arrhenius parameters k_0

and *Q* for each type of reaction can be calculated. Figure 3.30 and 3.31 show the plots from which these parameters are calculated. These parameters are listed in Tables 3.8.

Table 3. 8. Arrhenius parameters of absorption and desorption for different samples

Synthesis Route	Absorption		Desorption	
	Q (kJ/mole)	k_0	Q (kJ/mole)	k_0
Citrate Gel	51± 1	721 ± 3	213 ± 15	$5\ (\pm1) \times 10^{9}$
Precipitation	52 ± 1	412 ± 7	226 ± 10	$6\ (\pm1) \times 10^{9}$
Alanine Assisted	64 ± 2	2909 ± 23	324 ± 8	$4\ (\pm3) \times 10^{14}$
Pechini	57 ± 1	967 ± 1	332 ± 2	$9\ (\pm2) \times 10^{14}$
Copper Plate	39 ± 5	83 ± 3	391 ± 13	$2\ (\pm1) \times 10^{17}$
Penny	39 ± 5	2 ± 1	307 ± 8	$6\ (\pm2) \times 10^{13}$

As seen in Figure 3.32, in nearly all samples, negative absorption activation energy is observed above 850°C. (Zhu, Y., *et al.*, 2004) have also observed these negative activation energies and have attributed it to a low driving force and a lateral growth of CuO grains occurring as a result of a sintering effect.

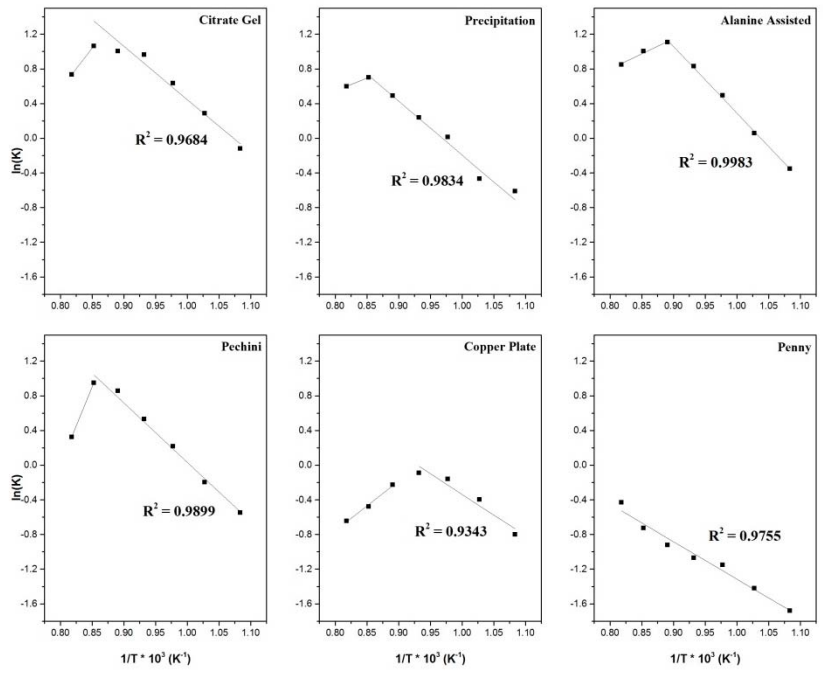

Figure 3.32. The *Arrheniun plots* of absorption runs

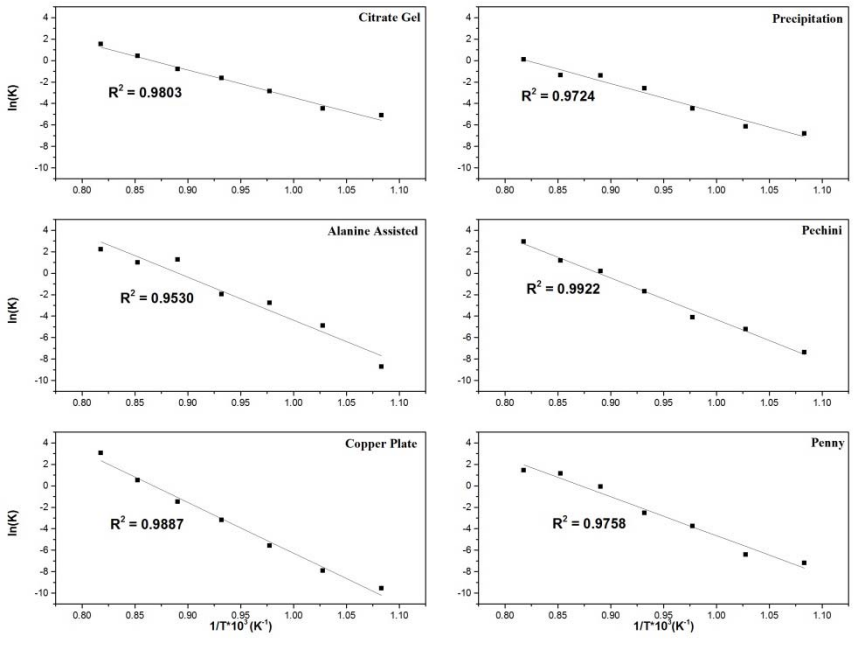

Figure 3.33. The *Arrheniun plots* of desorption runs

3.3.4.1. Oxygen sorption/desorption kinetics vs. surface Chemistry

The oxygen absorption/desorption activation energies have been plotted in Figure 3.34 as a function of surface Cu_2O concentration and O/Cu ratio calculated using the XPS data presented in section 3.3.2. The oxygen desorption kinetics has a clear dependence on the sorbents surface chemistry. Desorption activation energy increases with the Cu_2O content while it has a decreasing trend with the O/Cu ratio showing the role that the thermodynamic driving force plays in controlling the rate of the reaction. The higher concentration of the product (Cu_2O) as observed by its concentration and deviation from 1/1 ratio of O/Cu slows the rate of reaction therefore increasing the activation energy. The effect on the absorption kinetics is not significant because the absorption reaction is the Cu_2O oxidation, the surface chemistry of which is dependent on the temperature and was not measured in this work.

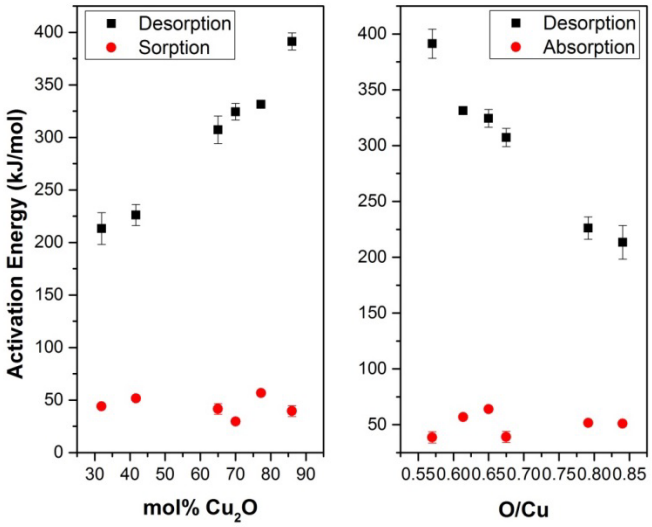

Figure 3.34. The dependence of absorption and deosprion activation energies on the surface chemistry of copper oxide samples.

3.4. Conclusion

Copper oxide can be an alternative for replacing the nonstoichiometric oxides with perovskite and perovskite/spinel structure for use as oxygen sorbent in high temperature air separation. The Sestak-Berggren method was able to describe the kinetics of both the oxygen desorption and absorption kinetics with good precision meaning the presence of an autocatalytic mechanism in these processes. The synthesis method was shown to be effective in controlling the kinetics of oxygen generation without seriously affecting the uptake rate. Surface chemistry was shown to be the parameter through which the kinetics is affected by the synthesis method. The citrate gel method was shown to be the most optimum method in in controlling the surface chemistry of oxide. Considering its ease and possibility to large scale development, the citrate gel method is highly recommended for development of other types of oxide for high temperature air separation and also chemical looping combustion.

Chapter 4: Evaluation of Copper-Aluminum Oxides as Sorbents for High Temperature Air Separation[1]

4.1. Introduction

Emission of CO_2 has been accepted to be a major contributor to global warming due to greenhouse gas effects. CO_2 capture and sequestration is considered as an important strategy for large scale reduction of this gas. The high cost of carbon dioxide capture using current technologies ($35-55 per ton of captured CO_2) is the main barrier for large scale emission-free power generation (Singh, D., *et al*., 2003). Oxy-fuel processes are considered one of the carbon capture technologies for reducing greenhouse gas emissions especially carbon dioxide. Carbon dioxide capture and sequestration techniques require separation of carbon dioxide from nitrogen which makes up the larger fraction of flue gases as air is currently used to burn fuels such as coal and natural gas. In oxy-fuel processes, an oxygen-enriched stream of carbon dioxide is produced to burn the fuel in oxygen rather than in air and as a result, a highly pure carbon dioxide exhaust is produced that requires little separation, facilitating carbon dioxide capture. Furthermore oxy-combustion reduces NO_x emissions while improving combustion characteristics such as unburned carbon (Buhre, B. J. P., *et al.*, 2005). The technology currently available for separation of carbon dioxide from nitrogen and other flue gases is cryogenic air separation which has very high energy consumption and relatively

[1] Part of this chapter was submitted for publication to journal of *Energy & Fuels*

low efficiency (Habib, M. A., *et al.*, 2011). An economically viable oxygen production method is essential to making oxy-combustion power plant a future option when carbon dioxide capture becomes a requirement. Cyclic Auto-thermal Recovery (CAR) process (Figure 4.11), a novel process proposed by (Krishnamurthy, K. R., *et al.*, 2007) and (Lin, Y.S., *et al.*, 2000) has a power consumption about 25% lower than cryogenic air separation which can reduce the total capital cost for about 50% (Nsakala, N.Y., *et al.*, 2004). The CAR process uses the oxygen storage capacity of perovskite oxide sorbents packed in two (or more) fixed beds. Absorption of oxygen occurs by passing air through one bed and the stored oxygen is then released by passing a sweep gas with lower oxygen partial pressure for use in the boiler. The sweep gas can be flue gas, steam or a mixture of the two (Yang, Z., *et al.*, 2002). The heat released by exothermic oxygen adsorption can be used to provide the heat for endothermic oxygen desorption. Low oxygen sorption capacity and desorption rate can be a drawback for CAR process when perovskite oxides are used as the sorbent. This issue is to some extent resolved when CO_2 is used as the sweep gas (Yang, Q., *et al.*, 2006) but the reversible carbonization reaction leads to formation of some excess CO_2 in the O_2 storage step which should be released into the air which means incomplete CO_2 capture (Li, Z., *et al.*, 2008). The sensitivity of mixed ionic electronic perovskite ceramics to acid gas species like SO_2 leads to gradual loss of their oxygen transport properties. Development of a sorbent with higher oxygen storage capacity and sorption/desorption rate and lower sensitivity to flue gas

species like H_2O and SO_2 is therefore necessary for replacing the cryogenic process with CAR or similar process and this is the focus of this study.

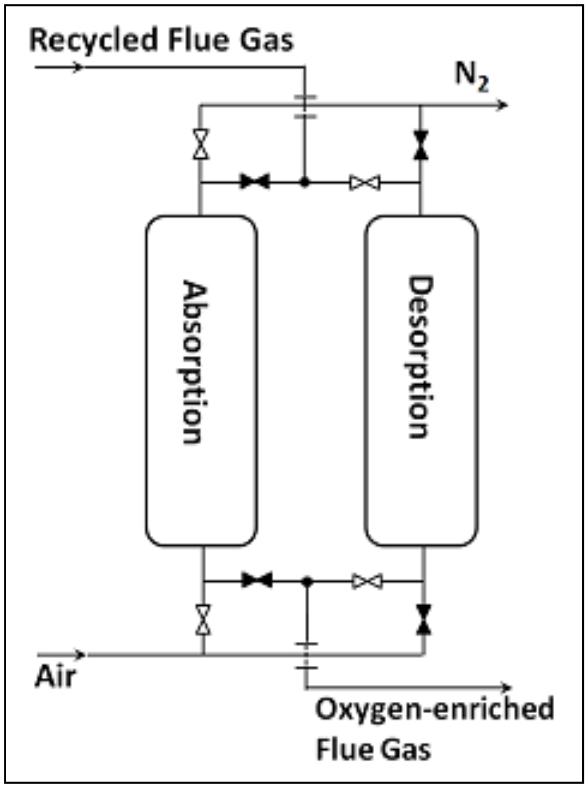

Figure 4. 1. Cyclic Auto-thermal Recovery (CAR) Process

(adapted from Krishnamurthy, K. R., *et al.*, 2007)

4.2. CuO /Cu_2O Equilibrium

In this work, use of CuO as an oxygen carrier for production of oxygen-enriched CO_2 was studied. The following reversible reaction is used to store and release oxygen: $2Cu_2O + O_2 = 4CuO$. FACTSage® was used to study the thermodynamics of the reaction and effect of other gas species on the equilibrium. Figure 4.2.a

shows the change in concentration of gaseous compound as a function of temperature whereas figure 4.2.b shows the same values for solid compounds. In both cases, the oxygen release stage under a typical flue gas with a composition given in Table 4.1 as purge gas was considered. The graphs in figures 4.2.a and 4.2.b show the lack of chemical affinity of CuO for the species in recycled flue gas which is an important requirement for oxygen carrier in the CAR process. The other advantage of CuO for use as oxygen carrier in CAR process is its potential capability to store energy. CuO/Cu_2O cycle has been reported to be a good candidate for chemical energy storage with insignificant loss in reactivity on repeated cycling. The difference in molar volume of the two compounds leads to cyclic swelling and shrinkage and the resultant pore formation increase the surface area therefore preventing the loss of reactivity without significant loss of mechanical properties which is a main requirement for a sorbent in the CAR process for significant periods of time (Yang, Q. and Lin, Y.S., 2006). The high temperature required for CuO dissociation under recycled flue gas as the purge atmosphere however is an important limitation for the use of CuO as a sorbent. The need for in high temperature use of CuO can be to some extent overcome by use of a material with high melting temperature as the support or dispersed second phase within the main phase. Addition of a second phase can affect the thermodynamics and kinetics of oxygen absorption and desorption depending on the support or second phase reactivity with copper oxides. Alumina is one of the most common materials used support or dopant (Andez, J., *et al.*, 2004). The next

section deals with the properties of Al_2O_3/CuO sorbents and their effect on oxygen sorptive/desorptive characteristics.

Table 4.1. Typical untreated flue gas composition

(Bordent, B. and Kluger, 2008)						
Compound	Ar	N_2	CO_2	SO_2	H_2O	O_2
Conc. (mol%)	2-2.1	4.8-5.0	58.9-60.1	0.1-0.5	31.8-32.0	1.9-3.0

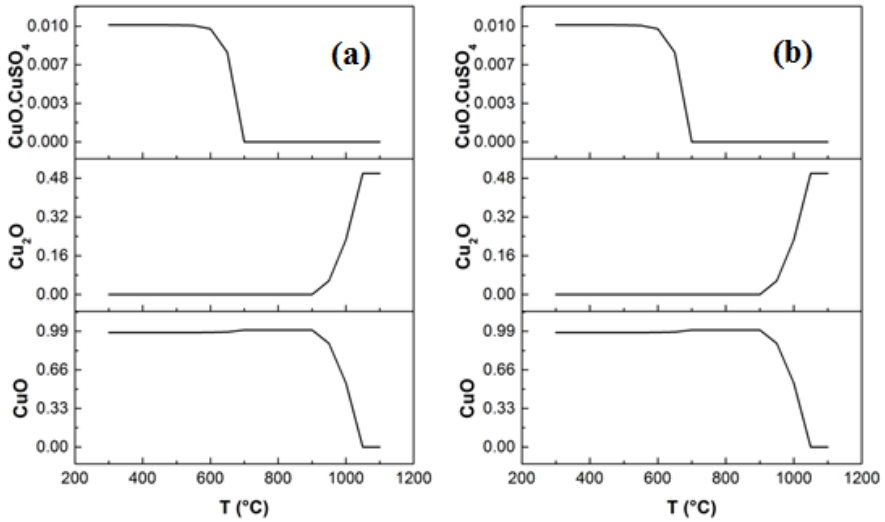

Figure 4.2. a: Solid compounds and b: gaseous compounds in equilibrium with CuO at different temperatures

4.2.1. Effect of Alumina Addition on the Equilibrium

Tenorite (CuO) and Alumina (Al_2O_3) have a high reactivity to form mixed oxide compounds which is a function of both temperature and oxygen partial pressure,

which is a quality that can be used for oxygen storage. Figure 4.3 represents the temperature vs. oxygen partial pressure diagram for Cu-Al-O system. Copper aluminum oxide appears into two structures of spinel ($CuAl_2O_4$) and delafossite ($CuAlO_2$). $CuAl_2O_4$ lowers the dissociation temperature of CuO. For pure CuO, the dissociation temperature is ~1032°C under air atmosphere (PO_2 = 0.21 atm) while by addition of $CuAl_2O_4$, the dissociation temperature is reduced to 942°C. Such dissociation temperatures are the upper limit for use of $CuO/CuAl_2O_4$ as high temperature oxygen sorbent. The lower limit depends on the oxygen partial pressure in the purge gas. In the CAR process where recycled flue gas is used as the purge gas, a value between 3-4% O_2 can be a reasonable assumption (Bordent, B. and Kluger, 2008) which leads to a lower temperature limit of about 757°C.

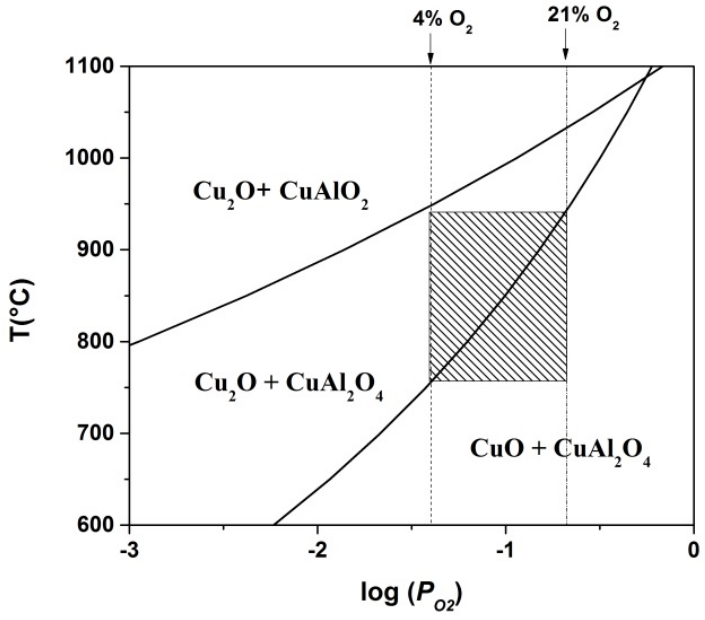

Figure 4.3. Temperature vs. log(P_{O2}) in the Al-Cu-O System, plotted using data from (Jacob, K.T.; Alcock, C.B., 1974)

4.3. Experimental Procedure

4.3.1. Sample Synthesis and Preparation

The citrate gel method (Baythoun, M.S.and Sale, F.R., 1982) was used to synthesize different CuO and CuO-Al_2O_3 samples. $Cu(NO_3)_2.6H_2O$ and $Al(NO_3)_3.9H_2O$ were used as precursors. The stoichiometry was chosen to produce different $CuAl_2O_4$ to CuO ratios. Samples with the molar ratio from 0% to 40% were synthesized using the following procedure (3 g of each sample):

1. Copper and aluminum nitrate were dissolved in distilled water by desired stoichiometric ratios and mixed in a beaker.
2. 50% molar excess citric acid relative to the total number of moles of nitrate ions was dissolved in distilled water and added to the nitrate solution.
3. The solution was heated to 95–100°C for 3–4 hrs for polymerization followed by condensation at 100 – 105°C for 3-4 hrs.
4. The gel-like product was then dried at 110°C for 24 hrs.
5. The dried gel was then ground by mortar and pestle and calcined at 650°C for 8 hrs in zirconia crucibles under an air flow of 20 ml/min.
6. The calcined powder was then ground by mortar and pestle and sintered at 950°C for 8 hrs in zirconia crucibles under an air flow of 20 ml/min.
7. Particle size distributions of the samples were measured using a Malvern mastersizer. All samples showed a narrow distribution with a $d_{0.5}$ around 100 mm.

4.3.2. Morphology and Crystal Structure

The morphology of samples was investigated using scanning electron microscopy (Hitachi S-2700) and the crystal structure was determined by X-ray diffraction (Rigaku rotating anode TTRAX III, Auburn Hills, MI) with Cu-Kα as the radiation. The X-ray diffraction patterns were refined using SIROQUANT®, based on Rietveld refinement algorithm, to determine the exact composition of the samples.

4.3.3. Oxygen Sorption/desorption Investigation by Thermogravimetric Analysis

A TA instrument SDT Q600 TGA instrument was used for thermogravimetric analysis. The instrument consisted of a stainless steel tube placed in a horizontal furnace that can be operated to temperatures up to 1200°C with a computer continuously recording the data. The instrument had two separate reactant gas inlets that can be operated automatically. Air and N_2/CO_2 were used as reactive gases for sorption and desorption stages. Small amounts of the sample (5-10 mg) were placed in alumina pans and heated with a heating rate of 50°C/min to 750-900°C under 250 ml/min of air and then gas is switched to a mixture of O_2 and CO_2 to study desorption. The oxygen concentration in the purge gas was adjusted using mass flow controllers with an accuracy of 0.1 ml/min. After complete desorption, the gas was switched to air to study absorption. As recommended by

(Ollero, P., *et al.*, 2002) to reduce the diffusion effects between the sample and bulk gas, sample pans were ground from the original 4 mm to about 0.5 mm deep.

4.4. Results and Discussion

4.4.1. Morphology of the Sorbents

Figure 4.4 shows the SEM micrograph of samples with different spinel phase content. The synthetic CuO sample shows a more porous structure compared to the commercial sample. A porous structure can improve the catalytic properties of the samples as investigated by (Zhou, K., *et al.*, 2006). The structure however becomes more porous with increase in the spinel phase content. Considering the relatively low sintering temperature, the increase in porosity can be explained by the fact that presence of second phase can inhibit the growth of the grains therefore the structure remains porous. The proposed mechanism for increase in porosity is in agreement with Hoque *et al.*'s work on Ni-Cu mixed spinels showing that above 10%, the porosity is increasing with the second phase content (Hoque, S., *et al.*, 2002).

However, due to difference in the density of the two phases (ρ_{CuO} = 6.51 and $\rho_{CuAl2O4}$ = 4.58 g/cm^3 (Jacob, K.T.; Alcock, C.B., 1974)) above a certain limit (30-40% $CuAl_2O_4$), agglomeration occurs which leads to separation of the two phases as shown by the backscattered electron micrographs of Figure 4.5. The spinel phase agglomeration is of crucial importance for thermodynamic feasibility

of oxygen desorption. As shown in Figure 4.3, presence of the spinel phase lowers the oxygen evolution temperature through formation of $CuAlO_2$. In addition, under recycled flue gas as the purge gas for desorption stage, the high oxygen partial pressure makes the presence of second spinel phase necessary. Cyclical stability of the sorbents can also be affected by phase separation due to the effect that it has on the kinetics of oxygen absorption and desorption. Over a long period of time, the phase separation can also lead to attrition and change in the particle size of the sorbents and their carry over by the gas stream to boiler or exhaust fume causing problems such as erosion in the reactor and decrease in the sorption capacity of the oxygen absorbers.

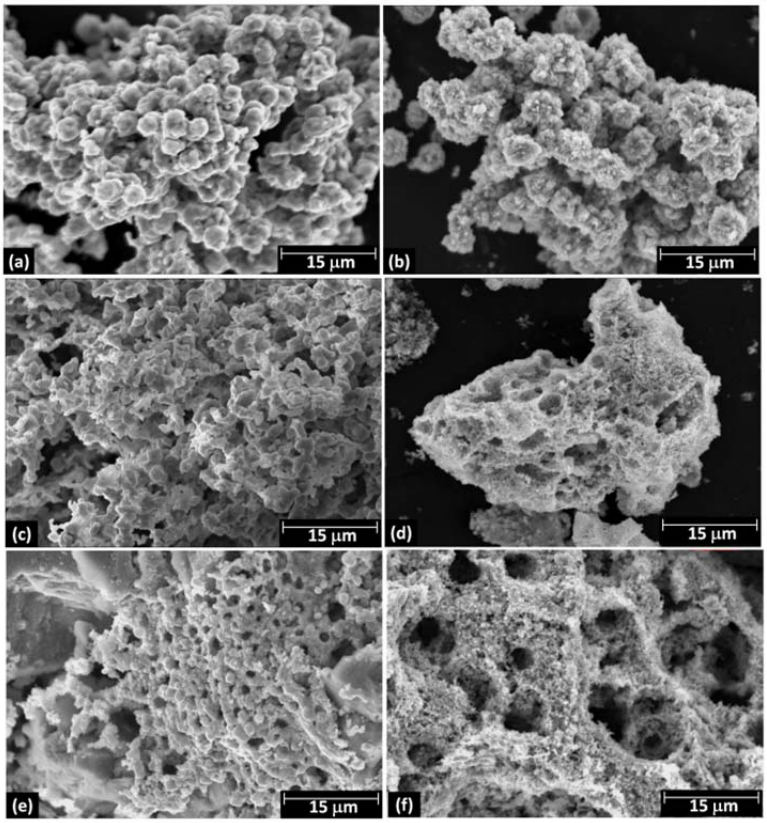

Figure 4.4. SEM micrographs of (a) Commercial CuO, (b)Synthesized CuO, (c) CuO-10% $CuAl_2O_4$, (d) CuO-20% $CuAl_2O_4$, (e) CuO-30% $CuAl_2O_4$, (f) CuO-40% $CuAl_2O_4$

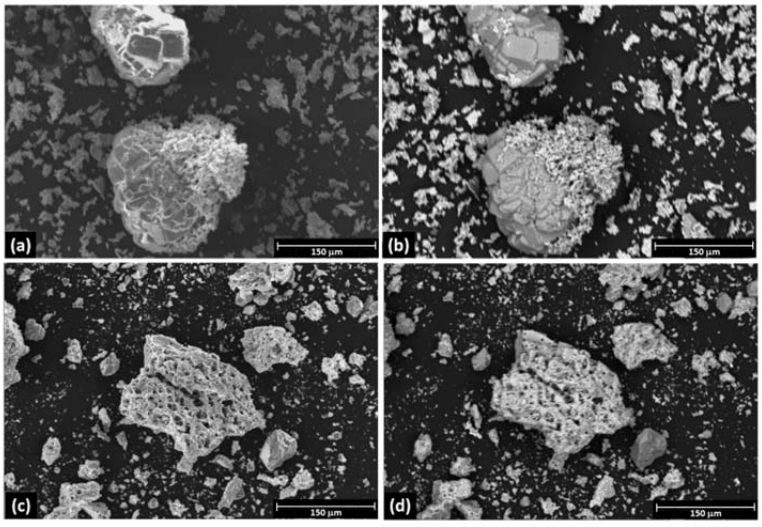

Figure 4.5 (a) Secondary electron micrograph of CuO-20%$CuAl_2O_4$, (b) Backscatterd electron micrograph of CuO-20%$CuAl_2O_4$, (c) Secondary electron micrograph of CuO-40%$CuAl_2O_4$, (d) Backscatterd electron micrograph of CuO-40%$CuAl_2O_4$

4.4.2. Crystal Structure Analysis of the Sorbents

Figure 6 shows the x-ray diffraction patterns of samples with different spinel phase content. Background, Kα2 and noise in all of the patterns have been removed to make the characterization easier. The figure shows the existence of distinct crystalline phases of two materials in the mixtures. The patterns were used to quantify the amount of phases in samples using Rietveld refinement with SIROQUANT^{TM} analysis software. The observed patterns for all profiles were analyzed by multiphase leas-square profile fitting of the calculated patterns using Rietveld instrumental parameters (Rietveld, H. M., 1969). The calculated patterns are derived using the crystal structure data bank available in the program. The derived pattern and the difference for each sample are shown in Figure 4.7.

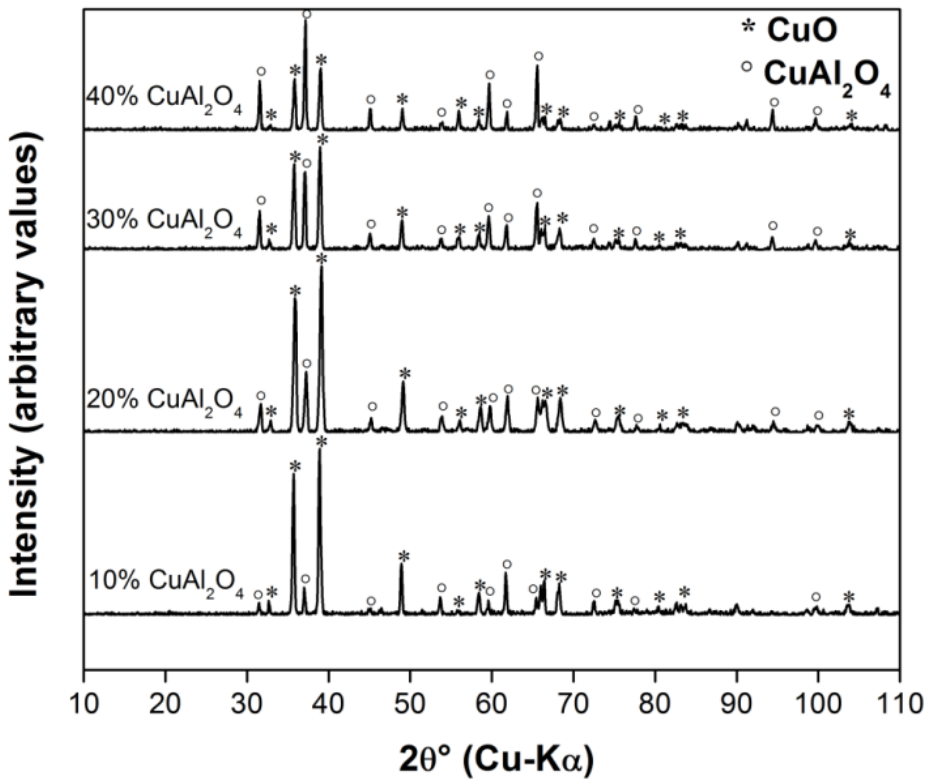

Figure 4. 6. XRD patterns of samples with different spinel phase content

The quantitative analysis of the samples is shown in Table 4. 2. It's clearly seen at higher aluminum content; the accuracy of the analyses is lower (χ^2 values in Table 4.2). This lower accuracy can be explained by the probability of the existence of other phases such as Cu_2O and $CuAlO_2$ as reported by (Kumekawa, Y., *et al*., 2009) Considering the fact that nitrate was used as precursor for synthesis of these samples and the possibility in variation of oxide yield from nitrates due to moisture absorption or dehydration during storage, the observed difference is reasonable.

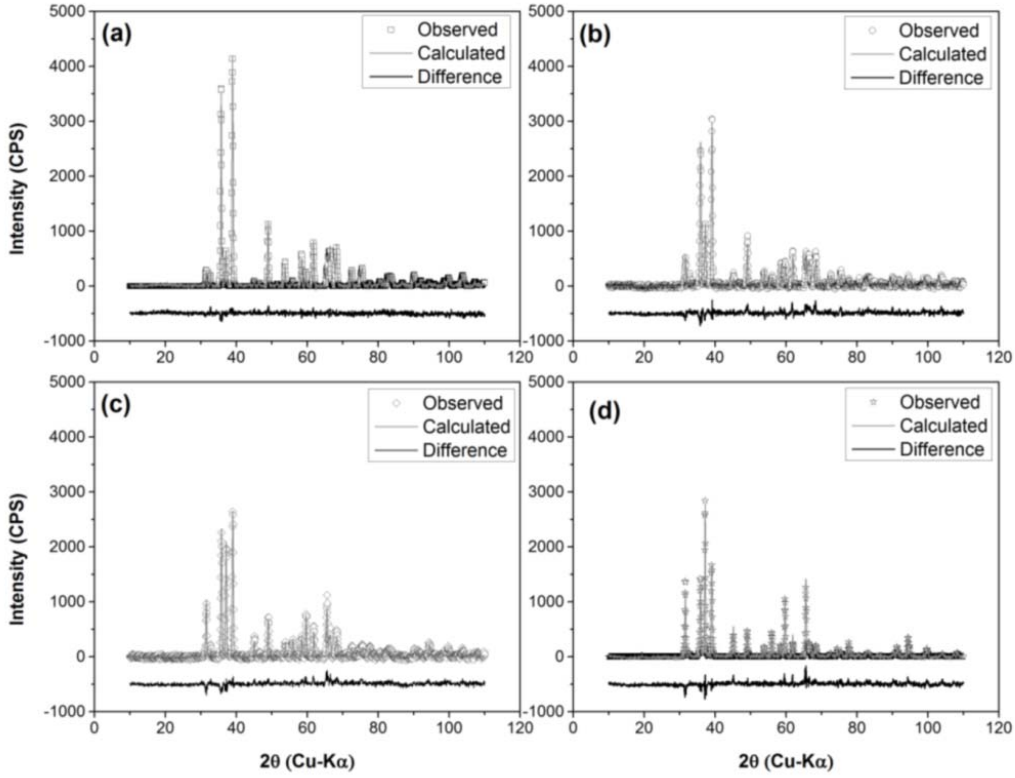

Figure 4.7. Rietveld refinement of a) CuO-10%$CuAl_2O_4$, b) CuO-20%$CuAl_2O_4$, c) CuO-30%$CuAl_2O_4$, d) CuO-40%$CuAl_2O_4$

Table 4.2. Phase Analysis of the sorbents calculated by X-ray Rietveld refinement and their comparison with the expected composition

Sample	Theoretical $CuAl_2O_4$ Weight	Measured $CuAl_2O_4$ Weight	χ^2
CuO-10%$CuAl_2O_4$	18.58 %	18.81% ± 0.25%	1.31
CuO-20%$CuAl_2O_4$	31.34%	31.61% ± 0.33%	1.20
CuO-30%$CuAl_2O_4$	40.64%	41.23% ± 0.33%	2.3
CuO-40%$CuAl_2O_4$	47.72%	48.51% ± 0.37%	2.5

4.4.3. Sorptive/Desorptive Characteristics of the Sorbents.

Figure 4.8 shows the oxygen desorption behavior of different samples over a range of temperatures under CO_2 atmosphere containing 0.1-5% Oxygen. These tests were performed under a total flow rate of 250 ml/min and a heating rate of 2.5°C/min. It is readily observed that the oxygen desorption rate is highly sensitive to the partial pressure of oxygen in the purges gas. By increasing the oxygen concentration above 0.1%, the oxygen desorption step is shifted to temperatures above 850°C from 650 °C. The total amount of oxygen released from each sample is however unaffected by this parameter.

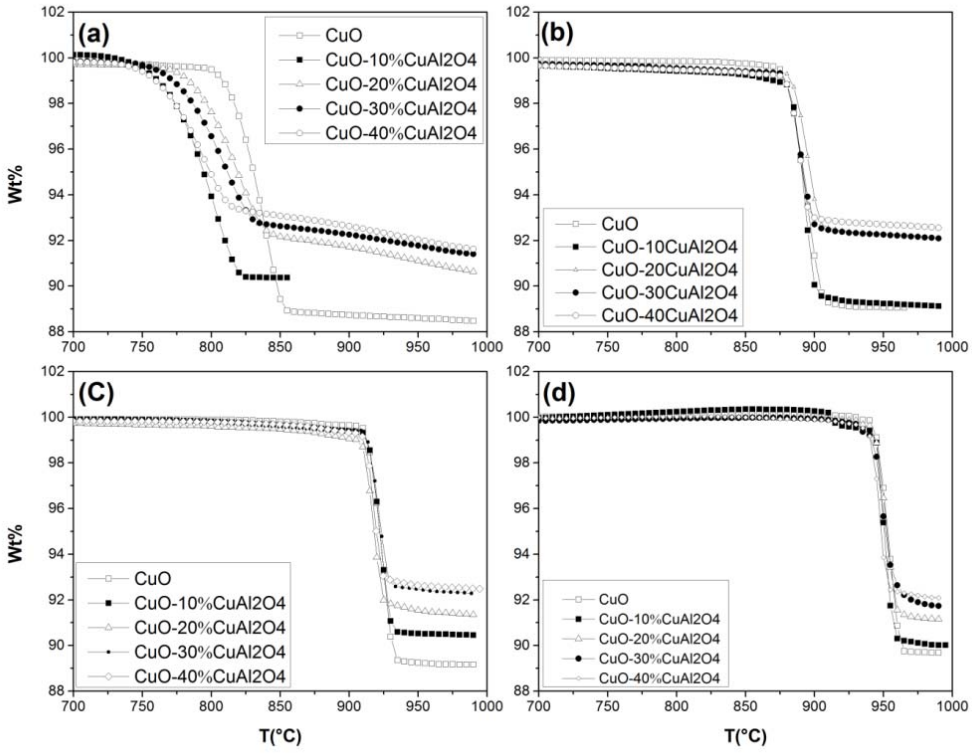

Figure 4.8. Effect of oxygen partial in purge gas on oxygen desorption behavior of samples with different spinel phase content over a certain range of temperature, a) 0.1%, b) 1%, c) 3%, d) 5% oxygen in CO_2/O_2 mixture

Conversion, *X*, is defined as:

$$X = \frac{w_0 - w_t}{w_0 - w_f} \quad \text{(Eqn. 4.1 (Brown, P.K., 2008))},$$

where w_0, w_t and w_f are initial weight, weight at time t and final weight of the sample. Figure 4.9 shows the conversion rate for different samples as a function of temperature. At low oxygen partial pressure (0.001 atm), the spinel phase reduces the oxygen desorption temperature. The effect is most significant for 10% $CuAl_2O_4$ content but decreases with increase in the ratio of the spinel phase. Agglomeration at higher spinel phase ratio (as shown in Figure 4.5) reduces this effect causing the desorption temperature to return to near its original values (as seen in Figures 4.9b,4.9c and 4.9d). At higher oxygen partial (≥1%), the effect is less significant. The weaker effect of spinel phase on oxygen exchange kinetics illustrates that thermodynamic effect of spinel phase presence is less significant than the dependence of oxygen desorption kinetics on its partial pressure in the atmosphere. In all samples containing the spinel phase regardless of oxygen partial pressure, desorption occurs in two distinct stages. The first stage can be attributed to CuO/Cu_2O whereas the second stage is the result of solid state reaction between CuO or Cu_2O and $CuAl_2O_4$. The solid state reaction stage having a much lower rate compared to the main reaction limits the range of operating temperature the sorbent can be used although under practical conditions of 0.03 atm. Oxygen partial pressure the range is automatically limited to the 900-950°C and the solid state reaction is avoided. Two reduction runs at 925°C under a stream of $97\%CO_2/3\%O_2$ have been performed on the sample with 40%

$CuAl_2O_4$ for durations of 15 and 45min. The reduced samples were analyzed using XRD. The XRD pattern (Figure 4.10) shows the evolution of structure with time. After 15 minutes, the $CuO/CuAl_2O_4$ structure transforms into a combination of CuO, Cu_2O and $CuAl_2O_4$. After 45 minutes, the structure is almost pure Cu_2O with trace amounts of $CuAl_2O_4$ and CuO. The $CuAlO_2$ phase is however not detected but the decrease in $CuAl_2O_4$ content can be the sign of the solid state reaction between CuO/Cu_2O and $CuAl_2O_4$.

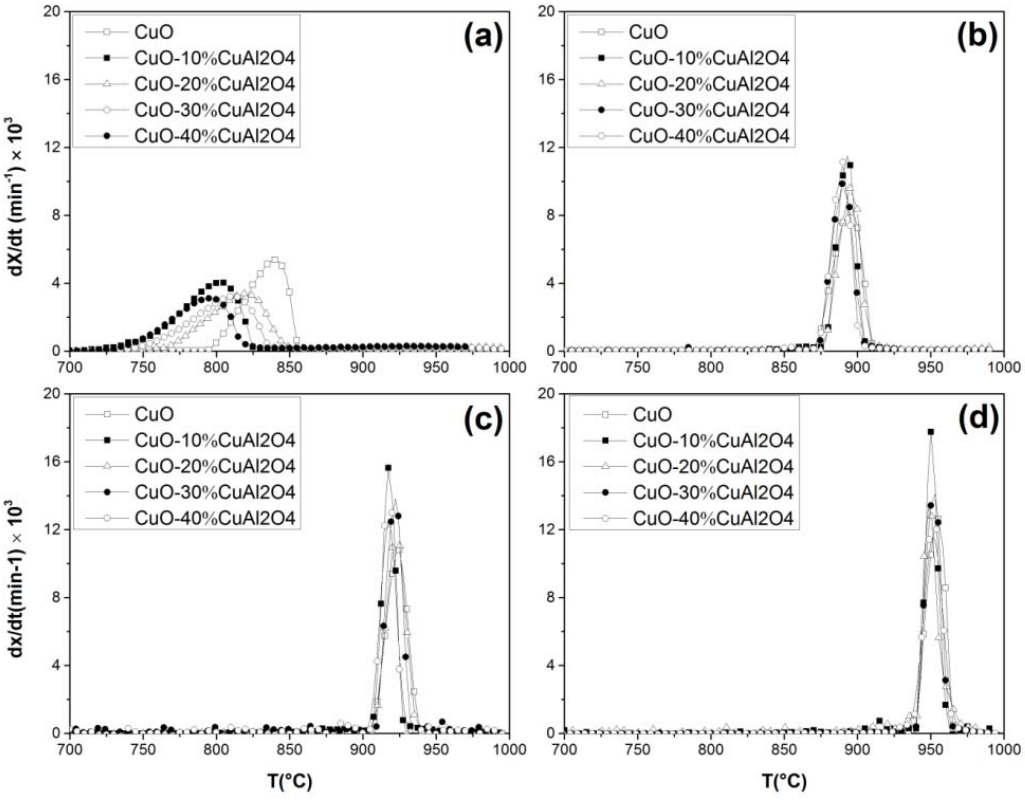

Figure 4.9. Effect of oxygen content in purge gas on oxygen desorption rate of samples with different spinel phase content over a certain range of temperature, a) 0.1%, b) 1%, c) 3%, d) 5% oxygen in CO_2/O_2 mixture

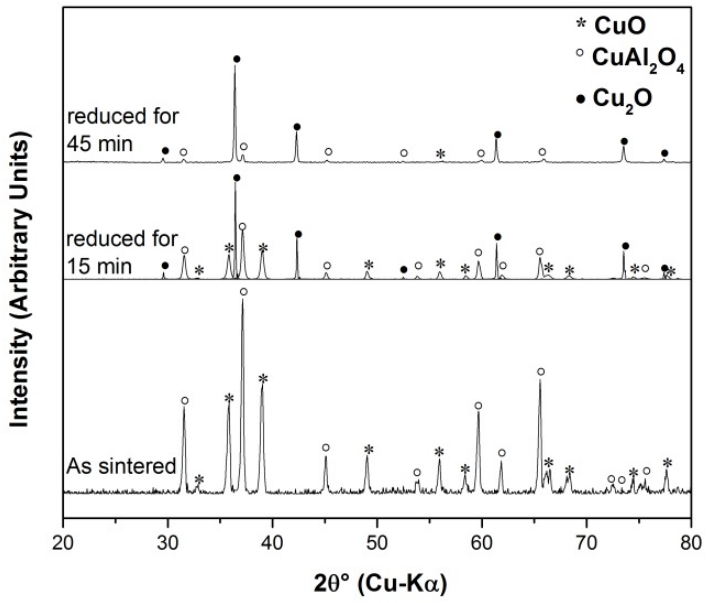

Figure 4.10. Evolution of crystal structure of CuO-40%$CuAl_2O_4$ with time under reducing condition

The data presented in Figure 4.9 was used to calculate the activation energy (Q_{des}) and rate constant ($k_{0,des}$) in the equation 4.2 that describes the kinetics of the desorption process (Eqn. 4.2):

$$\frac{dx_{des}}{dt} = k_{0,des} \exp\left(-\frac{Q_{des}}{RT}\right)\left(\frac{P_{O2}^{eq.} - P_{O2}}{P_{O2}^{eq.}}\right)(1 - x_{des})\left(-\ln(1 - x_{des})\right)^{2/3}$$

(Eqn. 4.2 (Brown, P.K., 2008)),

$P_{O2}^{eq.}$, the equilibrium oxygen partial pressure in the CuO/Cu_2O system was obtained from FACTSage®. The differential iso-conversional (Friedman) method (Brown, P.K., 2008) was used to calculate the rate equation constants. Table 4.3 lists the desorption equation parameters for different samples.

Table 4.3. Desorption equation parameters of different samples

Sample	$k_{0,des}$	$Q_{des}(\frac{kJ}{mol})$
CuO	$8.34(\pm0.1) \times 10^8$	320 ± 9
CuO-10%$CuAl_2O_4$	$8.5(\pm0.2) \times 10^8$	305 ± 2
CuO-20%$CuAl_2O_4$	$8.1(\pm0.1) \times 10^8$	321 ± 7
CuO-30%$CuAl_2O_4$	$8.1(\pm0.2) \times 10^8$	322 ± 8
CuO-40%$CuAl_2O_4$	$8.2(\pm0.1) \times 10^8$	322 ± 6

The sample with 10% spinel phase shows a decrease in desorption activation energy whereas the other samples have desorption parameters close to pure CuO. As mentioned before, this can be due to spinel phase agglomeration by increase in its amount (As seen in SEM micrographs in Figure 4.5). The scattered spinel phase has reduced the desorption temperature and increase the rate (Figure 4.9a) due to a decrease in desorption activation energy.

Figures 4.11 and 4.12 show the absorption curves for different samples at temperature range of 550-950°C. Similar to desorption, the spinel phase addition has a positive effect on absorption rate with the effect decreasing by increase in the second phase content. . The effect of second phase on absorption activation energy can be explained by contribution of dispersed spinel/delafossite phase particles as nucleation site and increasing the oxygen diffusion through CuO layers surrounding the Cu_2O causing the second stage to become faster compared to pure CuO. The absorption curves were used to calculate the oxygen sorption capacity (OSC) according to the following equation:

$$OSC = \frac{(w_f - w_0)/M_{O_2}}{w_0}\ (mmol/g) \qquad \text{(Eqn. 4.3)}$$

Where:

$$w_f = final\ weight, w_0 = initial\ weight\ and$$

$$M_{O_2} = Oxygen\ Molecular\ weight$$

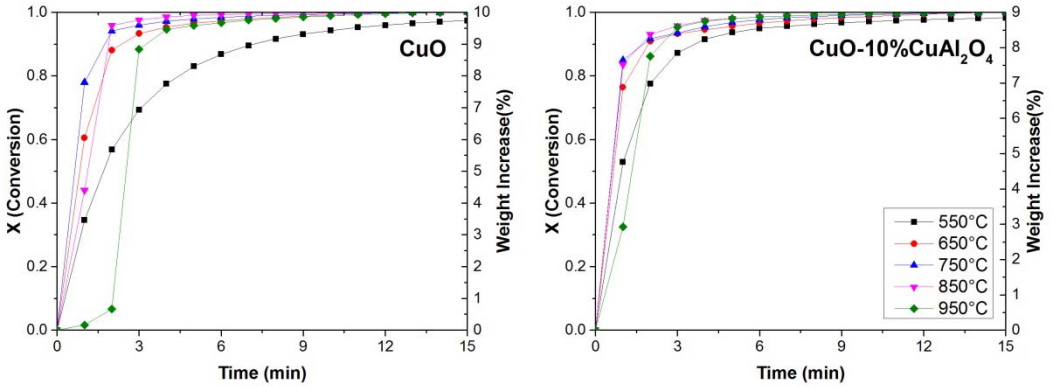

Figure 4.11.Oxygen absorption behavior of samples with 0% and 10% spinel phase content at 650-950°C

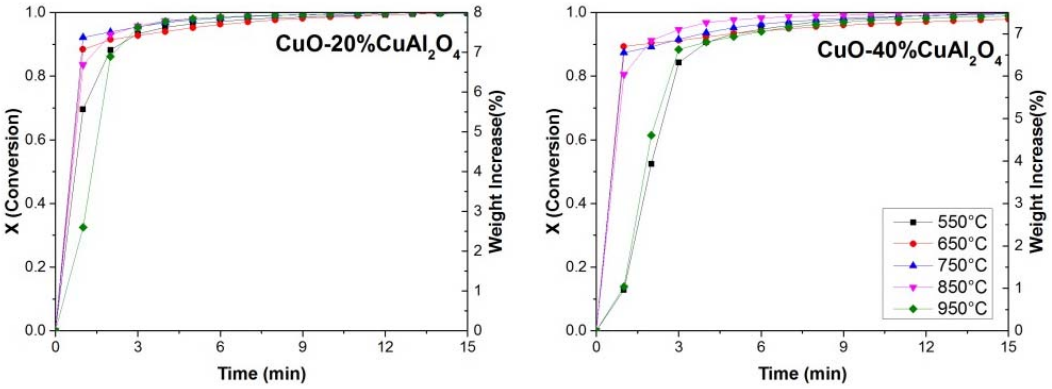

Figure 4.12. Oxygen absorption behavior of samples with 20% and 40% spinel phase content at 650-950°C

In all samples, below 800°C, the rate of absorption is very high and increases with temperature whereas above this temperature, this rate starts to fall. The decrease in oxygen absorption rate with temperature is more significant in samples with higher spinel phase content. The following rate equation was used to calculate the absorption activation energy (Q_{abs}) and rate constant, ($k_{0,abs}$) (Eqn. 4.4):

$$\frac{dx_{abs}}{dt} = k_{0,abs} \exp\left(-\frac{Q_{abs}}{RT}\right)\left(\frac{P_{O2} - P_{O2}^{eq.}}{P_{O2}^{eq.}}\right)(1 - x_{abs})^{2/3}$$

(Eqn. 4 (Brown, P.K., 2008))

Table 4.4 lists the absorption equation parameters for different samples. The absorption activation energy decreases by increasing the spinel phase content. The value reaches its minimum amount at 20% spinel phase but it remains relatively constant above 20%. The effect of spinel phase content on the absorption activation energy is similar to its effect on desorption with a difference that in the case of absorption, the maximum effect is at 20% whereas in the case of desorption, it is at 10%. The change from 10% to 20% shows that agglomeration of the spinel phase has a less significant effect on the kinetics of absorption compared to desorption

Table 4.4. Absorption equation parameters of different samples

Sample	$k_{0,abs}$	$Q_{abs}(\frac{kJ}{mol})$
CuO	$4.17(\pm1.1) \times 10^3$	72 ± 2
CuO-10%$CuAl_2O_4$	$1.11(\pm0.1) \times 10^3$	59 ± 1
CuO-20%$CuAl_2O_4$	$1.40(\pm0.6) \times 10^2$	29 ± 3
CuO-30%$CuAl_2O_4$	$2.45(\pm0.6) \times 10^2$	31 ± 2
CuO-40%$CuAl_2O_4$	$2.77(\pm0.1) \times 10^2$	28 ± 2

Figure 4.13 shows the variation of oxygen sorption capacity (OSC) with spinel phase content. The oxygen sorption capacities of all samples are above 2.5 mmol/g. Samples with spinel phase addition show a deviation from the expected sorption capacity based on the CuO content. Deviation from the expected OSC can be attributed to formation of delafossite phase during the desorption stage by the following reaction:

$$2CuO + 2CuAl_2O_4 \rightarrow 4CuAlO_2 + O_2$$ (Eqn. 4.5 (Jacob, K.T. and Alcock, C.B., 1974))

Through the following reaction, the delafossite phase can then produce additional cuprite (Cu_2O) which can cause the observed deviation:

$$8CuAlO_2 + O_2 \rightarrow 4CuAl_2O_4 + 2Cu_2O$$ (Eqn. 4.6 (Jacob, K.T. and Alcock, C.B., 1974))

In Cu_2O oxidation, formation of CuO slows the rate of oxidation. Presence of copper-aluminum oxides (spinel/delafossite) produces shorter oxygen diffusion pathways through the otherwise dense CuO layer and therefore increasing the rate of oxidation. At higher spinel content, the agglomeration of the phases reduces this positive effect. The existence of oxygen diffusion pathways however has disadvantages too. In long term cyclical oxidation-reduction, the difference in the density of the phases (Jacob, K.T. and Alcock, C.B., 1974) can produce stress in the material leading to attrition and crushing.

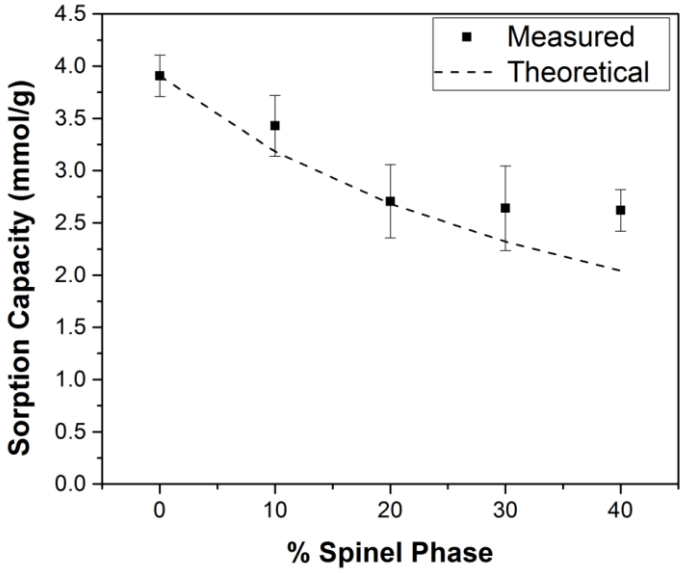

Figure 4.13. Oxygen absorption capacity of samples with different spinel phase content

4.4.4. Cyclical Stability of the Sorbents

Long-term stability is of great importance for selection of sorbents for high temperature air separation. All synthesized sorbents were tested at 900°C under an

atmosphere containing 97% CO_2 and 3% O_2 as the purge gas for a period of 8 hrs. The sorption and desorption time for all samples was chosen as 5 and 15 minutes respectively. The multiple-cycle tests were ended with an absorption step and the samples were collected for examination of the microstructure. Figure 4.14 shows the multiple sorption/desorption cycles of four of the samples as change in mass variation. The sorbents with 10% spinel reach a relative stability after a few cycles while the other sorbents show an unstable sorptive/desorptive performance. The pure copper oxide sample shows a decrease in both sorption and desorption rate. Figures 4.15 and 4.16 show the sorption and desorption rate at different cycles.

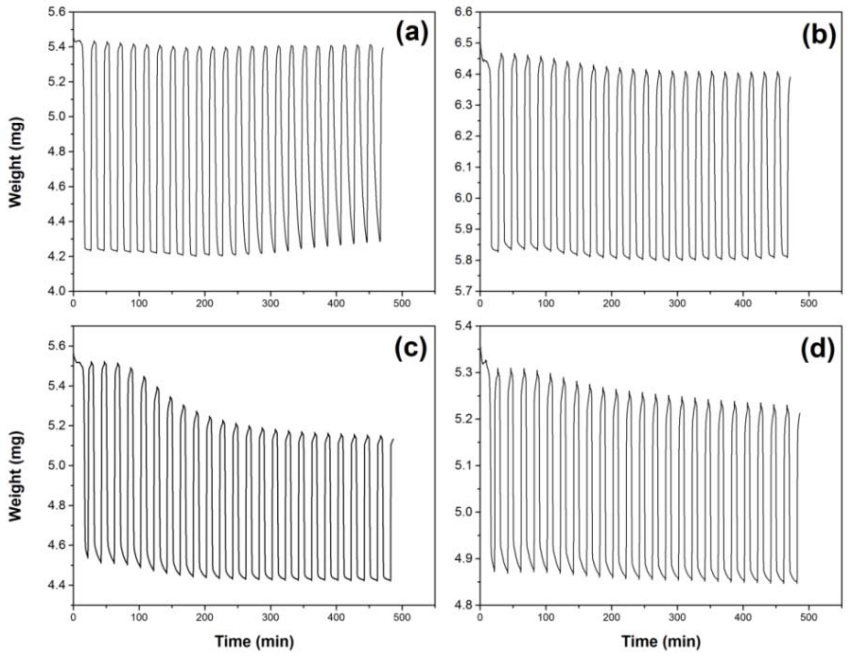

Figure 4.14. Multiple sorption/desorption cycles at 900°C under 97% CO_2/3% O_2 atmosphere of a) CuO, b) CuO-10%$CuAl_2O_4$, c) CuO-20%$CuAl_2O_4$, d) CuO-40%$CuAl_2O_4$

As seen in Figure 4.15, samples containing greater than 20% spinel phase, the absorption rate has an increasing trend over multiple cycles and reaches a constant value. In pure copper oxide, the sintering effect at the high temperature dominates the expansion/contraction effect occurring as a result of difference in CuO/Cu_2O density as observed by decrease in absorption and desorption rate and the change in morphology. The constant reactivity of spinel containing samples is in contrast with the loss of reactivity in copper oxide multiple cycle reduction/oxidation reported by (Chadda, D. and James, D.F., 1989). The reason can be the higher temperature used in this work required by the thermodynamics and kinetics of CuO reduction under recycled flue gas containing 3% O_2. The increasing trend in sorption rate can be explained by formation of delafossite phase in the desorption stage (Eqn. 4.5). The dalfossite phase increases the rate of oxygen diffusion through CuO layer therefore increasing the rate of oxidation. Agglomeration of **spinel** phase however limits the increasing effect of delafossite phase on absorption rate causing the rate to reach a stable value. Except for sample CuO-10%$CuAl_2O_4$, the desorption rate shows a decreasing rate in all samples. Decrease in rate of oxygen desorption for samples containing the spinel phase is however less significant. As seen in Figure 4.16-b, desorption rate in sample CuO-10%$CuAl_2O_4$ has remained unchanged. The stability of oxygen desorption rate proves the importance of the second phase dispersion on the stability of the samples.

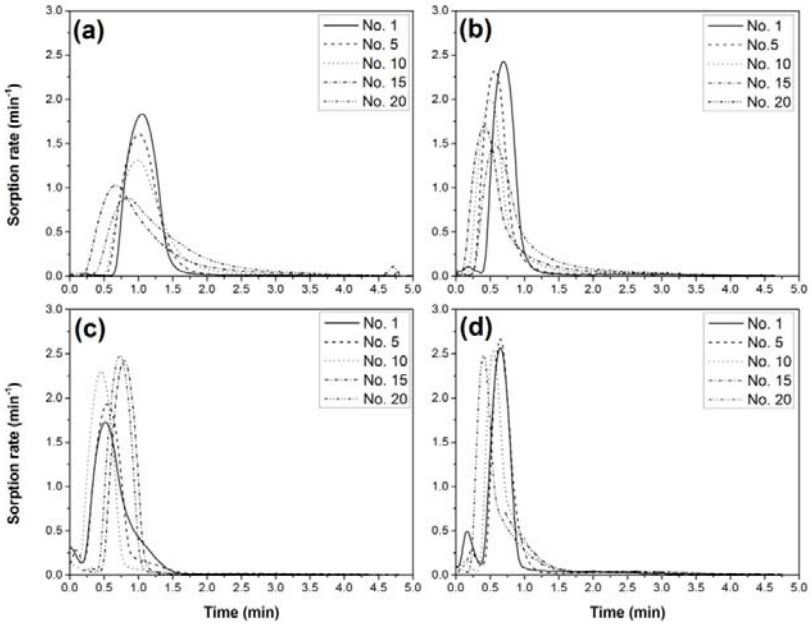

Figure 4.15. Sorption rate of a) CuO, b) CuO-10%$CuAl_2O_4$, c) CuO-20% $CuAl_2O_4$, d) CuO-40%$CuAl_2O_4$ at different cycles at 900°C

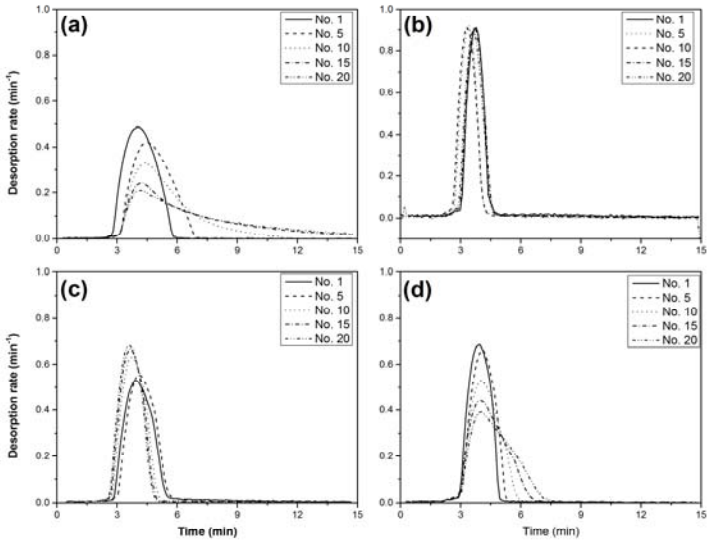

Figure 4.16. Desorption rate of a) CuO, b) CuO-10%$CuAl_2O_4$, c) CuO-20% $CuAl_2O_4$, d) CuO-40%$CuAl_2O_4$ at different cycles at 900°C

The effects observed in the change in the rate of sorption and desorption are also evidenced by the morphology of samples after multiple sorption/desorption cycles as shown by SEM micrographs in Figure 4.17. The pure CuO sample's morphology (Figure 4.17-b) has become more compact compared to as synthesized sorbents (Figure 4.4-b) showing the sintering effect's dominance. The cracks on the crystallites can also lead to attrition which is a major drawback for use of these materials in high temperature air separation. In sample CuO-10% $CuAl_2O_4$, only a minor coarsening is observed compared to its as-synthesized form (Figure 4.4-c). The minor coarsening observed is in agreement with the change in morphology reported by (Chadda, D. and James, D.F., 1989). In this example the spinel phase has not shown any qualitative increase in its size and acted as a nucleation site for the CuO/Cu_2O equilibrium reactions. Another important effect is the role of second phase in structural integrity of the sample. In samples with higher spinel content (Figures 4.16-c&d), although the morphology has changed compared to its as-synthesized form (Figures 4.4-c&e), the spinel phase can still contribute to the stability of samples by increasing the attrition resistance and sintering temperature of the material.

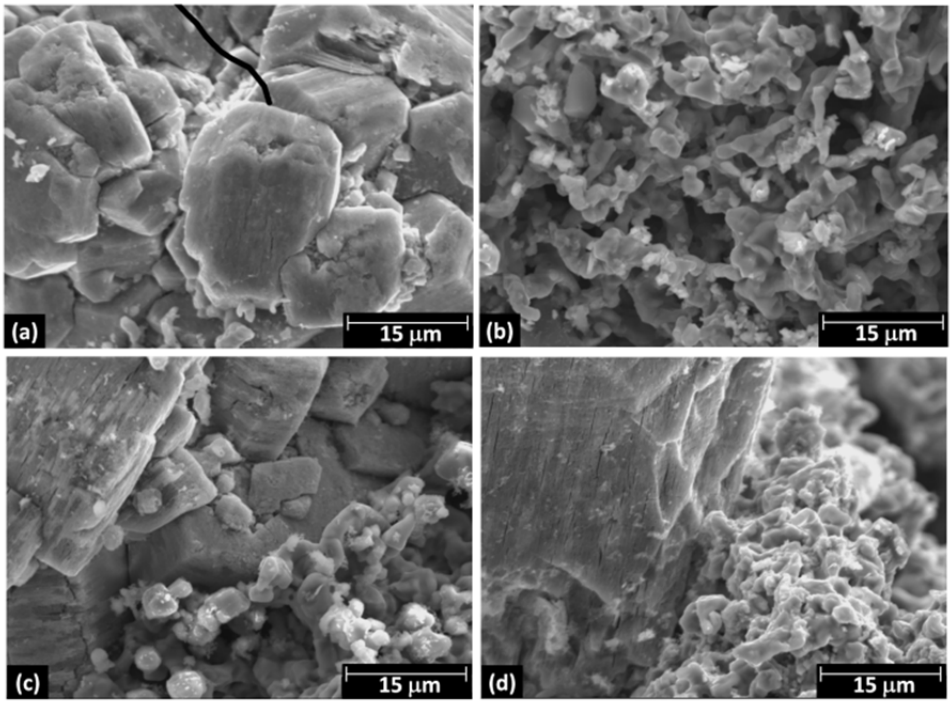

Figure 4.17. Micrograph of a) CuO, b) CuO-10%$CuAl_2O_4$, c) CuO-20% $CuAl_2O_4$, d) CuO-40%$CuAl_2O_4$ after 22 sorptive/desorptive cycles at 900°C

4.5. Conclusion

The conclusions derived from this work can be summarized as follows:

1) CuO-x$CuAl_2O_4$ sorbents show improved sorptive/desorptive properties including oxygen sorption capacity, sorption and desorption rate and neutrality to flue gas species. These improved properties make this type of material an important option for use in the CAR process. The high sorption capacity and oxygen delivery kinetics compared to the perovskite

materials can reduce the size of packed bed reactors and therefore the energy requirements of the air separation process.

2) The addition of alumina to CuO resulting in spinel phase ($CuAl_2O_4$) improves the oxygen sorption and desorption kinetics of the material depending on its amount, size and dispersion. A spinel content of 20% can be considered an optimum value for this purpose.
3) The spinel phase agglomeration cannot be prevented above spinel phase of 20% and can affect the attrition resistance of the sorbents through the separation of CuO and $CuAl_2O_4$ phases.
4) Addition of the spinel phase increases the long-term stability of the sorbents by increasing its sintering temperature. Long term stability is of crucial importance when recycled flue gas containing oxygen is used for oxygen generation. The presence of oxygen limits the desorption stage to temperatures above 950°C therefore the presence of high melting point species like alumina is necessary for long-term usage of the sorbent.

Chapter 5: ZrO_2-CuO Sorbents for High Temperature Air Separation

5.1. Introduction

Development of emission free power generation requires an air separation process that goes beyond the currently available technologies. Development of new sorbents is a key step in development of emission-free power generation processes such as in oxyfuel combustion. (Lin, Y.S., *et al* 2000) has introduced a new group of sorbents based on perovskite structure which have the potential to eliminate the drawbacks of current sorbents. These new sorbents are non-stoichiometric oxides in strontium-lanthanum-cobalt system which can selectively adsorb a considerable amount of oxygen at elevated temperatures (> 300°C). The nonstoichiometry of these oxides has an important consequence which is highly beneficial for oxygen separation. The oxygen-deficiency property makes these oxides highly selective to oxygen over nitrogen and other non-oxygen containing species as a result the effect of other gas species are expected to be minimal (Yang, Z. *et al.*, 2002). The obvious advantage of these processes over the conventional air separation techniques is their high selectivity for oxygen. Using these high temperature processes, production of nitrogen and oxygen at high purities are possible which cannot usually be reached with established processes (Yang Z.H. and Lin Y.S., 2003). However, these sorbents have major shortcomings that limit their application in air separation units of oxy-fuel combustion. Low oxygen desorption rate is the most important of these

disadvantages (Yang, Qing and Lin, Y.S., 2007). Carbonization by CO_2 as the purge gas (the main component of the boiler flue gas) drastically improves this property but has its own adverse effect on Carbon capture efficiency (Li, Z., *et al.*, 2008). Poisoning by sulfur oxides (usually found with variable concentrations in boiler flue gas) which affects the reactivity of perovskite sorbents is another shortcoming of perovskite oxides for use as oxygen sorbent in Ceramic Auto-thermal Recovery (CAR) Process (Rosso, M., *et al.*, 2003). Development of a sorbent with Oxygen sorptive/desorptive properties to resolve these shortcomings can be a major step in practical use of Oxyfuel power generation technologies. Transition metal oxides like Cu provide a chance of oxygen absorption and desorption through their multi-valence property. Compared to perovskite oxides, the high oxygen sorption capacity (OSC) of CuO/Cu_2O equilibrium is an important advantage. Other than SrO and BaO that are carbonate forming oxides (Lin, Y.S., *et al.*, 2009), copper oxide has a high OSC (Figure 3.2). The high OSC provides a chance for the oxide to be deposited on a support to increase high temperature resistance when used in air separation. In addition, loading copper oxide on zirconia below a certain concentration has the advantage of stabilizing this high temperature resistant material (Dongare, M.K., 2002). Despite afore mentioned advantages, copper oxide has some disadvantages in the context of high temperature air separation, such as high sensitivity of reduction rate to oxygen partial pressure and low oxidation rate at higher temperature (Chadda, D., *et al.*, 1989). Yttria stabilization of zirconia has been reported to lower the reduction temperature of copper oxide by increasing oxygen vacancy

concentration in bulk and surface of the support (Dow, W.P. and Huang, T.J., 1994). Using yttria stabilized zirconia (YSZ) as a support has also been reported to increase the dispersion of CuO particles, however increasing the copper oxide loading above a certain limit (5% by weight) destabilizes YSZ into multiple phases leading to formation of Y-rich cubic and monoclinic zirconia. Oxygen partial pressure also affects this phenomenon (Ruiz-Morales, J., *et al.*, 2008) which can have its own implication when CuO-doped YSZ is used as oxygen sorbent in the CAR process. Ceria-stabilized tetragonal zirconia is another option for use as the support. Ceria stabilized zirconia (CSZ) has the advantage of possessing improved mechanical properties especially toughness (Sharma, S.C., *et al.*, 2002) that is a very important property in increasing the attrition resistance of the sorbents. In this chapter various loadings of CuO on zirconia, YSZ and CSZ are studied for their suitability in high temperature air separation.

5.2. Experimental Description

5.2.1. Sorbent Synthesis and Preparation

Citrate-gel method (Baythoun, M.S., 1982) was used to synthesize ZrO_2, $Zr(Y)O_2$ and $Zr(Ce)O_2$ loaded with 0.2, 0.3 and 0.4 molar ratios of CuO. In all samples doped with Yttria and Ceria, a Y or Ce to Zr ratio of 0.02 was used. $Cu(NO_3)_2.6H_2O$, $ZrO.(NO_3)_2.1H_2O$, $Y(NO_3)_3.6H_2O$, $Ce(NO_3)_3.6H_2O$ with 99.999% trace metals basis purity were used as precursor. Figure 5.1 outlines the Citrate gel synthesis method.

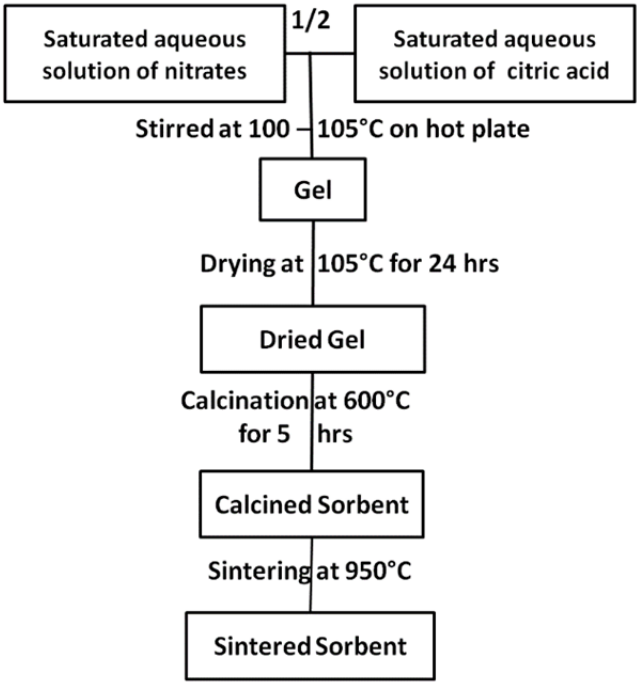

Figure 5.1. Citrate gel synthesis method

(Baythoun, M.S., 1982)

5.2.2. Morphology and Crystal Structure

The morphology of samples was investigated using scanning electron microscope (Hitachi S-2700) and the crystal structure was determined by X-ray diffraction (Rigaku rotating anode TTRAX III) with Cu-kα as the radiation. The X-ray diffraction patterns were refined using Siroquant® analysis software to determine the exact composition of the samples.

5.2.3. Particle Size distribution

A Malvern mastersizer® 2000 was used to measure the particle size distribution of the sorbents. The particles are passed through a focused laser beam. The particles scatter light at an angle that is inversely proportional to their size. The angular intensity of the scattered light is then measured by a series of photosensitive detectors and correlated to their size. Each measurement was repeated five times to consider for possible heterogeneity of the particles.

5.2.4. Oxygen sorption/desorption investigation by thermogravimetric analysis

Thermogravimetric analyses were done with a thermogravimetric analyzer (TGA) (SDT Q600). The analyzer consists of a stainless steel tube placed in a horizontal furnace which can be operated to temperature up to 1200°C; the analyzer is connected with a computer for continuous data recording. The instrument has two separate reactant gas inlets that can be operated automatically. Air and CO_2 were used as reactive gases for sorption and desorption process. In desorption study, samples (5-10 mg) were placed in platinum pans and heated to 1000°C with a heating rate of 5°C/min under a mixture of O_2 and CO_2. Desorption experiments were repeated under oxygen concentrations of 0.1%, 1%, 3% and 5% to study the effect of these parameters. The oxygen concentration in the purge gas was adjusted using mass flow controllers. After complete desorption, the gas was switched to air and the sample were heated to 1000°C with heating rates of 1, 2, 5,10 °C/min to study absorption. In order to reduce the diffusion effect between

the sample and bulk gas, sample pans were cut from the original 4 mm to about 0.5 mm deep, as recommended by (Ollero, P., *et al* 2002).

5.3. Results and Discussion

5.3.1. Morphology of the Sorbents

Figures 5.2, 5.3 and 5.4 show the backscattered scanning electron microscope micrograph of samples with 20%, 30% and 40% CuO loaded on ZrO_2, $Zr(Y)O_2$ and $Zr(Ce)O_2$ as support. In samples with 20% loading, the CuO particles are relatively fine and highly dispersed. In Yttria doped sample, no particle was observed at this magnification. By increasing CuO loading particles tend to coarsen, at 40% loading the support was fully covered by CuO particles and cracking of the support started. The same effect has been observed by others (Ruiz-Morales, J.C., *et al.*), however, their study was at a lower CuO loading and with different synthesis method. The higher dispersion of particles at higher CuO loading shows the positive effect that citrate gel synthesis has had on morphological features compared to solid state synthesis used in the previous works. The ceria doped samples are relatively denser, showing the promoting effect of CeO_2-ZrO_2 solid solution on sintering. Morphology and shape of CuO particles are also different, which can be explained by the solubility effect of CeO_2 in CuO as observed in use of CeO_2/CuO composite anodes in hydrocarbon solid oxide fuel cells (Lee, L., 2010). The solubility effect of CeO_2 in CuO can also have an advantage in improving the absorption/desorption kinetics by

increasing diffusion kinetics. Ceria has also been reported to be soluble in both ZrO_2 and Cu_2O (Linag, H., 2010). The solubility of CeO_2 in Zirconia and oxides of copper provides a bonding between the support and CuO/Cu_2O particles which can have an important effect on cyclical stability of the sorbents at high temperature.

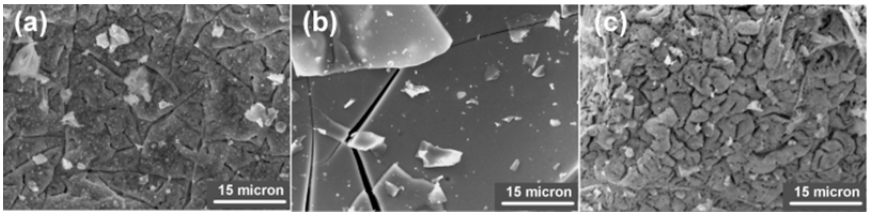

Figure 5.2. Backscattered electron micrograph of sorbents with 20% CuO loading, on a) ZrO_2, b) $Zr(Y)O_2$ and c) $Zr(Ce)O_2$

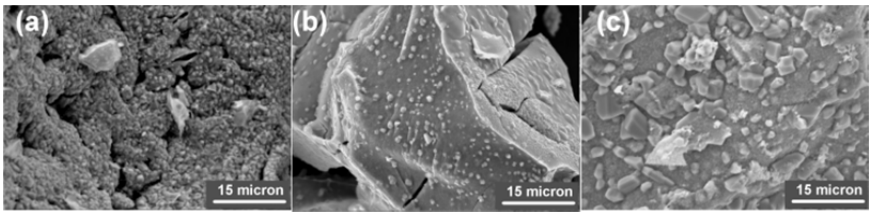

Figure 5.3. Backscattered electron micrograph of sorbents with 30% CuO loading, on a) ZrO_2, b) $Zr(Y)O_2$ and c) $Zr(Ce)O_2$

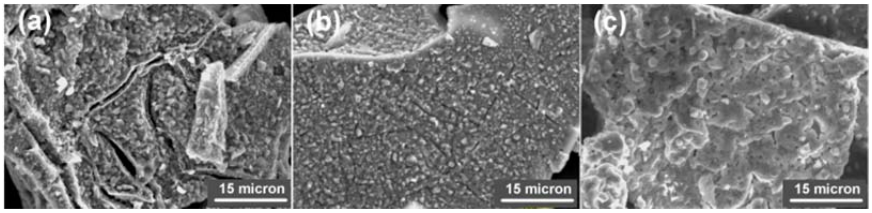

Figure 5.4. Backscattered electron micrograph of sorbents with 40% CuO loading, on a) ZrO_2, b) $Zr(Y)O_2$ and c) $Zr(Ce)O_2$

5.3.2. Particle Size Distribution

Figure 5.5 shows the particle size distribution of the synthesized samples. The samples with 20% CuO show a relatively narrower distribution with a $d_{(50)}$ around 100 μm. The samples with higher CuO loading have a broader particle size distribution. The broader particle size distribution can be due to the separation of copper oxide particles from the support and attrition of the sorbents as observed in the SEM micrographs.

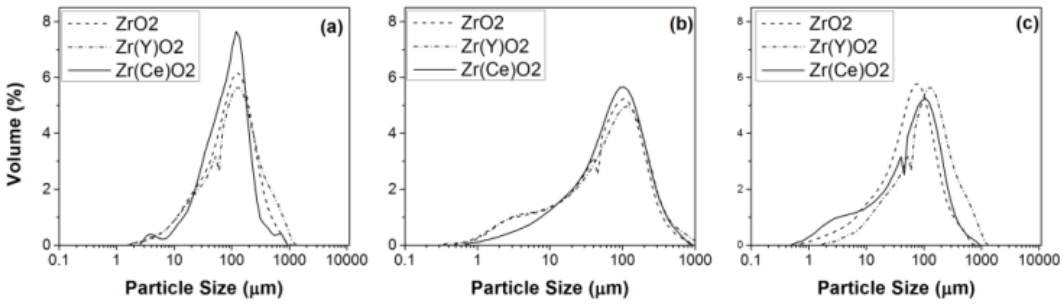

Figure 5.5.Particle size distribution of sorbents with a) 20% CuO, b) 30% CuO and c) 40% CuO

5.3.3. Crystal Structure Analysis of the Sorbents

Figure 5.6 shows the X-ray diffraction pattern of samples with 20% CuO loading. The sample doped with yttria showed significantly different structure compared to the other two samples. The major phase in this sample is yttria stabilized zirconia with tetragonal structure. In the other two samples zirconia with monoclinic structure is observed. In the yttria doped sample, the CuO peaks are more broadened representing the finer crystallite size of this compared to other samples. Addition of ceria has not significantly affected the crystal structure of the zirconia phase and only trace amount of ceria is detectable in the sorbent containing ceria. The intensity of all peaks is however greater in the ceria doped sample showing the effect that this compound has had on the sintering behavior of the sample as mentioned in the previous section. A comparison of the three patterns shows the overlap of peaks of the available phases. The overlap of peaks makes quantitative analysis using Rietveld refinement impossible. Figure 5.7 shows the same patterns for samples with 30% CuO loading. The ZrO_2 and $Zr(Ce)O_2$ samples show the same type of crystalline phases however the $Zr(Y)O_2$ sample's behavior was different compared to the previous case. Two types of zirconia phases exist in this sample: A Y-rich tetragonal zirconia and the monoclinic zirconia. The existence of multiple Zirconia phases can be explained by the instability effect of copper oxide on yttria stabilized zirconia as already reported by other authors (Ruiz-Morales, J. *et al.*, 2008). At this copper concentration, formation of compounds

like CuY_2O_5 is also expected (Zhang,W. and Osamura, K.), however they're difficult to observe at this resolution.

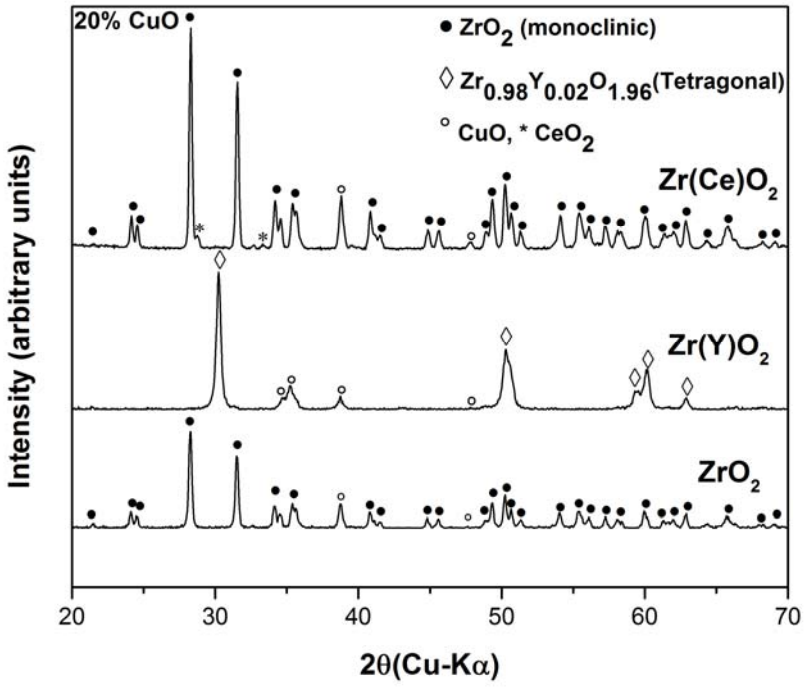

Figure 5.6. X-ray diffraction pattern of sorbents with 20% CuO

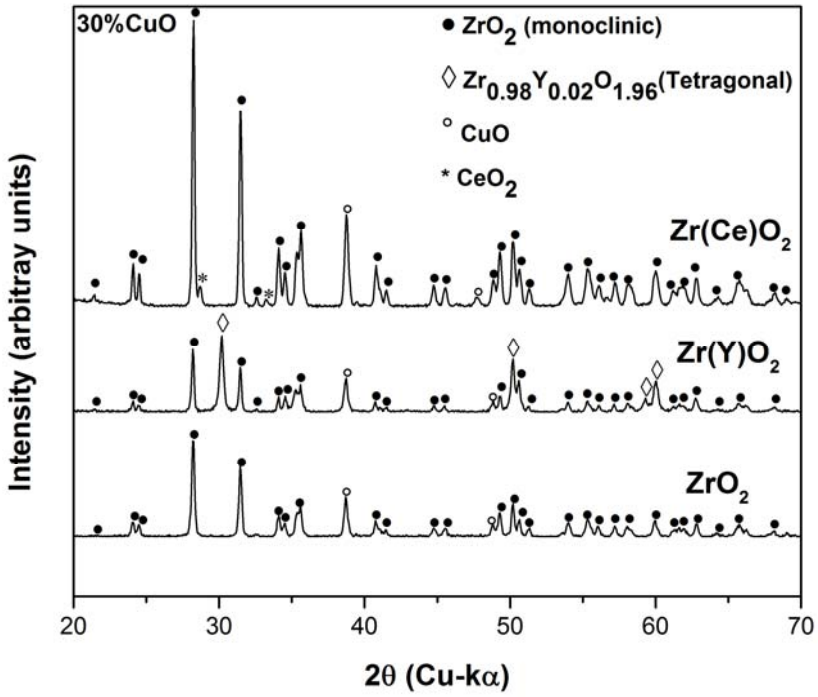

Figure 5.7. X-ray diffraction pattern of sorbents with 30% CuO

Figure 5.8 shows the patterns for samples doped with 40% CuO. No significant change is detectable compared to the samples with 30% CuO other than finer CuO peak widths and higher intensities which is due to coarsening of the CuO particles as observed in the SEM micrographs in Figures 5.2 to 5.4.

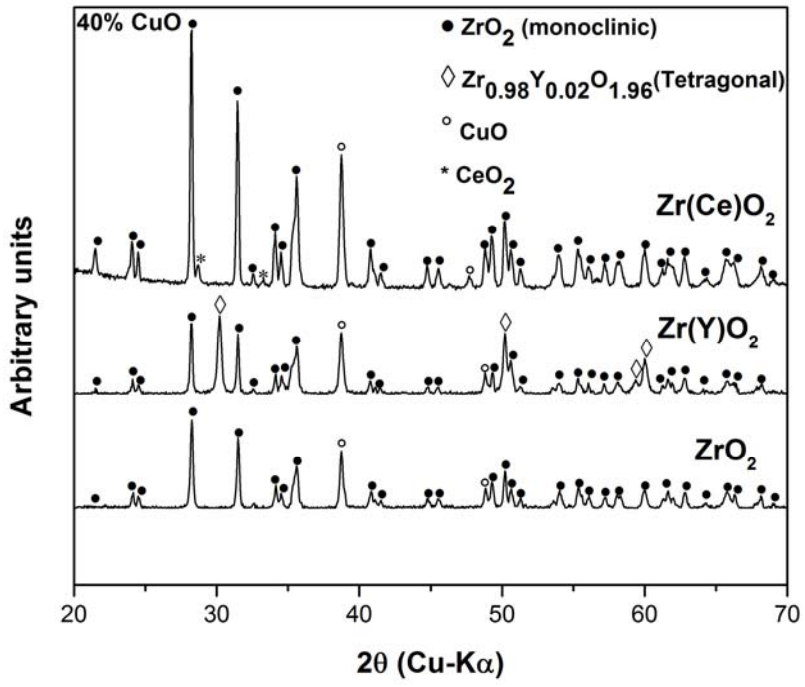

Figure 5.8. X-ray diffraction pattern of sorbents with 40% CuO

5.3.4. Oxygen desorption behavior of the Sorbents

Figures 5.9, 5.10 and 5.11 respectively compare the oxygen desorption behavior of samples with 20%, 30% and 40% CuO loading over a range of temperature under CO_2 atmosphere containing 0.1-5% Oxygen. These tests were performed under a total flow rate of 250 ml/min and a heating rate of 2.5°C/min. In nearly all samples and at oxygen concentrations lower than 5%, the major weight loss occurring above 750°C is preceded by a weight loss of with constant slope which can be due to desorption of surface or nonstoichiometric oxygen species available in the sorbents. The sorbents with ceria stabilized support tend to have a higher desorption onset temperature compared to the sorbents with zirconia and yittria

stabilized zirconia support. The higher desorption onset temperature of ceria stabilized zirconia sorbents is due to higher size of CuO particles as observed in the SEM micrographs shown in Figures 5.2 to 5.4. The difference observed between sorbents with ZrO_2 and $Zr(Y)O_2$ is less significant in these graphs.

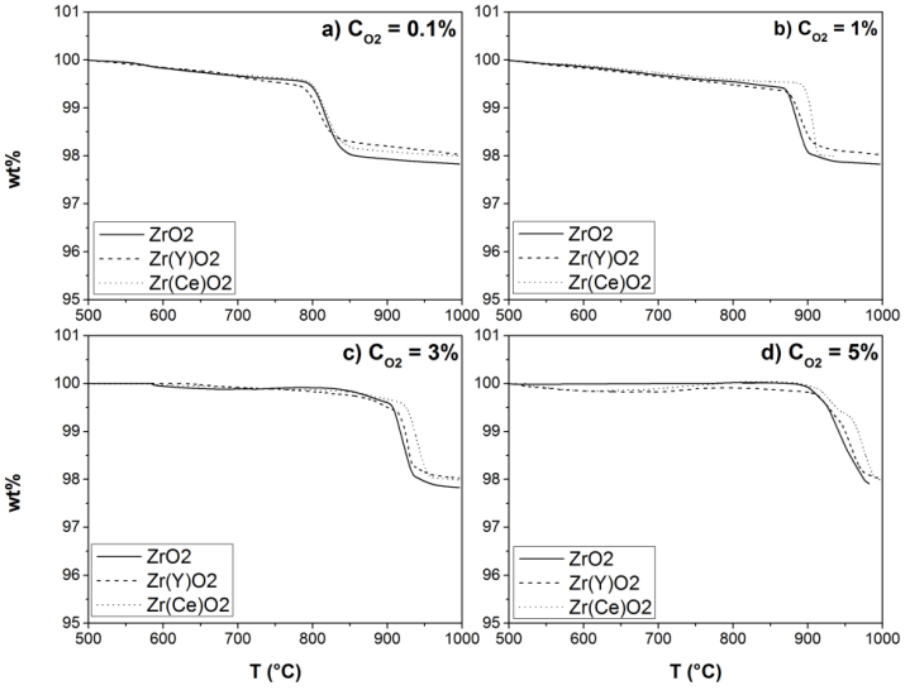

Figure 5.9. TG desorption curves of sorbents with 20% CuO

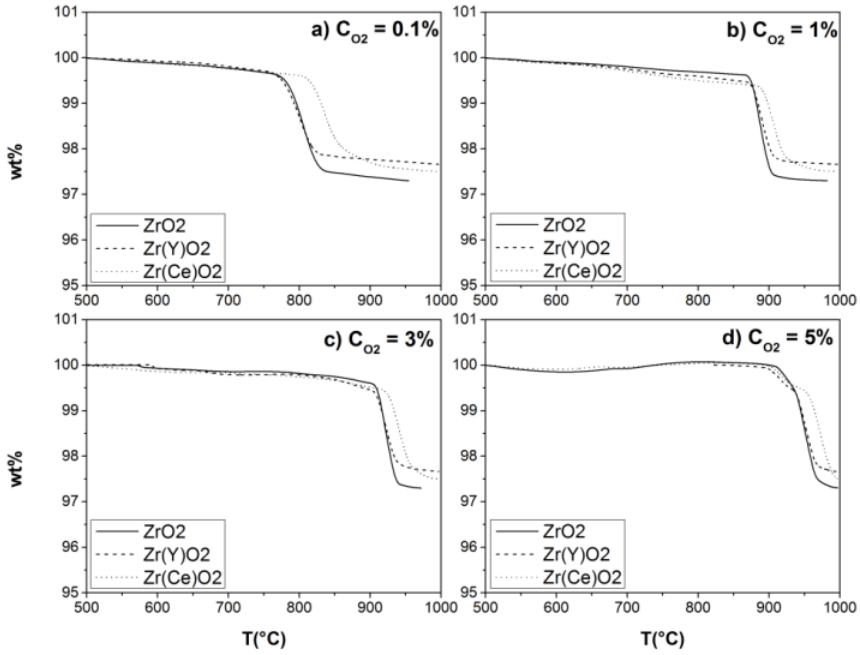

Figure 5.10. TG desorption curves of sorbents with 30% CuO

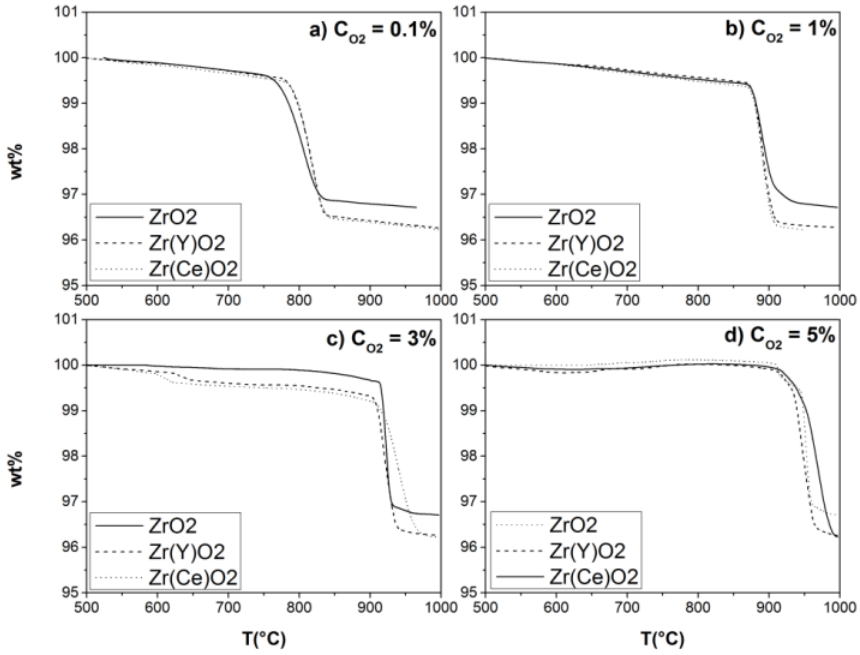

Figure 5.11. TG desorption curves of sorbents with 40% CuO

Conversion, X, is defined as:

$$X = \frac{w_0 - w_t}{w_0 - w_f}$$ (Eqn. 5.1 (Brown, M.E. and Gallagher, P. K., 2008))

Where w_0, w_t and w_f are initial weight, weight at time t and final weight of the sample. The conversions were fitted by smoothing spline to calculate the conversion rate which is shown for different samples as a function of temperature in Figures 5.12 to 5.14.

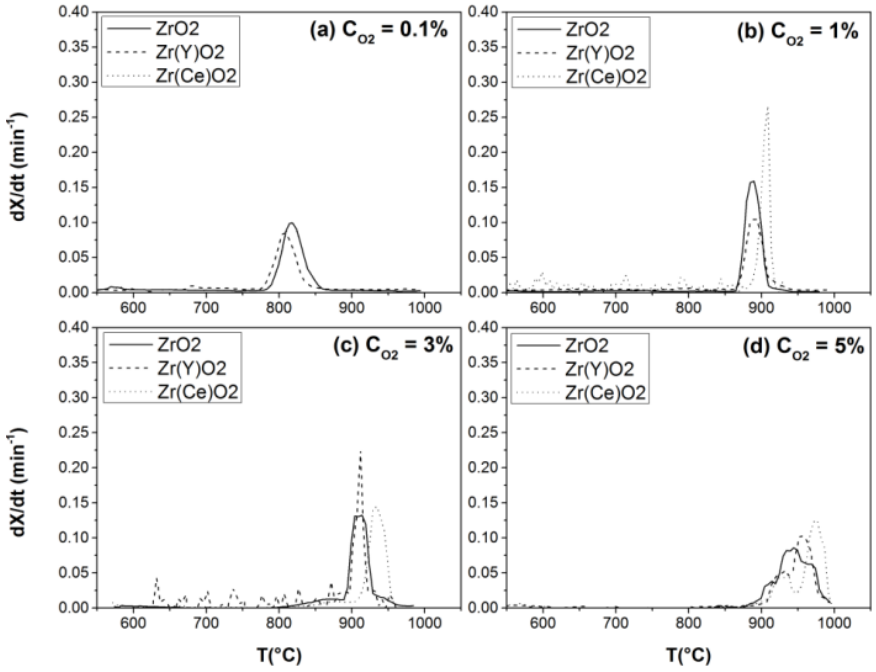

Figure 5.12. Desorption rate behavior of sorbents with 20% CuO under a) 0.1%, b) 1%, c) 3% and d) 5% oxygen mixed with CO_2 as the major component

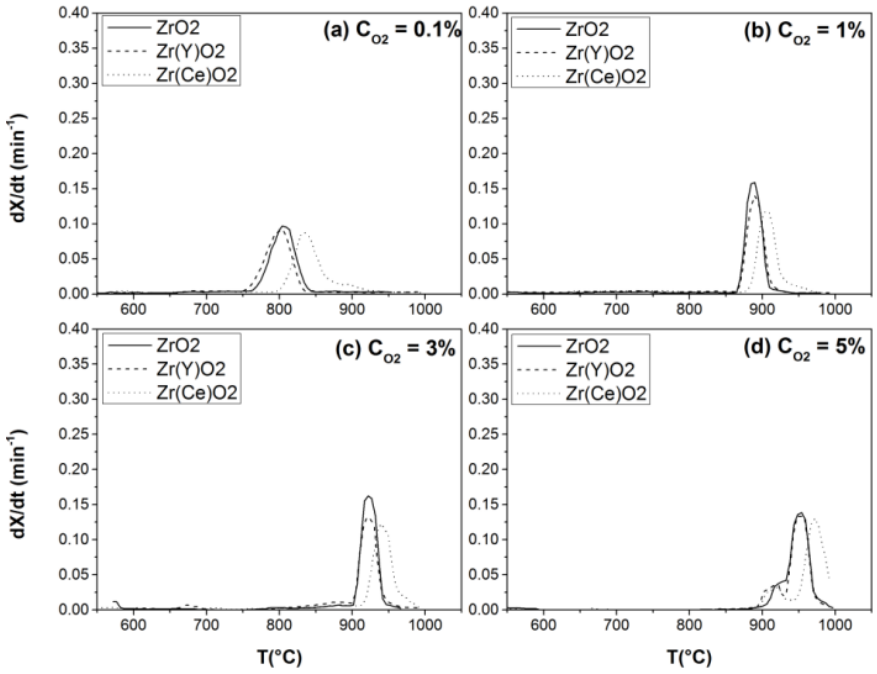

Figure 5.13. Desorption rate behavior of sorbents with 30% CuO under a) 0.1%, b) 1%, c) 3% and d) 5% oxygen mixed with CO_2 as the major component

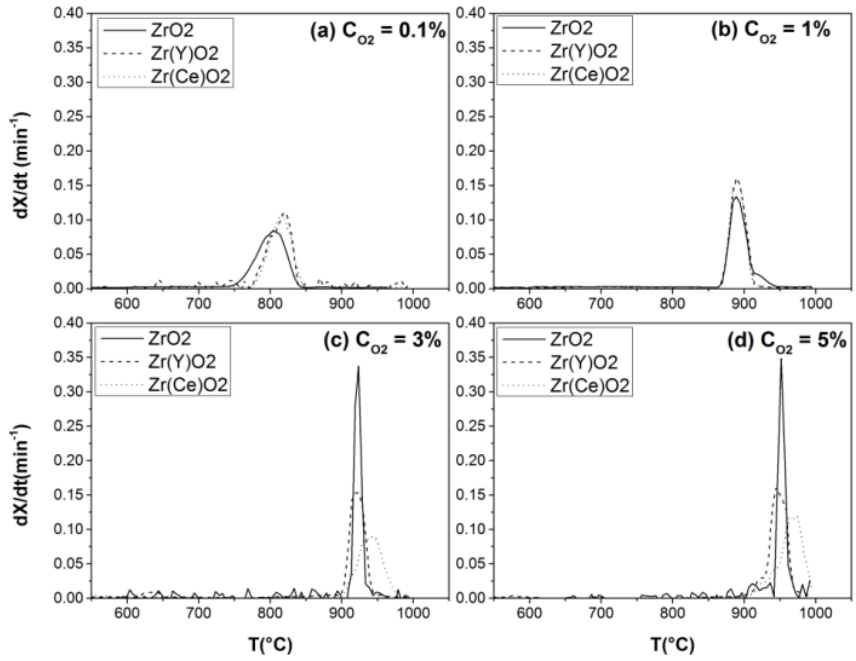

Figure 5.14. Desorption rate behavior of sorbents with 40% CuO under a) 0.1%, b) 1%, c) 3% and d) 5% oxygen mixed with CO_2 as the major component

The above data was used to calculate the activation energy (Q_{des}) and rate constant ($k_{0,des}$) in the following equation that describes the kinetics of the desorption process:

$$\frac{dX_{des}}{dt} = k_{0,des} \exp\left(-\frac{Q_{des}}{RT}\right)\left(1-\frac{P_{O2}^{eq}}{P_{O2}}\right)^{0.6}\left(1-X_{des}\right)\left(-\ln\left(1-X_{des}\right)\right)^{2/3}$$

(Eqn. 5.2 (Brown, M.E. and Gallagher, P. K., 2008))

P_{O2}^{eq}, the equilibrium oxygen partial pressure in the CuO/Cu_2O system was obtained from FACTSage®. The Friedman method (Brown, M.E. and Gallagher,

P. K., 2008) was used to calculate the rate equation constants. These values are listed in Table 5.1 and plotted in Figure 5.15 The stabilization by yttria and ceria addition did not have a significant effect on desorption kinetics. The $Zr(Y)O_2$-20CuO was the only sample with single phase tetragonal support, and showedthe lowest activation energy. The low desorption activation energy of the sorbent with single phase tetragonal support is in agreement with the results reported by (Kundakovic, L., *et al.*, 1998) where the tetragonal support had been shown to reduce the reduction temperature and increasing the rate of oxygen evolution. In all the samples, the activation energy increased with CuO loading. The increase of desorption activation energy with CuO loading can be due to the agglomeration effect that occurs when the copper oxide content goes above 20%.

Table 5.1. Desorption equation parameters of different samples

Sample	$k_{0,des}$	Q_{des} (kJ/mol)
ZrO_2-20CuO	$1.91(\pm0.01) \times 10^7$	181 ± 3
ZrO_2-30CuO	$8.19 (\pm0.21) \times 10^8$	221 ± 2
ZrO_2-40CuO	$9.57 (\pm0.32) \times 10^8$	224 ± 8
$Zr(Y)O_2$-20CuO	$8.03 (\pm0.3) \times 10^9$	240 ± 7
$Zr(Y)O_2$-30CuO	$1.47 (\pm0.36) \times 10^7$	182 ± 11
$Zr(Y)O_2$-40CuO	$4.42 (\pm5.97) \times 10^7$	196 ± 2
$Zr(Ce)O_2$-20CuO	$3.31 (\pm0.67) \times 10^7$	186 ± 5
$Zr(Ce)O_2$-30CuO	$1.06 (\pm0.02) \times 10^8$	201 ± 3
$Zr(Ce)O_2$-40CuO	$5.89 (\pm0.03) \times 10^8$	220 ± 7

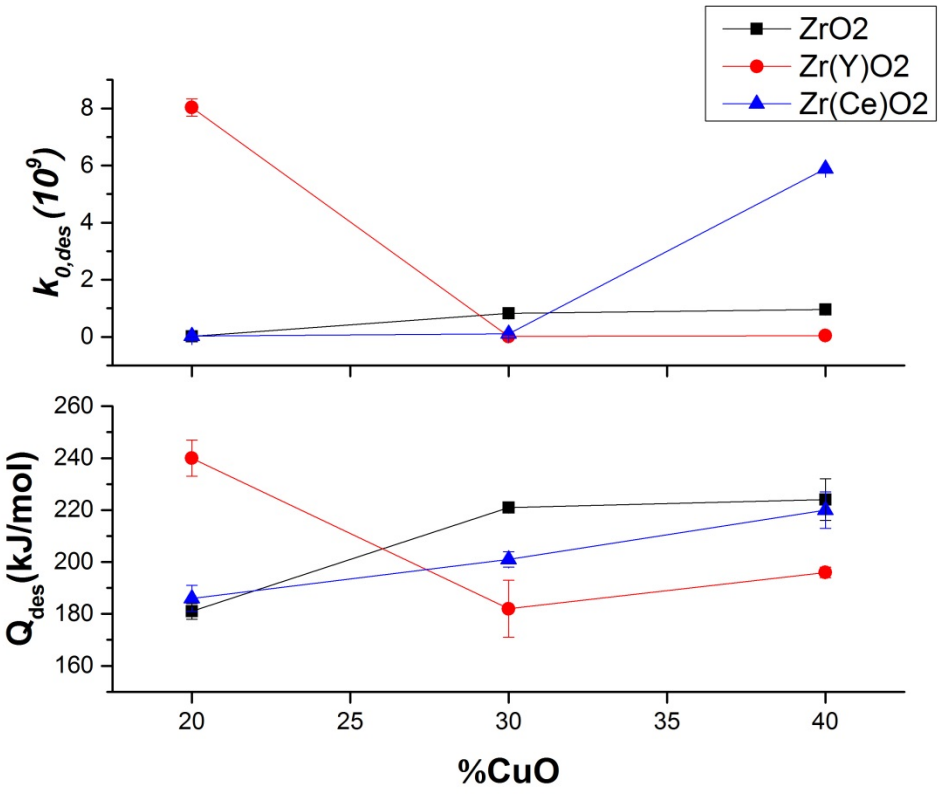

Figure 5.15. Dependence of desorption kinetic parameters of copper oxide-doped zirconia samples on CuO content

5.3.5. Oxygen absorption behavior of the sorbents

Figures 5.16, 5.17 and 5.18 compare the oxygen absorption behavior of samples with 20%, 30% and 40% CuO loading, respectively, over a range of temperatures under an air flow rate of 250 ml/min with different heating rates (β).

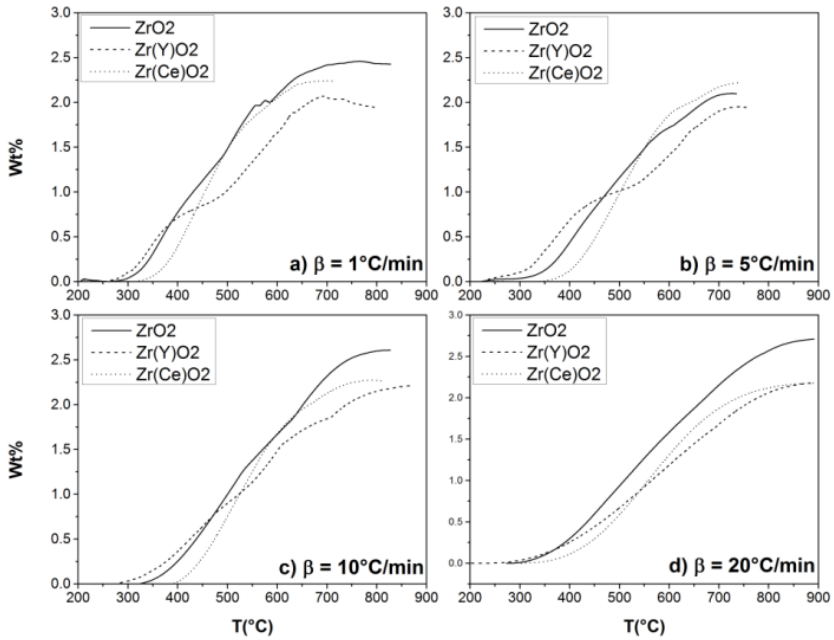

Figure 5.16. TG absorption curves of sorbents with 20% CuO

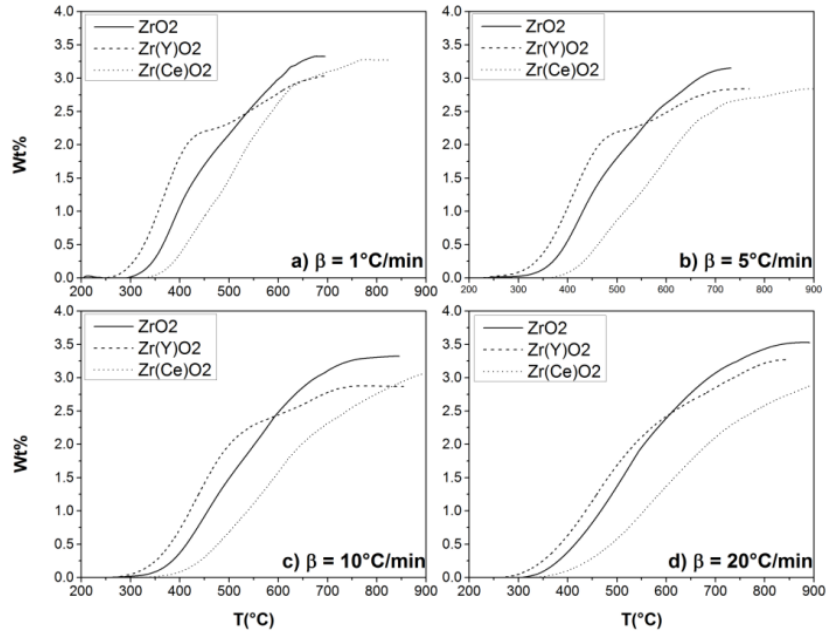

Figure 5.17. TG absorption curves of sorbents with 30% CuO

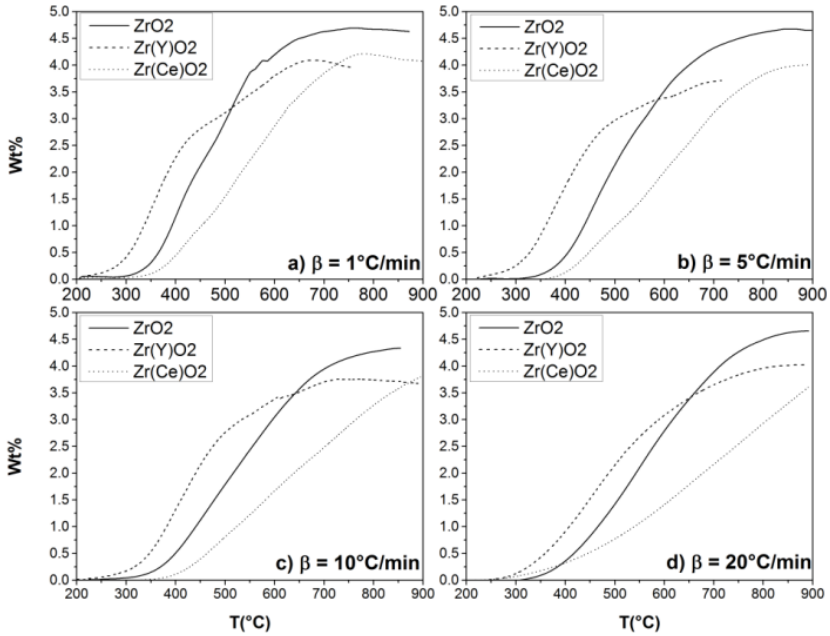

Figure 5.18. TG absorption curves of sorbents with 30% CuO

Conversion, *X*, is defined as:

$$X = \frac{w_t - w_0}{w_f - w_0}$$ (Eqn. 5.3 (Brown, M.E. and Gallagher, P. K., 2008))

Where w_0, w_t and w_f are initial weight, weight at time t and final weight of the sample. The conversions were fitted by smoothing spline to calculate the conversion rate which is shown for different samples as a function of reaction temperature (Figures 5.19, 5.20 and 5.21). It is readily observed that multistage reaction is followed. This can be explained by formation of a CuO layer on Cu_2O particles and its limiting effect on oxygen diffusion. At 20% copper loading,

samples with $Zr(Ce)O_2$ as the support show a higher rate compared to the other samples which can be explained by the positive effect of ceria in oxygen diffusion through the CuO layer. At higher copper content, this effect is limited and the ceria containing samples have a lower absorption rate compared to the other samples.

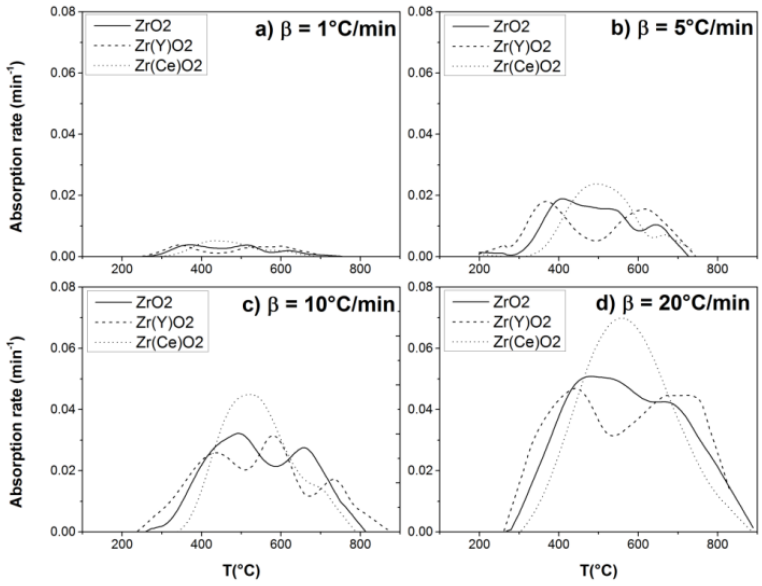

Figure 5.19. Oxygen absorption rate of sorbents with 20% CuO under different heating rate

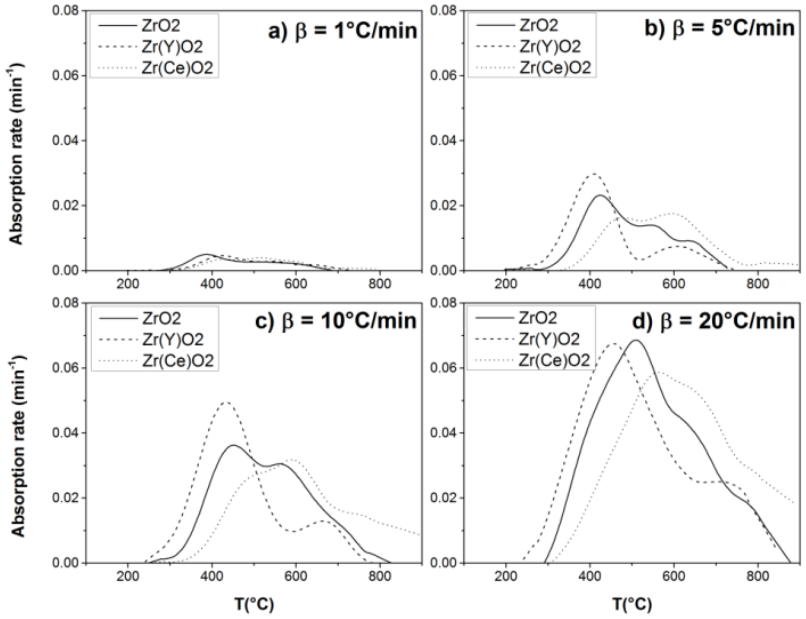

Figure 5.20. Oxygen absorption rate of sorbents with 30% CuO under different heating rate

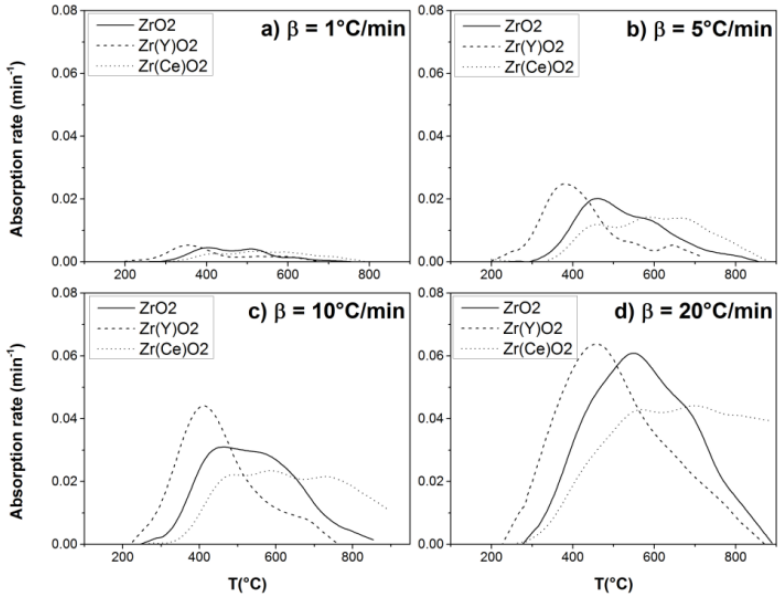

Figure 5.21. Oxygen absorption rate of sorbents with 40% CuO under different heating rate

The complexity of the absorption process necessitates the use of a model free kinetic analysis. To do this, a direct Arrhenius plot of ln (rate) vs. reciprocal of temperature was used to calculate the pre-exponential factor ($k_{0,\,abs}$) and activation energy (Q_{abs}) which are listed in Table 5.2. The absorption activation energy increases with copper oxide loading which shows the effect that CuO dispersion has on the rate of the reaction. The sorbents doped with yttria and ceria show a relatively lower activation energy which can be due the effect that dissolution of these compounds have on the diffusion of oxygen in CuO layer around Cu_2O particles.

Table 5.2. Absorption equation parameters of different samples

Sample	$k_{0,abs}$	Q_{abs}(KJ/mol)
ZrO_2-20CuO	$2.09(\pm0.67) \times 10^7$	114 ± 2
ZrO_2-30CuO	$9.51(\pm0.18) \times 10^8$	150 ± 8
ZrO_2-40CuO	$1.24(\pm0.76) \times 10^8$	160 ± 3
Zr(Y)O_2-20CuO	$1.04(\pm0.09) \times 10^9$	111 ± 1
Zr(Y)O_2-30CuO	$8.08(\pm0.04) \times 10^8$	147 ± 6
Zr(Y)O_2-40CuO	$1.78(\pm0.33) \times 10^9$	151 ± 1
Zr(Ce)O_2-20CuO	$1.02(\pm0.89) \times 10^8$	106 ± 6
Zr(Ce)O_2-30CuO	$9.42(\pm0.42) \times 10^8$	144 ± 4
Zr(Ce)O_2-40CuO	$3.59(\pm0.99) \times 10^{10}$	157 ± 8

5.3.6. Cyclical Stability of the Sorbents

Long-term stability of sorbents is of great importance in high temperature air separation process. All the synthesized sorbents were tested at 900°C under an atmosphere containing 97% CO_2 and 3% O_2 as the purge gas for a period of 8 hrs. The sorption and desorption time for all samples were chosen as 5 and 15 minutes

respectively. The multiple-cycle tests were ended with desorption step and the samples were collected for examination with micrograph. Figures 5.22, 5.23 and 5.24 show the multiple sorption/desorption cycles of the samples with 20, 30 and 40% CuO loading, respectively as change in weight percent. All sorbents show a stable behavior in cyclic sorption/desorption.

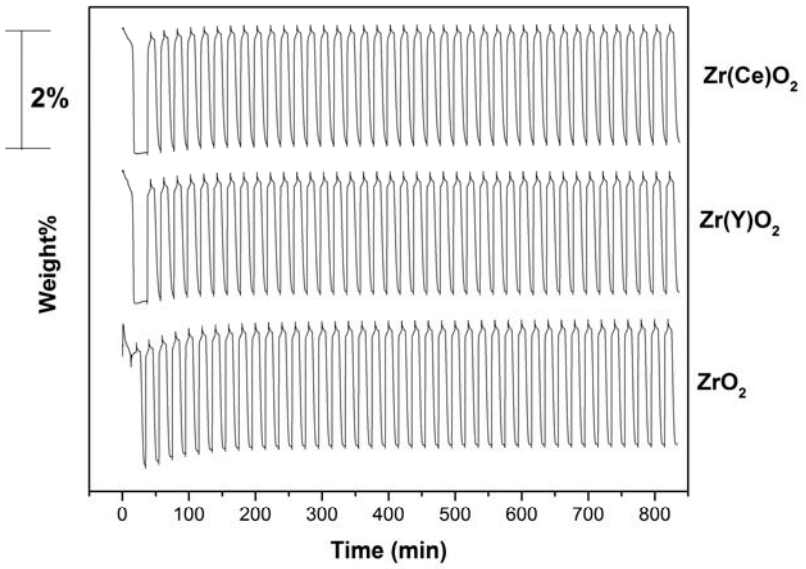

Figure 5.22. Multiple sorption/desorption cycles at 900°C under 97% CO_2/3% O_2 atmosphere of sorbent with 20% CuO

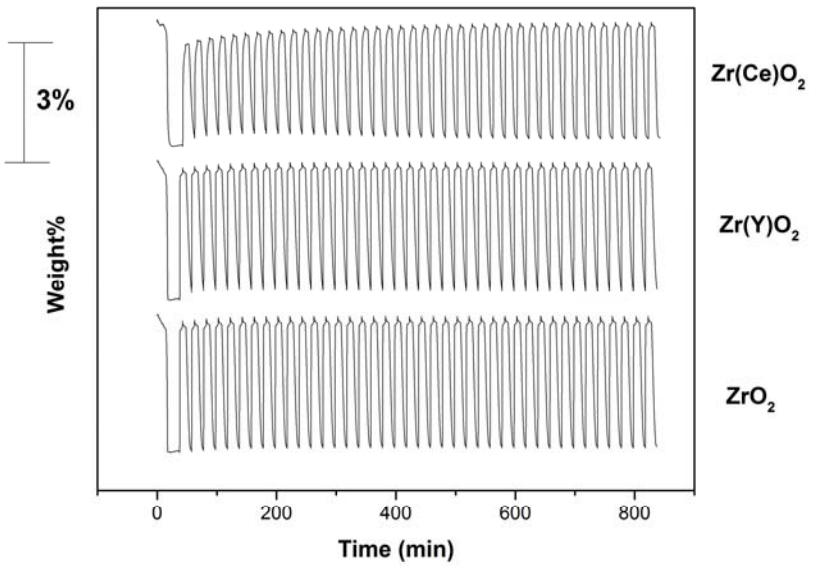

Figure 5.23. Multiple sorption/desorption cycles at 900°C under 97% CO_2/3% O_2 atmosphere of sorbent with 30% CuO

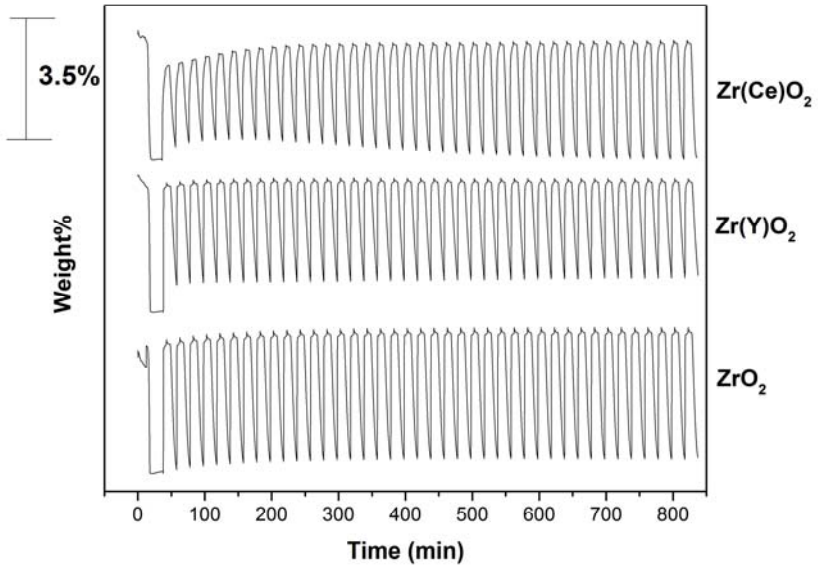

Figure 5.24. Multiple sorption/desorption cycles at 900°C under 97% CO_2/3% O_2 atmosphere of sorbent with 40% CuO

All sorbents were examined by SEM after the cyclic tests, the micrographs of which are shown in Figure 5.25 to 5.27.

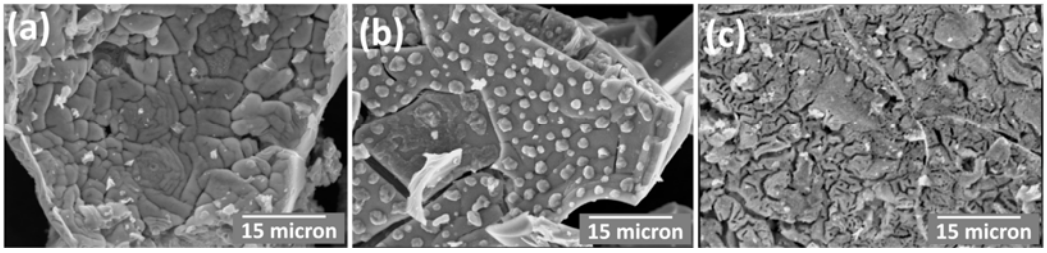

Figure 5.25. Backscattered electron micrograph of sorbents with 20% CuO loading, on a) ZrO_2, b) $Zr(Y)O_2$ and c) $Zr(Ce)O_2$ after multiple sorptive/desorptive cycles at 900°C

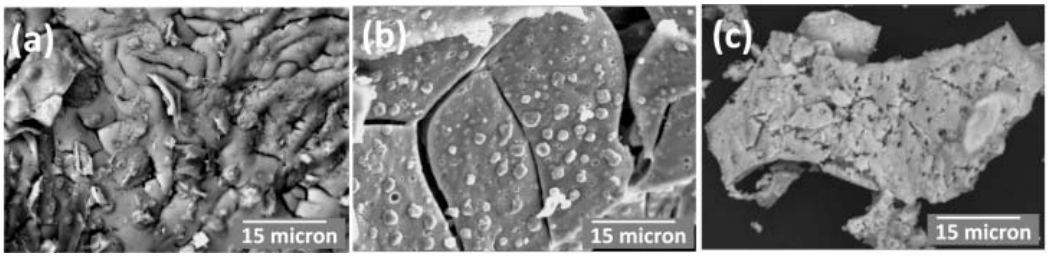

Figure 5.26. Backscattered electron micrograph of sorbents with 30% CuO loading, on a) ZrO_2, b) $Zr(Y)O_2$ and c) $Zr(Ce)O_2$ after multiple sorptive/desorptive cycles at 900°C

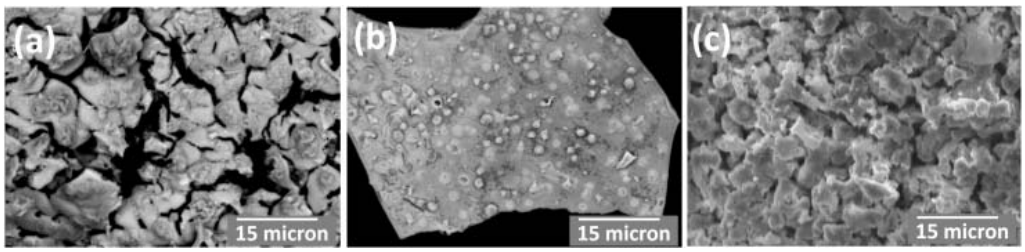

Figure 5.27. Backscattered electron micrograph of sorbents with 40% CuO loading, on a) ZrO_2, b) $Zr(Y)O_2$ and c) $Zr(Ce)O_2$ after multiple sorptive/desorptive cycles at 900°C

In all sorbents, there were significant changes in morphology compared to the as-synthesized samples shown in Figures 5.2 to 5.4. In sorbents with ZrO_2 as the support, the densification was more significant and a weaker atomic number contrast was observable between the particles and the support. The weaker atomic number contrast observed between the CuO particle and the support can be due to partial solubility between the copper oxide and zirconia under reducing condition (Kundakovic, L., *et al.*, 1998). To verify the partial solubility between copper oxide and zirconia, the ZrO_2 supported sorbents were heated up to 900°C under reducing conditions (97%CO_2, 3%O_2) and held for 15 minutes and the morphology of the samples were examined again which are shown in Figure 5.27.

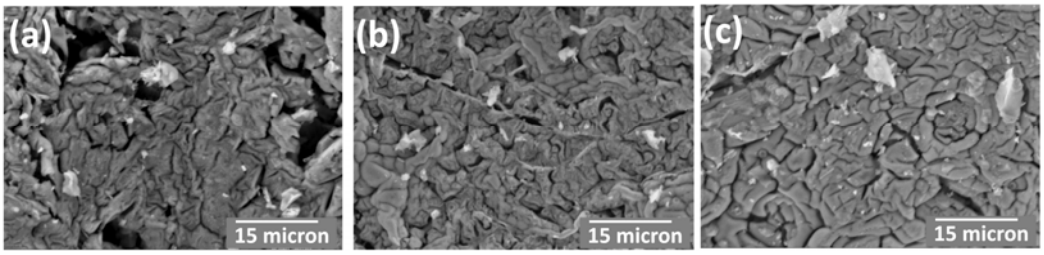

Figure 5.28. Morphology of samples with a) 20%, b) 30% and c) 40% CuO on ZrO_2 after one desorption cycle at 900°C

It is clearly seen that the change in morphology was highly similar to the one shown for the same samples in Figures 5.25, 5.25 and 5.27. In the sample with 40% CuO however cracks and pores have been developed which can be due to the cyclic shrinkage/expansion as a result of CuO/Cu_2O transformation. The sorbents with Zr(Y)O_2 support show a significant growth in CuO particle size. The growth in CuO particle size can lead to attrition and detachment of the CuO particles from the support and has negative effect on the stability of the sorbents. In the sorbents with Zr(Ce)O_2 as support, scattered pores and cracks are developed but the change in morphology was not significant.

5.4. Copper Oxide vs. Perovskite based sorbents

Kinetics of oxygen desorption is a controlling parameter in use of these sorbents in high temperature air separation. Figure 5.29 compares the desorption rate at half length of the reaction for the sorbents based on copper oxide. For perovskite

based sorbents under these conditions (T=800°C, P_{O2}= 0.04 atm), the rate of reaction is very low and no oxygen can be generated.

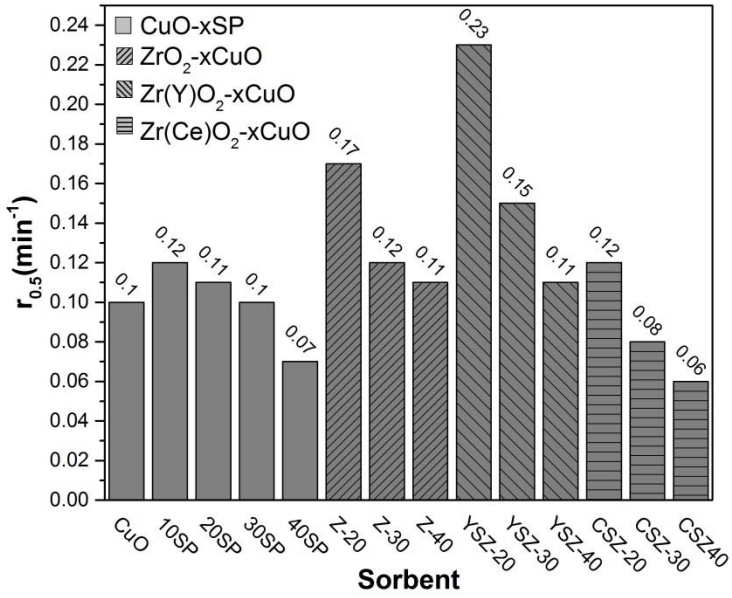

Figure 5. 29. Comparison of desorption rate of different samples at 50% of the reaction at 800°C and P_{O2} = 0.04 atm

The significantly higher oxygen sorption capacity (≈ 3-4 times in mmol/g) of copper oxide compared to perovskite and spinel-perovskite oxides can contribute greatly in reducing the bed size and energy requirements of air separation system. Neutrality to flue gas species (especially oxygen) avoids the need for flue gas treatment before using it as sweep gas for supplying oxygen to the boiler. Its main disadvantages i.e. low desorption rate and high temperature instability have been improved by doping with alumina and by using zirconia-based supports. Figure 5.30 compares the oxygen sorption capacity of different oxides synthesized and studied in this work. Figure 5.31 compares the amount of sorbent required for production of 1 ton per hour of oxygen with a bed temperature of 800°C and three

cycles per hour based on 5 minute absorption and 15 minute desorption cycles (which were found to have been stable and achievable in this work).

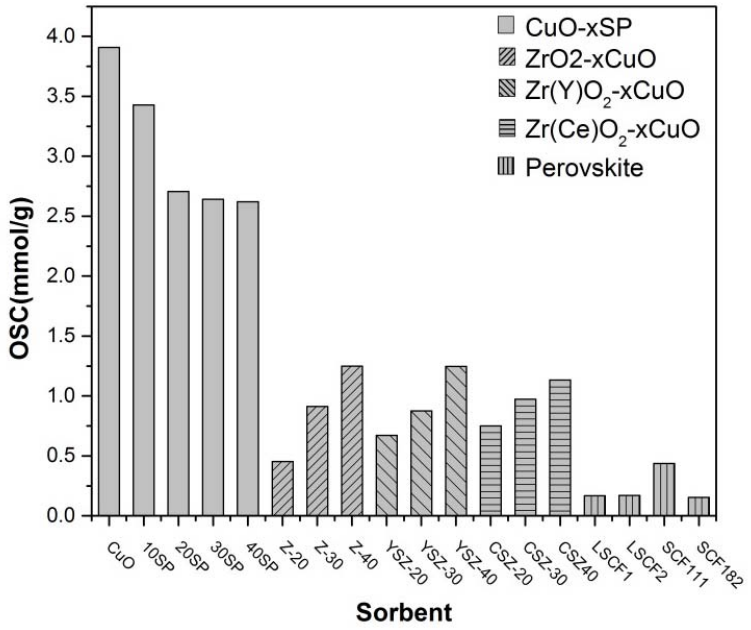

Figure 5. 30. Comparison of oxygen sorption capacity of different sorbents

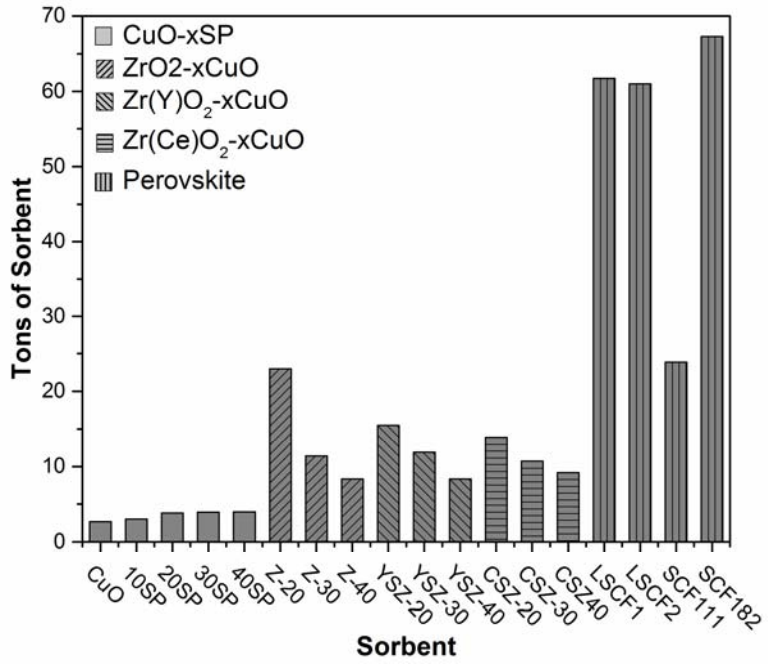

Figure 5. 31. Tons of sorbent required for production of 1 ton/hr of oxygen at 800°C

Table 5.3 shows the calculation steps of these values using the sorption capacities in the specified time periods and temperature for producing 1 ton/hr of oxygen. For perovskite and perovskite/spinel sorbents, due to high sensitivity that both oxygen sorption capacity and oxygen desorption rate have on the oxygen partial pressure the oxygen generating gas stream (0.04 atm used in the desorption stage of the multiple cycle tests used in this work), the OSC measured CO_2 with oxygen partial pressure of 0.00001 have been used in the calculations.

Table 5. 3. Procedure for calculation of the amount of sorbent required for generation of 1 ton/hr of oxygen at T = 800°C and P_{O2} = 0.04 atm

Sample	W_i (mg)	W_f(mg)	$OSC = \frac{(W_f - W_i)/32}{W_i} \times 10^3$	$W_{Sorbent} = \frac{10^3}{32\times3\times OSC}$ (ton)
CuO	5.14	5.78	3.91	2.67
CuO-10$CuAl_2O_4$	6.12	6.80	3.43	3.04
CuO-20$CuAl_2O_4$	7.11	7.73	2.71	3.85
CuO-30$CuAl_2O_4$	9.13	9.90	2.64	3.95
CuO-40$CuAl_2O_4$	4.13	4.47	2.62	3.98
ZrO_2-20CuO	5.15	5.22	0.45	22.98
ZrO_2-30CuO	6.12	6.30	0.91	11.42
ZrO_2-40CuO	7.13	7.41	1.25	8.34
Zr(Y)O_2-20CuO	9.84	10.05	0.67	15.49
Zr(Y)O_2-30CuO	7.42	7.62	0.88	11.90
Zr(Y)O_2-40CuO	6.13	6.38	1.25	8.35
Zr(Ce)O_2-20CuO	6.13	6.27	0.75	13.88
Zr(Ce)O_2-30CuO	6.84	7.05	0.97	10.70
Zr(Ce)O_2-40CuO	9.14	9.47	1.13	9.20
LSCF1	7.12	7.16	0.17	61.73
LSCF2	7.15	7.19	0.17	60.99
SCF111	4.15	4.21	0.44	23.87
SCF182	5.27	5.30	0.15	67.27

5.5. Conclusion

The conclusions derived from the results presented in this chapter can be summarized as follows:

1. Use of ZrO_2 and stabilized $Zr(Y)O_2$ and $Zr(Ce)O_2$ as high temperature resistant supports for CuO improves performance of candidate sorbents for high temperature air separation. The high temperature Stability decreases by increasing the copper loading. 20wt% copper oxide content is the limit for destabilization of the support. Sorbents at this copper content still have a higher oxygen sorption capacity (1.5 times) than the perovskite and perovskite spinel oxides and higher oxygen desorption kinetics.
2. Addition of yttria does not have a significant effect on oxygen sorption kinetics while improving desorption for sorbents with copper loading below 20%. Addition of ceria improves the sorption kinetics by increasing the oxygen diffusion rate through CuO layers formed around Cu_2O particles during the oxidation stage. However, this solubility effect leads to destabilization of the support in sorption/desorption cycles.
3. Yttrium doping improves dispersion of CuO on the support therefore leading to higher desorption rates. Yttria doping also prevents the agglomeration of Cu_2O particles in desorption cycles making the rate of desorption and absorption stable over long timer periods.

4. For copper oxide loading lower than 20%, addition of yttria improves the cyclic stability of the sorbents. The tetragonal structure of YSZ has a higher compatibility with the structural change in CuO/Cu_2O transformation therefore prevents the detachment of copper oxide particles form the support and increasing the attrition resistance of the sorbent.

Chapter 6: Conclusion and Recommendations

6.1. Conclusions

6.1.1. Dual Phase Sorbents

Dual phase sorbents with spinel/perovskite structures provide improvements over single phase perovskite sorbents. Increase in oxygen sorption capacity and at the same time desorption rate is a considered an important advantage over the original perovskite oxide. In dual phase sorbents, no Lanthanum is used which can most likely reduce the cost of the sorbent for large scale production since Lanthanum is very expensive. The dual phase sorbent had a lower CO_2 uptake therefore reducing the CO_2 emission in the absorption stage.

6.1.2. Copper Oxide as Oxygen Sorbent

Higher oxygen sorption capacity, neutrality to gas species in untreated flue gas, and lower cost are the main reasons for using CuO as an alternative to nonstoichiometric perovskite and perovskite/spinel oxides for high temperature air separation. The oxygen sorption capacity in nonstoichiometric oxide is highly sensitive to the difference between oxygen partial pressure in the air and the sweep gas while in copper oxide no such dependence exists and the weight change in CuO/Cu_2O equilibrium is independent of oxygen partial pressure provided the thermodynamic condition, temperature, is satisfied. The rate of oxygen desorption however decreases with increases in oxygen partial pressure in the purge gas requiring use of temperatures higher than 850°C depending on the oxygen content.

6.1.3. Effect of Synthesis Method on CuO as Oxygen Sorbent

Synthesis route is an effective method for improving the oxygen desorption rate from CuO. The citrate gel method proved to be the most effective method for the purpose of oxygen sorbent synthesis. Cu_2O content and O/Cu ratio in the surface are the factors through which the synthesis methods affect the desorption rate.

6.1.4. Effect of Doping with Alumina

Addition of alumina up to 30 mole percent increases the oxygen sorptive/desorptive properties of copper oxide. These include the rate of oxygen desorption and cyclic stability at high temperatures (>= 900°C). This improvement is the result of formation of $CuAl_2O_4$ phase and its effects on thermodynamics and kinetics of oxygen absorption and desorption. The presence of such a higher melting point compound also increases the sintering temperature of the material making a more suitable choice for high temperature processes like CAR and CLC.

6.1.5. Zirconia-based Oxides as Support for CuO

Yttria stabilized zirconia was shown to be a support with high cyclic stability for up to 20 wt% copper oxide loading. Improvement in oxygen desorption kinetics, cyclic stability and attrition resistance makes it a candidate for use in high temperature air separation and chemical looping with oxygen uncoupling.

6.1.6. CuO-based oxides vs. Perovskite based Oxides

The higher sorption capacity and oxygen desorption rate of the CuO-based oxides compared to those of the perovskite-based oxides provide a major advantage for use of these materials as oxygen sorbent in high temperature air separation. Depending on the CuO content, oxygen content of the sorbents can reach to values one order of magnitude higher than that of perovskite oxides. The higher oxygen desorption rate of CuO-based oxide makes use of recycled flue gas with oxygen content up to 4% possible for generation of oxygen-enriched CO_2 stream. Neutrality to SO_x and NO_x is another major advantage of CuO-based oxides as oxygen source when flue gas is used as the purge gas.

6.2. Recommendations

Based on the experimental and theoretical studies carried out in this dissertation, the following recommendations are suggested for future work:

- Firstly, I would recommend that the effect of oxides of sulphur and nitrogen and moisture on the performance of these sorbents be investigated.
- A limited number of synthesis methods were tried in this work. A greater number of methods like sol-gel, carbonization, spray pyrolysis, combustion synthesis, hydrothermal synthesis and carbon fiber impregnation are available which can improve the properties of copper

oxide as an oxygen sorbent, catalyst and energy storage material through the effects they have on pore structure, surface chemistry, grain geometry and other physical and chemical properties of the material.

- Alumina was used as dopant on copper oxide in this work. Addition of other types of oxides like Fe_2O_3, Co_3O_4, NiO, MnO and CeO_2 as dopants can have positive effects on the properties of CuO for oxygen absorption and other applications, so should be investigated.
- Inert supports (zirconia-based) were studied in this work. Reactive supports such as $CuAl_2O_4$ and $MgAl_2O_4$, despite their disadvantages like stability, can have positive effects on oxygen sorption/desorption kinetics that requires further investigation.
- Use of naturally occurring minerals such as kaolinite as a support can reduce the cost of sorbent synthesis which is crucial to large scale development of high temperature air separation.
- TGA was used for investigating the oxygen sorption/desorption properties of the materials studied in this work. Packed bed or fluidized bed experiments are necessary for gaining a better understanding of these materials as high temperature oxygen sorbents.
- Combination of high purity CO_2 and oxygen were used as purge gases in conducting the desorption experiments in this work. Effect of sulfur oxides and steam in the purge gas should be studied to get a better understanding of the kinetics under real conditions provided the safety requirements are available.

- XRD and SEM were the main characterization techniques used in this dissertation. For better understanding of the processes involved in synthesis and high temperature air separation, use of TEM is highly recommended.
- Last but not the least, an investigation of techno-economic evaluation of different sorbents in oxygen production is recommended.

7. References

Adanez, J. de Diego, L. F., Garcia-Labiano, F., Gayan, P. and Abad, A., "Selection of Oxygen Carriers for Chemical-Looping Combustion", *Energy & Fuels*, 2004, 18, 2, 371-377

Anson, A., Kuznicki, S.M., Kuznicki, T., Dunn, B.C., Eyring, E. M. and Hunter, D.B., "Separation of Argon and Oxygen by Adsorption on a Titanosilicate Molecular Sieve", *Separation Science and Technology*, 2009, 44, 1604–1620

Baltes, C. S., Vukojevi, C. and Schuth, F., "Correlations between synthesis, precursor, and catalyst structure and activity of a large set of $CuO/ZnO/Al_2O_3$ catalysts for methanol synthesis. *Journal of Catalysis*, 2008, 258, 334–344

Barsoum, M.W., Fundamentals of Ceramics, *Taylor & Francis*, New York, 2003

Baythoun, M.S., "Production of strontium-substituted lanthanum manganite perovskite powder by the amorphous citrate process", *Journal of Materials Science*, 1982, 2757-2769.

Bluthardt, C., Fink C., Flick K. and Hagemeyer, A., "Aqueous synthesis of high surface area metal oxides", *Catalysis Today*, 2008, 137, 132–143

Bordent, B. and Kluger, F, "Thermodynamic Modelling of the Corrosive Deposits in Oxy-Fuel Fired Boilers", *Materials Science Forum*, 2008, 595-598, 261-269.

Brown, P. K. and Gallagher, P. K., Handbook of Thermal Analysis and Calorimetry, *Elsevier*, 2008

Buhre, B. J.P., Elliott, L.K., Sheng, C.D., Gupta, R. P. and Wall, T. F., “Oxyfuel combustion technology for coal-fired power generation.”, *Progress in Energy and Combustion Science*, 2005, 31, 4, 283–307.

Burdyny, T. and Struchtrup, H., "Hybrid membrane/cryogenic separation of oxygen from air for use in the oxy-fuel process", *Energy*, 2010, 35, 1884–1897

Burnham, A.K. and Braun, R.L., “Global Kinetic Analysis of Complex Materials”, *Energy & Fuels*, 1999, 13, 1-22.

Chadda, D., James, D.F., “Chemical Energy Storage by the Reaction Cycle CuO/Cu_2O”, *International Journal of Energy Research*, 1989, 13, 63-73.

Chou,C., Ju, D. and Chang, S., "Simulation of a Fractionated Vacuum Swing Adsorption Process for Air Separation", *Separation Science and Technology*,1998,33, 13, 2059-2073.

Chuang, S.Y., Dennis, J.S., Hayhurst, A.N. and Scott, S.A. ”Development and performance of Cu-based oxygen carriers for chemical-looping combustion”, *Combustion and Flame*, 2008, 154, 109-121.

Davis, M.E. and Lobo, R.F., "Zeolite and Molecular Sieve Synthesis", *Chemistry of Materials*, 1992, 4,156-768.

Dongare, M.K., Dongare , A.M., Tare, V.B. and Kemnitz, E., “Synthesis and characterization of copper-stabilized zirconia as an anode material for SOFC”, *Solid State Ionics*, 2002, 152– 153, 455– 462.

Dow, W.P. and Huang, T., "Effect of Oxygen Vacancy of Yttria-stabilized Zirconia Support on Carbon Monoxide Oxidation over Copper Catalyst", *Journal of Catalysis*, 1994, 147, 322-332.

Du, G.H., Van Tendeloo, G., "$Cu(OH)_2$ nanowires, CuO nanowires and CuO nanobelts", *Chemical Physics Letters*, 2004, 393, 64–69.

Filipic, G and Cvelbar, U., "Copper oxide nanowires: a review of growth", *Nanotechnology,* 2012, 23, 1-16.

Garcia-Labiano, F. L., de Diego, F., Ada´nez, J., Abad, A. and Gaya´n, P., " Reduction and Oxidation Kinetics of a Copper-Based Oxygen Carrier Prepared by Impregnation for Chemical-Looping Combustion", *Industrial & Engineering Chemistry Research*, 2004, 43, 26, 8168-8177.

Garcia-Marquez, A., Portehault, D. and Giordano, C., "Chromium nitride and carbide nanofibers: from composites to mesostructures.", *Journal of Materials Chemistry*, 2011, 21, 2136–2143.

Grzeski, Z. and Migdalska, M., "On the mechanism of Cu_2O Oxidation at High Temperature", *Defect and Diffusion Forum*, 2009, 289-292, 229-236.

Habib, M. A., Badr, H. M., Ahmed, R., Ben-Mansour, K. and Mezghani, S., "A review of recent developments in carbon capture utilizing oxy-fuel combustion in conventional and ion transport membrane systems", *International Journal of Energy Research*,2011, 35, 9, 741-764.

Heffelfinger, J.R., Bench, M.W, Carter, B., “On the faceting of ceramic surfaces”. *Surface Science*, 1995, 343, L1161-L1166.

Hellfritsch S, Gampe U. Modern coal-fired oxyfuel power plants with CO_2 Capture - energetic and economical evaluation. Germany: Dresden University

Hadjipaschalis, I., Kourtis, G., Poullikkas, A., “Assessment of oxyfuel power generation technologies”, *Renewable and Sustainable Energy Reviews*, 2009, 13, 9, 2637–2644.

Hoque S.M., Chudhurry, M.A. and Islam, M.F., “Characterization of Ni–Cu mixed spinel ferrite”, *Journal of Magnetism and Magnetic Materials*, 2002, 251, 292-303.

Ishida, M. and Jin, H., "A New Advanced Power-Generation System Using Chemical-Looping Combustion", *Energy*, 1994, 19, 4, 415-422.

Jacob, K.T. and Alcock, B.C., “Thermodynamics of $CuAlO_2$ and $CuAl_2O_4$ and Phase Equilibria in the system Cu_2O-CuO-Al_2O_3”, *Journal of the American Ceramic Society*, 1974, 58, 6, 192-195.

Jadhav, P. D., Chatti, R. V., Biniwale, R. B., Labhsetwar, N. K. Devotta, S. and Rayalu, S. S. "Monoethanol Amine Modified Zeolite 13X for CO_2 Adsorption at Different Temperatures", *Energy and Fuels*, 2007, 21, 6, 35555-35559.

Jayaraman, A. and Yang, R.T., “Stable Oxygen-Selective Sorbents for Air Separation”, *Chemical Engineering Science*, 2005, 60, 625-634.

Jordal, K., Anheden, M., Yan, J. and Stromberg, L. "Oxyfuel combustion for coal-fired power generation with CO_2 capture - opportunities and challenges", *Seventh conference on greenhouse gas technologies*, 2004

Kakaras, E., Koumanakos, A., Doukelis, A., Giannakopoulos, D. and Vorrias, I. "Oxyfuel boiler design in a lignite-fired power plant", *Fuel*, 2007, 86, 14, 2144–2150.

Klug, H.P., X-ray Diffraction Procedures for Polycrystalline and Amorphous Materials, *Wiley Inter-Science Publications*, 1954

Kingery, W.D., Bowen, H.K. and Uhlmann, D.R., Introduction to Ceramics, *John Wiley & Sons*, 1976.

Kobayashi, H., and Prasad, R., "A Review of Oxygen Combustion and Oxygen Production Systems", Praxair Technology, Inc., 1999

Krishnamurthy, K. R., Barton, T., Braunberger, B., Omar, K. and Sethi, V.; "Demonstration of a Novel, Low-Cost Oxygen Supply Process and its Integration with Oxy-Fuel Coal-Fired Boilers", *Sixth Annual Conference on Carbon Capture & Sequestration, Pittsburgh*, 2007, Pennsylvania.

Kroger, F.A. and Vink, H.J., "Relations between the concentrations of imperfections in solids", *Journal of Physics and Chemistry of Solids*, 1958, 5, 3, 208-214.

Kumekawa Y., Hirai, M., Kobayashi, Y., Endoh, S., Oikawa, E. and Hashimoto, T.; "Evaluation of thermodynamic and kinetic stability of $CuAlO_2$", *Journal of Thermal Analysis and Calorimetry*, 2009, 99, 57–63.

Lee L., "Performance and evaluation of Cu-based nano-composite anodes for direct utilisation of hydrocarbon fuels in SOFCs", *Fuel cells*, 2010, 10, 1, 145-155.

Li, G.Q. and Govind, R., "Separation of Oxygen from Air Using Coordination Complexes: A Review", *Industrial and Engineering Chemistry Research*, 1994, 33, 755-783

Li, J. and Wang, S. Q., "Oxygen diffusion-induced phase boundary migration in copper oxide thin films. *Physical Reviews B*, 1989, 39, 12367-1270.

Li, Z., Zhang, T. and Cai, N.S., " Experimental Study of O_2-CO_2 Production for the Oxyfuel Combustion Using a Co-Based Oxygen Carrier", *Industrial & Engineering Chemistry Research*, 2008, 47,19, 7147-7153.

Liang, H., Xingwang, Z., Lin, C. and Lechng, L., "Promotional effect of CeO_2 and Y_2O_3 on CuO/ZrO_2 catalysts for methane combustion", *Journal of Rare Earths*, 2010, 30, 2, 123-127.

Lin, Y. S., Mclean, D. L., Zeng, Y., "High Temperature Adsorption Process", US Patent 6059858, 2000.

Lin, Y.S., Yang, Q. and Ida, J. “High temperature sorption of carbon dioxide on perovskite-type metal oxides”, *Journal of the Taiwan Institute of Chemical Engineers*, 2009, 40, 276–280.

Lin, Y.S. and Zhang, T., “Fixed-bed performance for production of oxygen-enriched carbon dioxide stream by perovskite-type ceramic sorbent”, *Separation & Purification Technology*, 2006, 49, 27-35.

Lu, F.H. and Dieckmann, R. “Point defects in oxide spinel solid solutions of the type (Co, Fe, Mn)$_{3-\delta}$O$_4$ at 1200°C”. *Journal of Physical Chemistry of Solids*, 1995, 56, 5, 725–33.

Malek, J. (1992) The kinetic analysis of non-isothermal data. *Thermochimica Acta*, 200, 257-269

Marcilly, C., Cqurty, P. and Delmqn, B., “Preparation of Highly Dispersed Mixed Oxides and Oxide Solid Solutions by Pyrolysis of Amorphous Organic Precursors”, *Journal of the American Ceramics Society*, 1970, 53, 1, 56-57.

Marion J. “Technology options for controlling CO2 emissions from fossil-fuelled power plants. “, *Proceedings of the third annual conference on carbon sequestration*, 2004.

Mattisson, T., Lyngfelt, A.and Leion, H., “Chemical-looping with oxygen uncoupling for combustion of solid fuels”, *International Journal of Greenhouse Gas Control*, 2009, 3, 11–19.

Mizusaki J., Yoshihiro, M., Yamahuchi, S. and Fueki, K., "Nonstoichiometry and structure of perovskite-type oxides $La_{1-x}Sr_XFeO_{3-\delta}$", *Journal of Solid Sate Chemistry*, 1985, 58, 257-264.

Mizusaki J., Yoshihiro, M., Yamahuchi, S. and Fueki, K., "Nonstoichiometry and structure of perovskite-type oxides $La_{1-x}Sr_XCoO_{3-\delta}$", *Journal of Solid Sate Chemistry*, 1989, 80, 102-110.

Navrotsky, A. (Editor), Perovskite: a structure of great interest to geophysics and materials science, *American Geophysical Union*, Washington D.C., 1989.

Nsakala, N.y; Liljedahl, G.N.; Marion, J., Levasseur, A.A., Turek, D. and Chamberland, R., "Oxygen-fired circulating fluidized bed boilers for greenhouse gas emissions control and other applications", *Proceedings of Third Annual Conference on Carbon Sequestration*, 2004, Alexandria, VA, USA.

Ollero, P., Serrera, R.A.; Alcantarilla, S., " Diffusional effects in TGA gasification experiments for kinetic determination", *Fuel*, 2002, 81, 15, 1989-2000.

Pechini, M.P., US Patent No.3.330.697 July 1, 1967

Poulston, S., Parlett, P. M., Stone, P. and Bowker, M., "Surface Oxidation and Reduction of CuO and Cu_2O Studied Using XPS and XAES", *Surface Science and Interface Analysis*, 1996, 24, 811-820.

Raja, M.W., Mahanty, S. Ghosh, P., Basu, R.N. and Maiti, H.S., "Alanine-assisted low-temperature combustion synthesis of nanocrystalline $LiMn_2O_4$ for lithium-ion batteries", *Materials Research Bulletin*, 2007, 42, 1499–1506.

Raynaud, G. M., William, A.T. and RAPP, R. A., " In Situ Observation of Copper Oxidation at High Temperatures", *Metallurgical Transactions A.*, 1984, 15, 573-579.

Rege, S.U. and Yang, R.T., "Limits for Air Separation with LiX Zeolite", *Industrial and Engineering Chemistry Research*, 1997, 36, 5358 -5365.

Reinecke, N. and Taglauer, E., " The kinetics of oxygen-induced faceting of Cu(115) and Cu(119) surfaces", *Surface Science*, 2000, 454–456, 94–100.

Rietveld, H. M., "A Profile Refinement Method for Nuclear and Magnetic Structures", *Journal of Applied Crystallography*, 1969, 2, 65-71.

Rosso, M., Saracco, G., Specchia, V., "Tackling the problem of sulfur poisoning of perovskite catalysts for natural gas combustion", *Korean Journal of Chemical Engineering*, 2003, 20, 2, 222-229.

Ruiz-Morales, J. Canales-Va´zquez, J. Marrero-Lo´pez, D., Pen˜a-Martı´nez, J., "Is YSZ stable in the presence of Cu?", *Journal of Materials Chemistry*, 2008, 18, 42, 5072-5077.

Ruthven, D.M., Principles of Adsorption and Adsorption Processes, *John Wiley & Sons*, New York, 1984.

Ruthven D.M., Farooq, S., and Knaebel, K. S., Pressure swing adsorption, *VCH Publishers Inc.*, New York, 1994.

Scheffknecht, G., Al-Makhadmeh1, L., Schnell, U. and Maier, J., "Oxy-fuel coal combustion.A review of the current state-of-the-art", *International Journal of Greenhouse Gas Control*, 2011, 5S, S16–S35.

Sharma, S.C., Gokhale, N. M, Dayal, R. and Lal, R., "Synthesis, microstructure and mechanical properties of ceria stabilized tetragonal zirconia prepared by spray drying technique", *Bulletin of Materials Science*, 2002, 25, 1, 15-20.

Singh, D., Croiset, E., Douglas, P. L. and Douglas, M. A., "Technoeconomic study of CO_2 capture from an existing coal-fired power plant: MEA scrubbing vs. O_2/CO_2 recycle combustion", Energy Conversion and Management, 2003, 44, 19, 3073–3091.

Sircar, S., Rao, M.B. and Golden T.C., "Fractionation of Air by Zeolites", *Studies in Surface Science and Catalysis*, 1998, 120, 395-423.

Sunarsoa, J., Baumannb, S., Serrac, J.M., Meulenbergb, W.A., Liua, S., Lin, Y.S. and Diniz da Costa, J.C., "Mixed ionic–electronic conducting (MIEC) ceramic-based membranes for oxygen separation", *Journal of Membrane Science*, 2008, 320, 13–41.

Tannyan, N.J., Plasencia, G. and Utigard, T.A., " High Temperature Oxidation of Copper and Copper Aluminum Alloys", *Canadian Metallurgical Quarterly*, 2002, 41, 2, 213-218.

Tejuca, L. G., Fierro, J. L.G., and Tascon, J.M.D, "Structure and Reactivity of Perovskite-type Oxides", *Advanced Catalysis*, 1989, 36, 237-296.

Tobin, J. P., Hirschwald, W. and Cunningham, J., "XPS and XAES Studies of Transient Enhancement of Cu1 at CuO Surfaces during Vacuum Outgassing", *Applications of Surface Science*, 1983, 16, 441-452.

Toftegaarda, M.B., Brixa, J., Jensena, P.A., Glarborga, P. and Jensena, A.D., "Oxy-fuel combustion of solid fuels", *Progress in Energy and Combustion Science*, 2010, 36, 36581-625

Toporov, D., Forster, M. and Kneer, R., "Combustion of pulverized fuel under oxycoal conditions at low oxygen concentrations", *Third international conference on clean coal technologies for our future*; 2007.

Wall, T., Liu, Y., Spero, C., Elliot L. and Khare, S., "An overview on oxyfuel coal combustion-State of the art research and technology development", *Chemical Engineering Research and Design*, 2009, 87, 3, 1003-1016

Watterud, G. PhD Thesis Norwegian University of Science and Technology (2005). Determination of oxygen transport coefficients in perovskites and perovskite related materials with mixed conductivity.

Wei, Z. and Osamura, K., "Phase Diagram of Cu_2O-CuO-Y_2O_3 System in Air", *Metallurgical Transactions A*, 1990, 21, 8, 2243-2248.

Wood, G. C. and Stott, F. H., "The Influence of an Intermediate Annealing Treatment on the Oxidation of Copper and Nickel", *Oxidation of Metals*,1980, 14, 3, 187-205.

Xu, L., Wang, J., Li, Z.and Cai, N.", Experimental Study of Cement-Supported CuO Oxygen Carriers in Chemical Looping with Oxygen Uncoupling (CLOU)", *Energy Fuels*, 2013, 27, 1522−1530.

Yang, Q. and Lin,Y.S., "Improved Sorbent for High-Temperature Production of Oxygen-Enriched Carbon Dioxide Stream", *Industrial and Engineering Chemistry Research*, 2007, 46, 18, 6025-6031.

Yang, Q., Lin, Y.S., Bulow, M., "High Temperature Sorption Separation of Air for Producing Oxygen-Enriched CO_2 Stream", *AIChE Journal*, 2006, 52, 2, 574-581.

Yang, Z., Lin, Y. S. and Zeng, Y, "High-Temperature Sorption Process for Air Separation and Oxygen Removal", *Industrial and Engineering Chemistry Research*,2002, 41, 2775-2784.

Yang, Z. H. and Lin, Y. S., "High-Temperature Oxygen Sorption in a Fixed Bed Packed with Perovskite-Type Ceramic Sorbents", *Industrial and Engineering Chemistry Research*, 2003, 42, 4376-4381.

Yin, Q., Kniep, J. and Lin, Y.S., "Oxygen sorption and desorption properties of Sr–Co–Fe oxide", *Chemical Engineering Science*, 2008, 63, 2211 – 2218.

Zhang, T., Li, Z. and Cai, N.", "Continuous O_2-CO_2 Production Using a Co-Based Oxygen Carrier in two Parallel fixed-bed reactors", *Korean Journal of Chemical Engineering,* 2008, 26, 3, 845-849.

Zhou, K., Wang, R., Xu, B. and Li, Y.; "Synthesis, characterization and catalytic properties of CuO nanocrystals with various shapes", *Nanotechnology*, 2006, 17, 3939-3943.

Zhu, Y., Mimura, K. and Isshiki, M., "Oxidation Mechanism of Cu_2O to CuO at 600-1050 °C", *Oxidation of Metals*, 2004, 62, 3/4, 207-222.